

DEVELOPMENT OF PRECAST CONCRETE AND STEEL HYBRID SPECIAL
MOMENT-RESISTING FRAMES

by

Yuntian Wu

A Dissertation Presented to the
FACULTY OF THE GRADUATE SCHOOL
UNIVERSITY OF SOUTHERN CALIFORNIA
In Partial Fulfillment of the
Requirements for the Degree
DOCTOR OF PHILOSOPHY
(CIVIL ENGINEERING)

December 2008

Acknowledgements

The author would like to thank Professor Yan Xiao for his expertise and continuous support at all stages of research of this project. Without his guidance and support in both study and life the completion of this research would not be possible. The author also would like to thank Professor James C Anderson for his help and support during the author's entire academic life at USC.

The research project described in this report was supported by the National Science Foundation under the contract number CMS-0220067. The NSF project director was Dr. Perumalsamy N. Balaguru. The reinforced concrete precast columns were donated by Pomeroy Corporation, and SSI Express Inc. The NMB Splice-sleeve systems were donated by Splice Sleeve North America, Inc. Mr. D. Mooradian, Director of PCMAC coordinated the industrial collaborations for this research program. The authors would like to appreciate the helps and supports of all the sponsoring agencies.

The authors would also like to thank Mr. Zhu, Pingsheng, graduate research assistant for their helps in preparing the testing. Corporations from laboratory manager, Mr. Lance Hill are specially appreciated.

Table of Contents

| | |
|--|----|
| Acknowledgements | ii |
| List of Tables | v |
| List of Figures | vi |
| Abstract | x |
| Chapter 1: Introduction | 1 |
| 1.1 Research Background | 1 |
| 1.2 Objective of Research | 5 |
| 1.3 Composite Structure vs. Hybrid Structure | 6 |
| 1.4 Proposed Hybrid PCS Beam-column Connection | 7 |
| 1.5 Yield-line Theory for End-plate Design | 7 |
| Chapter 2: Capacity-Based Design and Construction of PCS Moment Frames | 11 |
| 2.1 Proposed Hybrid Beam-column Connection Details | 11 |
| 2.2 Development of System Capacities | 14 |
| 2.3 Splice Design and Construction | 19 |
| 2.3.1 Design of Dowel Anchorage Base Connection | 22 |
| 2.3.2 Design of Splice Sleeves Base Connection | 26 |
| Chapter 3: Experimental Program | 27 |
| 3.1 Selection of Beam-column Connection Testing Method | 27 |
| 3.2 Objective of Experimental Program | 30 |
| 3.3 Design of Test Models | 31 |
| 3.3.1 Steel Beam Design | 33 |
| 3.3.2 Precast Concrete Column Design | 37 |
| 3.3.3 Precast Concrete Footing Design | 42 |
| 3.3.4 Design of Bolted End-plate Beam-column Connection | 48 |
| 3.4 Construction of Test Models | 53 |
| 3.4.1 Construction of RC Columns and Footings | 53 |
| 3.4.2 Fabrication of Steel Beams and Steel Plates | 55 |
| 3.4.3 Connection between Columns and Footings | 56 |
| 3.4.4 Connection between Columns and Beams | 60 |
| 3.5 Test Setup | 61 |
| 3.6 Instrumentation | 63 |
| 3.7 Test Regimen | 65 |
| 3.8 Experimental Results and Discussions | 67 |
| 3.8.1 General Observations | 67 |
| 3.8.2 Horizontal Force-Displacement Response | 71 |

| | | |
|---|--|-----|
| 3.8.3 | Overstrength Factor of RBS | 74 |
| 3.8.4 | Post-tensioning Steel Rods | 75 |
| 3.8.5 | Beam-column Joint Region | 77 |
| 3.8.6 | PC Column Base | 77 |
| 3.8.7 | Yield Sequence of Test Subassembly Components | 80 |
| 3.9 | Conclusions | 81 |
| Chapter 4: Comparative Study of S, PCS and RC Building Design | | 84 |
| 4.1 | Introduction | 84 |
| 4.2 | Prototype Buildings | 85 |
| 4.3 | Characteristics of Seismic Design of Prototype Buildings | 88 |
| 4.3.1 | Building Period T_a | 88 |
| 4.3.2 | Seismic Weight W | 88 |
| 4.3.3 | Design Base Shear V | 89 |
| 4.3.4 | Vertical Distribution of Design Base Shear | 90 |
| 4.3.5 | Lateral Displacement and Inter-story Drift | 92 |
| Chapter 5: Nonlinear Modeling of PCS Beam-column Connection | | 94 |
| 5.1 | Modeling Philosophy | 94 |
| 5.2 | Rotation of Hybrid Beam-column Connection | 95 |
| Chapter 6: Conclusions and Future Research | | 101 |
| 6.1 | Conclusions | 101 |
| 6.2 | Future Research | 103 |
| Notation | | 105 |
| Bibliography | | 108 |
| Appendix A: Structural Design of Prototype Buildings | | 110 |
| Appendix B: Experimental Results | | 138 |
| Appendix C: Material Test Results | | 156 |

List of Tables

| | |
|--|-----|
| Table 3.1 Seismic compact section check for W12X26 | 33 |
| Table 4.1 Fundamental period of prototype buildings | 88 |
| Table A.1 Member size of 13-story prototype building | 112 |
| Table A.2 Equivalent Concrete Column Sizes | 114 |
| Table A.3 Equivalent Concrete Beam Sizes | 114 |
| Table A.4 Member Size of 13-Story RC Prototype Building | 115 |
| Table A.5 Member Size of 13-Story PCS Prototype Building | 116 |
| Table A.6 Seismic Weight of Prototype Buildings | 118 |
| Table A.7 Seismic Forces and Story Shears of Steel Building | 122 |
| Table A.8 Seismic Forces and Story Shears of PCS Building | 123 |
| Table A.9 Seismic Forces and Story Shears of RC Building | 123 |
| Table A.10 Lateral Displacements and Drifts of Prototype Buildings | 126 |
| Table A.11 Reduced Beam Section Design Results | 133 |
| Table A.12 Service Dead and Live Axial Load for An Edge Column | 134 |
| Table A.13 Service Dead and Live Axial Load for A Corner Column | 135 |
| Table A.14 Longitudinal Reinforcement for PCS Building | 135 |

List of Figures

| | |
|--|----|
| Figure 1.1 Hybrid PCS beam-column connection | 9 |
| Figure 1.2 Yield line pattern and virtual displacement | 10 |
| Figure 2.1 Proposed hybrid PCS Beam-column connection | 11 |
| Figure 2.2 Loading conditions of PCS beam-column joint | 13 |
| Figure 2.3 Yield line pattern of endplate | 16 |
| Figure 2.4 Shipment and splice plan of PCS frame | 20 |
| Figure 2.5 Splice of columns using embedded sleeves | 21 |
| Figure 2.6 Dowel anchorage base connection | 23 |
| Figure 2.7 Bond slip of column rebars | 25 |
| Figure 2.8 Design critical section of splice sleeve connection | 26 |
| Figure 3.1 Typical test specimen | 28 |
| Figure 3.2 Deformed shape of frame structure | 29 |
| Figure 3.3 Loading diagram of simple connection test | 29 |
| Figure 3.4 Special moment resisting frame elevation and test model | 32 |
| Figure 3.5 Reduced beam section parameters | 34 |
| Figure 3.6 Forces developed at plastic hinges | 36 |
| Figure 3.7 P-M interaction curve of reinforced column section | 38 |
| Figure 3.8 Column to footing connection details | 43 |
| Figure 3.9 7U-X sleeve details | 44 |
| Figure 3.10 Reinforcement details of footing of test model 1 | 45 |

| | |
|---|----|
| Figure 3.11 Reinforcement details of footing of test model 2 | 46 |
| Figure 3.12 Details of column in test model 1 | 47 |
| Figure 3.13 Details of column in test model 2 | 48 |
| Figure 3.14 Models of beam-column connection for calculation | 50 |
| Figure 3.15 Endplate details | 51 |
| Figure 3.16 NMB splice sleeves and dowel rebars | 54 |
| Figure 3.17 Steel cages of footings | 55 |
| Figure 3.18 Steel beam details | 56 |
| Figure 3.19 Test frame | 57 |
| Figure 3.20 Column to footing connection | 58 |
| Figure 3.21 SS mortar | 58 |
| Figure 3.22 Filling of SS mortar into sleeves | 59 |
| Figure 3.23 NMB splice sleeve test | 59 |
| Figure 3.24 Column-footing connection of test model 2 | 60 |
| Figure 3.25 Test setup | 62 |
| Figure 3.26 Instrumentation for steel beam | 64 |
| Figure 3.27 Instrumentation for beam-column joint | 65 |
| Figure 3.28 Instrumentation for curvature at column plastic hinge | 65 |
| Figure 3.29 Interstory drift | 67 |
| Figure 3.30 Buckling of steel beam RBS of TS1 | 68 |
| Figure 3.31 Cracking of beam-column joint of TS2 | 68 |
| Figure 3.32 Cracking of column of TS1 | 69 |

| | |
|---|----|
| Figure 3.33 Cracking of column of TS2 | 69 |
| Figure 3.34 Horizontal force-drift ratio relationship of TS1 | 72 |
| Figure 3.35 Horizontal force-drift ratio relationship of TS2 | 73 |
| Figure 3.36 Typical hysteresis hoop of TS1 and TS2 | 73 |
| Figure 3.37 Overstrength of RBS of TS1 | 75 |
| Figure 3.38 Overstrength of RBS of TS2 | 75 |
| Figure 3.39 Deformation-force relationship of post-tensioning rod | 76 |
| Figure 3.40 Curvature-moment relationship of TS1 | 79 |
| Figure 3.41 Curvature-moment relationship of TS2 | 79 |
| Figure 3.42 Yield sequence of TS1 | 81 |
| Figure 3.43 Yield sequence of TS2 | 81 |
| Figure 4.1 Typical floor plan of Steel building | 86 |
| Figure 4.2 Typical floor plan of PCS building | 87 |
| Figure 4.3 Typical floor plan of RC building | 87 |
| Figure 4.4 Seismic weight comparison | 89 |
| Figure 4.5 Design base shear of prototype buildings | 90 |
| Figure 4.6 Vertical distribution of design base shear | 91 |
| Figure 4.7 Story shear of prototype buildings | 91 |
| Figure 4.8 Lateral displacement of prototype buildings | 92 |
| Figure 4.9 Inter-story drift of prototype buildings | 93 |
| Figure 5.1 Chord-hinge model of steel beam | 96 |
| Figure 5.2 Hinge moment rotation relationship | 97 |

| | |
|---|-----|
| Figure 6.1 Suggest test setup | 103 |
| Figure A.1 Plan view of perimeter frames | 111 |
| Figure A.2 Elevation of perimeter frame | 112 |
| Figure A.3 Geometrical parameters of reduced beam section | 132 |
| Figure A.4 Light-weight concrete floor slab system | 137 |
| Figure A.5 Composite beam section | 137 |
| Figure B.1 Testing Data of Test Model 1 | 138 |
| Figure B.2 Testing Data of Test Model 2 | 143 |
| Figure C Material test results | 157 |

Abstract

In this NSF sponsored research project, an innovative hybrid steel precast concrete column (PC) and steel beam (S) moment resisting system was proposed and studied. The proposed hybrid PCS beam-column frame is structurally unique in that its system continuity and toughness is solely provided by the post-tensioning force of beam-column connection. The proposed PCS system is also economically efficient due to the mixed use of precast concrete and steel beam. Compared with conventional steel structure, PCS system has lower material cost while better dynamic characteristics. Compared with conventional reinforced concrete system, PCS frame is lighter, lesser labor cost and faster construction speed.

To validate the use of hybrid PCS special moment resisting frame in moderate to high seismic regions, a capacity-based design methodology was developed and applied to design of prototype building. The effectiveness of the proposed design approach was also examined through large scale quasi-static testing of beam-column-footing subassembly. Test results showed that the hybrid PCS moment frame can be designed to have adequate strength, stiffness and energy dissipation capacity.

Some considerations on the nonlinear modeling of the proposed hybrid PCS beam-column connection are also presented. The purpose of the proposed modeling method is to capture the rotational behavior of the PCS beam-column connection.

Chapter 1: Introduction

1.1 Research Background

The steel and concrete composite and hybrid structures first appeared in the United States and Japan due to its potential cost-effectiveness in 1960's. In Japan, construction contractors substituted reinforced concrete beams by steel beams in conventional reinforced concrete retailing stores to make longer floor span. In the United States, contractors substituted steel columns by reinforced concrete columns in conventional steel structures to reduce the total material cost. Those early-emerging steel and concrete composite and hybrid buildings were mostly low-rise and located in low seismic regions. The composite beam-column connection was only considered to resist shear caused by gravity loads. Soon after successful applications of steel and concrete composite and hybrid construction in gravity load resisting systems in both countries, the call for research aiming to expand the use of composite structures into seismic load resisting system was raised by the construction industries. As a response to the request for research, the US-Japan cooperative structural research project on composite and hybrid structure was then launched aiming to develop composite and hybrid moment resisting frame system consisting of concrete column and steel beam suitable to be used in medium and high-rise buildings located in moderate to high seismic regions. In the following decade of years, a great deal of experimental and analytical research was conducted on the reinforced concrete (RC) and steel (S) or RCS composite and hybrid system, where the

steel beam goes through the cast-in-place RC column. According to previous studies (Sheikh 1989; Griffis 1992), the merits and advantages of the RCS moment resisting frame include

- 1) Concrete columns are more cost-effective than steel columns in providing lateral stiffness and strength in high rise buildings;
- 2) Concrete columns are superior to steel columns in dynamic characteristics. Concrete material has better damping behavior than steel;
- 3) Concrete column has better fire resistance than steel column;
- 4) Steel beam is more cost-effective than concrete beam in providing long floor span. Use of steel beam can reduce the total seismic load of structure;
- 5) Use of steel beam can further reduce the labor cost for formwork and shoring and then improve the construction efficiency.

The studies under the US-Japan cooperative program indicated that monolithic RCS moment frames, where the steel beam runs through cast-in-place RC column, can be designed with seismic deformation capacity and toughness comparable to traditional structural steel or reinforced concrete construction (Chou and Uang 1998; Deierlein 2004).

However, research has rarely been conducted on hybrid moment resisting frame consisting of precast concrete column and steel beam where the beam-column connection is not monolithic but jointed, despite of its potential benefits in construction speed due to

the use of precast columns. The lack of research on the precast concrete (PC) and steel (S) hybrid frames, or the PCS hybrid frames, is largely due to the fact that the previous or existing building codes are mainly based on existing data with cast-in-place construction only. As an “undefined structural system”, the hybrid PCS system cannot be easily designed and detailed such that it can respond to seismic loading essentially equivalent to cast-in-place or monolithic moment systems due to its jointed nature. However, it has become more and more recognized by researchers and practicing professionals in recent years that structural systems that do not fully satisfy the prescriptive requirements of current building codes can possibly provide satisfactory seismic performance. The desirable seismic characteristics must be validated by analysis and laboratory tests. Following this understanding, a series of innovative precast concrete seismic resisting systems, such as the precast hybrid moment resisting frame (Stone and Cheok etc. 1992) and precast concrete unbonded post-tensioned wall system (Kurama etc. 1999), were developed and validated in the PRESS (PREcast Seismic Structural Systems) research program and other research programs. Besides their inherent advantages and merits, these innovative precast systems were designed to ensure adequate continuity of components, effective load transfer mechanism and sufficient post-yield deformation capacity. Deviating from the typical cast-in-place emulation approach, the above-mentioned design methods may allow the post-yield deformation to occur at the connections. This relocation of system post-yield deformation may reduce the shear and flexural loads at beam end and thus mitigate the beam end concrete crushing. In a well-detailed hybrid precast concrete seismic system, the beam-column joint region may stay essentially

elastic since the mild steel that are placed at top and bottom of beam end section and extended into column joint region with certain debonded length is the energy dissipation device to endure most of the system post-yield deformation.

Another trend in the development of innovative lateral force resisting system is the wide application of post-tensioning technology. As one may know, the post-tensioning technology is originally developed to be used in precast and prestressed reinforced concrete. With post-tensioning tendons going through structural components such as concrete beam, concrete slab in building structures and bridge deck in bridge superstructures, the structure can be more wide-span, less vertical deflection and improved serviceability. In recent years, the post-tensioning technology has been adopted to the development of innovative precast lateral force resisting system. In precast moment resisting frames, the post-tensioning steel is used to connect precast beams to precast column. In precast shear wall system, post-tensioning tendons go through the wall body and fasten the wall to the foundation, providing significant restoring capacity to resist the overturning force under lateral loads.

The proposed hybrid precast concrete and steel moment frame system, or the PCS system, may develop seismic characteristics of both precast and composite constructions. Previous research on precast concrete seismic resisting systems has proved the effectiveness of jointed beam-column connections in the load transfer and energy dissipation mechanisms. Compared with precast concrete frame systems, more design merits and flexibility may be achieved if steel beam is used. The relatively lightweight of

steel beam along with the use of metal deck and lightweight concrete slab system can significantly reduce the weight of the structure thus further limiting the seismic demand imposed on the beam-column connection. The hybrid PCS system also allows the use of reduced beam section (RBS) of steel beam to provide post-yield deformation ductility and energy dissipation capacity.

1.2 Objectives of Research

The main objective of this research is to validate the use of the proposed PCS moment resisting frame in the design point of view. Here the design methods include both the conventional capacity-based design as well as the performance-based design. The purpose of the capacity-based design is to provide the PCS moment frame with reasonable capacity hierarchy among structural components such that the lateral structural system can yield in a ductile manner. The performance-based design, on the other hand, focus on the evaluation of the lateral deformation capacity of the PCS system. The effectiveness of the proposed capacity-based design of the PCS moment frame is evaluated through the interpretation of the test results of two large scale beam-column subassemblies. The performance-based design is carried out by conducting a series of nonlinear and dynamic analysis. The current research, however, focused on the development of capacity-based design methodology. The nonlinear modeling of critical structural components is discussed for the future development of performance-based design.

1.3 Composite structure vs. hybrid structure

In many circumstances composite structure and hybrid structure are treated as the same concept, referring to a structural system where structural steel and reinforced concrete are mixed together. However, considering the diverse natures of different mixed structural systems, the author highly recommends a reasonable separation of composite system and hybrid system. Composite structure refers to a structural system where the beams, or columns, or even both are mixed. For example, a composite structure can be formed by using Steel and Reinforced Concrete (SRC) member, which consists of a structural steel shape encased in concrete. Concrete Filled Tube (CFT) columns, where reinforced concrete is filled into steel rectangular or circular tube, are also common in composite structures. Due to its superior seismic resisting performance, composite structure is very popular in Japan even the cost of composite construction is very expensive. Hybrid structure, on the other hand, is appropriate to denote a structural system composed of conventional steel beam and conventional reinforced concrete column.

The RCS moment resisting frame type studied under the US-Japan cooperative project is both hybrid and composite. Although a RCS moment frame only consists of steel beam and concrete column, its beam-column connection is composite since the steel beam that runs through the concrete column is fully bonded to the column joint concrete. The performance of such composite connection partly relies on the bonding strength.

The proposed PCS moment frame, on the other hand, is pure hybrid since any bonding between steel beam and concrete column at the joint region is avoided.

1.4 Proposed hybrid PCS beam-column connection

The proposed hybrid PCS beam-column connection consists of a steel end-plate that is shop welded to beam end and then post-tensioned to precast concrete column, as shown in Figure 1.1. The post-tensioning steel rods are absolutely debonded from column joint concrete, since the diameter of the ducts is larger than that of the rods. The debonding of steel rods and column concrete at joint region can avoid the damage to joint caused by the repeated elongation of steel rods. The continuity of the beam-column connection is ensured by the post-tensioning force of the steel rods. The shear resistance is provided by friction as the connection is designed to be slip-critical, indicating a total neglecting of dowel effect. Another important feature of the hybrid post-tensioned connection is the gap opening between end-plate and column face after the tension force of post-tensioning rods exceed the pre-applied post-tensioning force.

1.5 Yield line theory for end-plate design

The beam-column connection type using steel end-plate and pre-tensioned fasteners was originally an optional choice for conventional steel structures. It attracted the attention of

structural designers because of its convenience of construction that only involves installation of fasteners. Any field welding can be avoided.

The typical moment resisting end-plate connection is designed as slip-critical type, i.e. the shear transfer is accomplished by the friction between end-plate and column face. To provide adequate moment resistance, a rational failure mechanism must be selected first. According to previous research, the yield line theory can well predict the upper bound of the bending moment strength of end-plate. The equation governing the yield line analysis based on virtual work method is

$$W_i = W_e$$

Where W_i is the internal work of the steel end-plate; W_e is the external work done to the end-plate based on the assumed yield line pattern.

$$W_i = \sum_{n=1}^N m_p (\theta_{nx} L_{nx} + \theta_{ny} L_{ny})$$

where θ_{nx} and θ_{ny} are the x- and y- components of the relative rotation of the rigid end-plate segments along the yield line; L_{nx} and L_{ny} are the x- and y- components of the yield line length; m_p is the plastic moment strength of the end-plate per unit length,

$$m_p = F_{yp} Z_p = \frac{1}{4} F_{yp} t_p^2$$

Where F_{yp} is the yield strength of plate material; Z_p is the plastic modulus per unit width of the end-plate and t_p is thickness of the end-plate.

$$W_e = M_{pl} \theta = M_{pl} \left(\frac{1}{h} \right)$$

Where M_{pl} is the flexural strength of the end-plate; θ is the applied virtual displacement and h is the distance from the centerline of the compression flange to the tension side edge of the end-plate. Figure 1.2 depicts a typical yield line pattern of steel end plate.

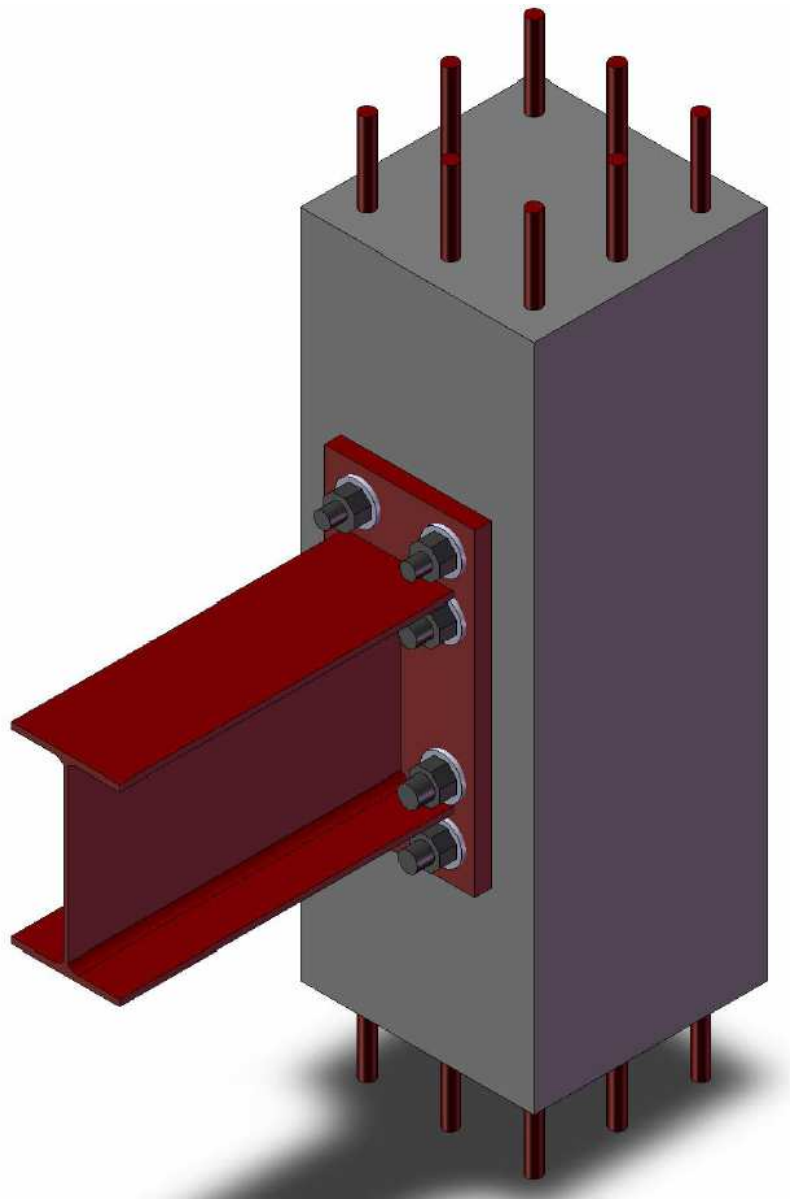


Figure 1.1: Hybrid PCS beam-column connection

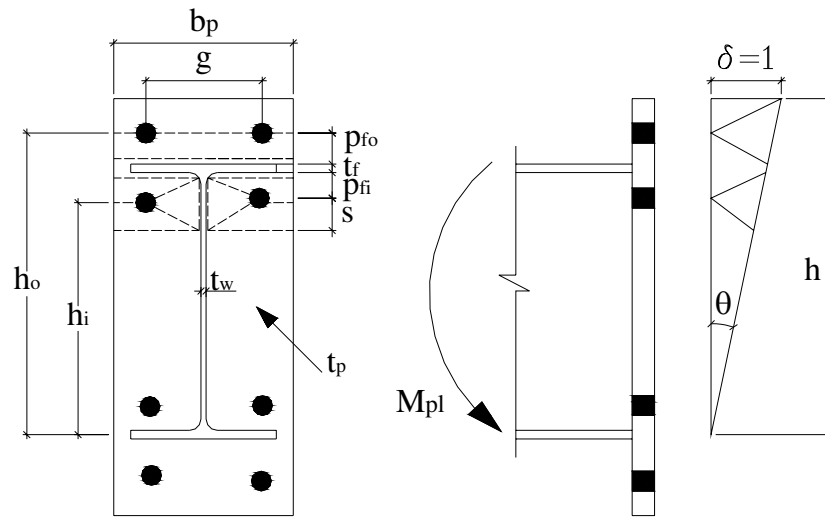


Figure 1.2: Yield line pattern and virtual displacement

Chapter 2: Capacity-based Design and Construction of PCS Moment Resisting Frames

2.1 Proposed Hybrid PCS Beam-column Connection Details

The proposed hybrid PCS beam-column connection, as shown in Figure 2.1, consists of a steel plate that is shop welded to the steel beam end, and then post-tensioned to the PC column using high strength steel rods that are fully unbonded to the PC concrete. The prestressing force of the post-tensioning rods is then transferred to PC column joint region through end plate. Thus the PC column joint concrete is subject to a pre-compressive stress before any seismic loading.

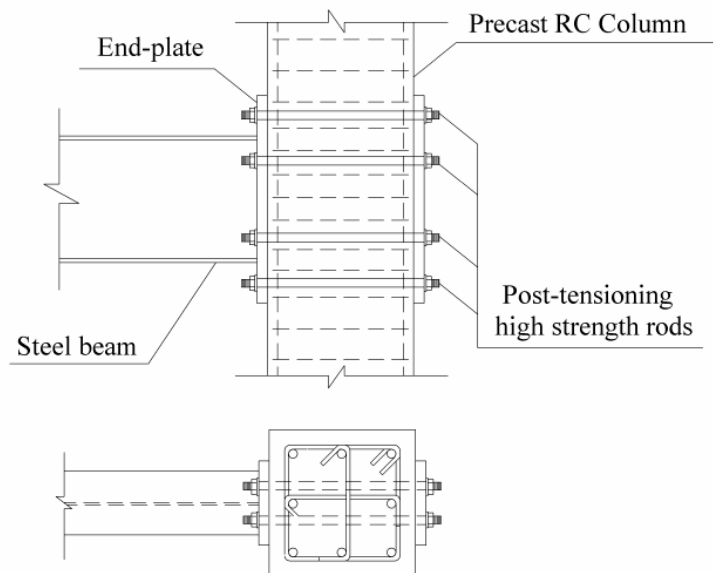


Figure 2.1: Proposed hybrid PCS beam-column connection

As a result of these features, the behavior of the post-tensioned end-plate connection is significantly different from that of a monolithic connection. Firstly, the earthquake-induced flexural moment at beam end is resisted by the combined reaction of end plate and the steel rods that causes the decompression of joint concrete. The extent of decompression depends on the pretension force level of steel rods and the magnitude of earthquake-induced moment transmitted to the connection. Following the total decompression of the PC column joint concrete, a gap is expected to be opened between the end plate and the adjoining column face, as exaggeratedly depicted in Figure 2.2. This earthquake-induced gap is unavoidable unless the pretension force level of steel rod is large enough. However, applying too much pretension to steel rod increases the difficulty as well as construction cost. In this sense, the steel rods and the corresponding PC column joint region are designed as a partial prestressed system that allows partial or total decompression of the column joint region at ultimate loading condition. Secondly, the primary shear resisting mechanism at the beam-column connection interface is friction, and the dowel effects of the rods are ignored. At service load level, the friction-mobilizing normal force is provided by the pretension force of the post-tensioning rods. At ultimate loading condition, the friction is mobilized by either the residual pretension force of steel rods or the seismic-induced reaction force between end-plate and PC column face, whichever is greater. Thirdly, the post-tensioning force of steel rod provides a restoring force that tends to close the seismic-induced gap. However, the inelastic deformation of steel rods may cause the loss of the pretension force of steel rods. The

usable restoring force of the steel rods is dependent on the magnitude of the steel rod pretension and type of steel material of the rods. Therefore, the main design parameters of post-tensioned end-plate connection include the thickness of end plate, size of steel rods and magnitude of pretension of steel post-tensioning rods.

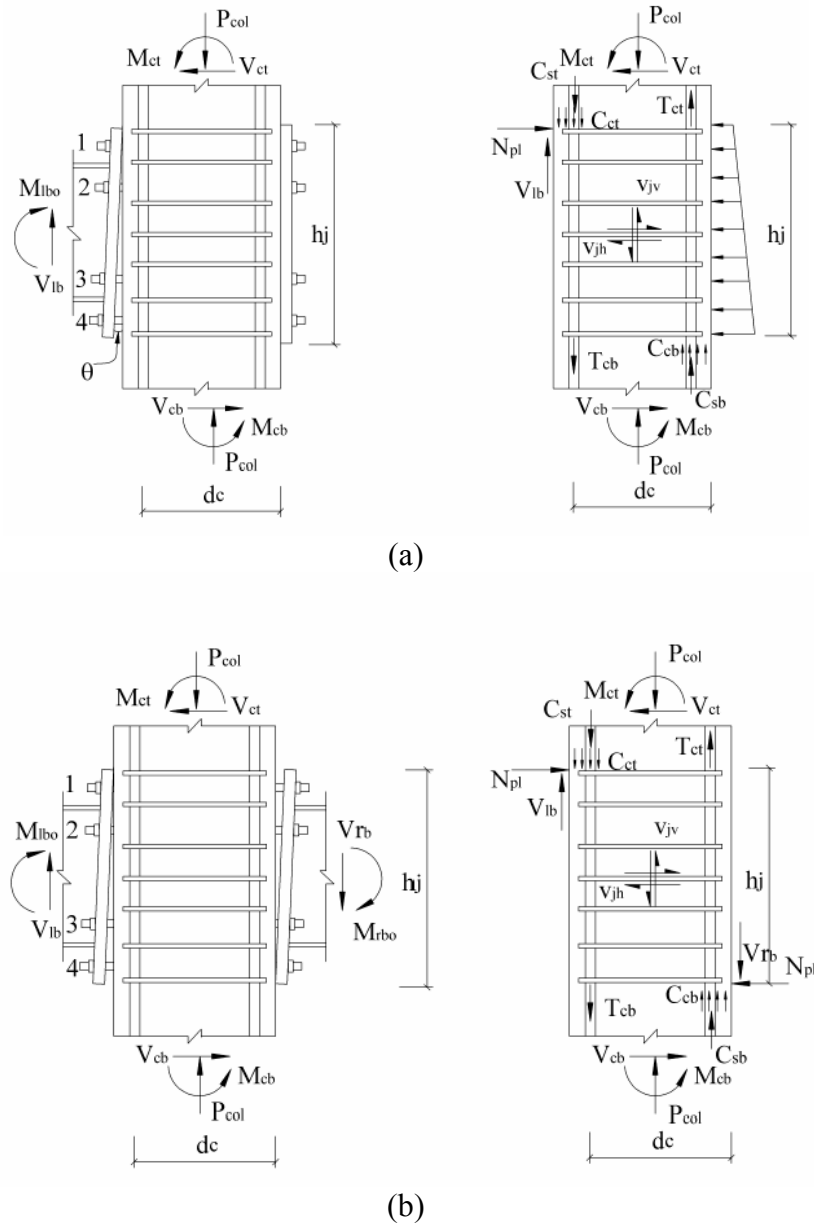


Figure 2.2: Loading conditions of PCS beam-column joint

2.2 Development of system capacities

The design approach following strong column-weak beam concept is adopted to design the composite PCS moment frame structure. The system post-yield deformation capacity is assumed to be provided by the plastic hinges formed at the reduced beam sections (RBS) located close to the beam ends. The relocation of plastic hinge from the beam column interface protects the welds of the end plate from excessive inelastic deformation. Use of reduced beam section can also decrease the width to thickness ratios of beam critical sections to prevent early local buckling of flanges. The ideal flexural moment capacity at the reduced beam section $M_{i,RBS}$ is:

$$M_{i,RBS} = Z_{RBS} F_y \quad (\text{Eqn. 2.1})$$

where, Z_{RBS} is the plastic sectional modulus of reduced beam section. The corresponding flexural moment at beam end M_{BE} is:

$$M_{BE} = M_{i,RBS} + \frac{2M_{i,RBS}}{L_c} L' \quad (\text{Eqn. 2.2})$$

where, L_c is the span between reduced beam sections at beam ends; L' is the distance measured from the reduced beam section to the adjacent column surface. This beam end moment M_{BE} can be regarded as the minimum nominal strength required for end plate and steel rods. To ensure an effective use of material, M_{BE} must be within 85% to 100% of the most probable plastic moment of the beam end section $M_{pr,BE}$. If M_{BE} turns out to be less than $0.85M_{pr,BE}$, or exceeds $M_{pr,BE}$, the reduced beam section must be redesigned until this requirement is satisfied. Because the nominal capacity at the reduced beam section must be developed to accommodate the system post-yield deformation, the over-

strength factor λ_o must be introduced when $M_{i,RBS}$ is used in the design of end-plate and steel rods.

End-plate

In this research program, the end plate is designed to have a thickness such that the prying force imposed on steel rods can be assumed being eliminated. The thickness of end plate was determined by the yield line theory using virtual work method. According to the design guidelines of steel moment resisting end plate (Murray and Summer, 2004), the nominal end-plate yielding strength M_{pl} can be estimated by,

$$M_{PL} = F_{py} t_p^2 Y \quad (\text{Eqn. 2.3})$$

where, F_{py} is the yield strength of plate material; t_p is the plate thickness; and Y is the parameter reflecting the controlling yielding mechanism shown in Figure 2.3. It is defined by,

$$Y = \frac{b_p}{2} \left[h_i \left(\frac{1}{p_{fi}} + \frac{1}{s} \right) + h_o \frac{1}{p_{fo}} - \frac{1}{2} \right] + \frac{2}{g} h_i (p_{fi} + s) \quad (\text{Eqn. 2.4})$$

Therefore, the plate thickness t_p can be determined by,

$$\lambda_o M_{BE} = \phi_{pl} F_{py} t_p^2 Y \quad (\text{Eqn. 2.5})$$

Observe that the end plate cannot yield provided that λ_o / ϕ_{pl} is appropriately chosen.

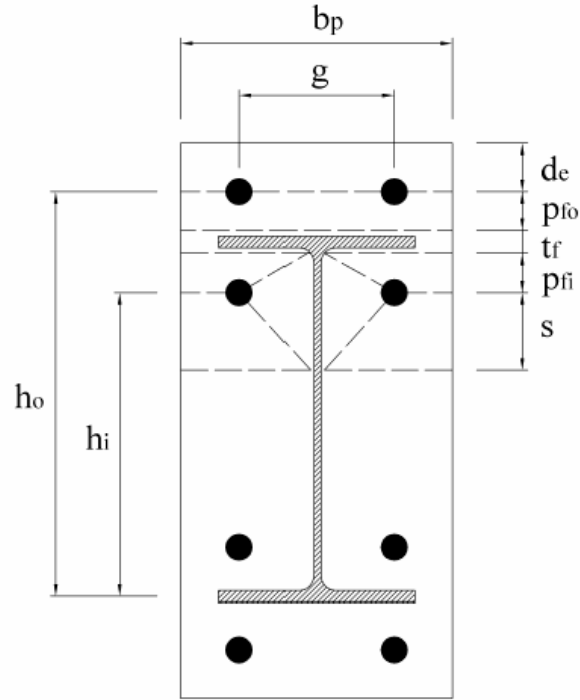


Figure 2.3: Yield line pattern of endplate

Steel Rods

Following the configuration shown in Figure 2.2, the nominal moment strength that the steel rods group can develop is given by

$$M_R = 2F_t \sum_{i=3}^4 d_i \quad (\text{Eqn. 2.6})$$

where, F_t is the tensile strength of steel rod; d_i is the distance between i -th row of rods and the end-plate edge about which it rotates. If no prying force is introduced, the following equation can be used to determine the required rod diameter D ,

$$\lambda_o M_{BE} = \phi_r \left[\frac{\pi D^2}{2} f_t \left(\sum_{i=3}^4 d_i \right) \right] \quad (\text{Eqn. 2.7})$$

where, D is the nominal diameter of the steel rod and f_t is the tensile capacity of each steel rod. The expected strain magnitude of steel rods can be obtained provided λ_o / ϕ_r is appropriately chosen.

Shear Transfer Mechanism

The shear transfer mechanism at the interface of the end plate and the PC column surface is considered to be provided by friction, and the dowel effects of the post tensioned bars are ignored. The minimum post-tensioning force P_{pre} applied to each steel rod should provide a total normal force satisfying:

$$\gamma_D V_D + \gamma_L V_L < \sum P_{pre} f \quad (\text{Eqn. 2.8})$$

where, f is the coefficient of friction; P_{pre} is the pretension force of each rod; V_D and V_L are the shear demand due to the dead and live loads, respectively; and γ_D and γ_L are the load combination factors for dead load and live load, respectively. In this study, γ_D and γ_L were taken as 1.4 and 1.7, respectively.

The shear force corresponding to the ultimate loading condition consists of the shear due to gravity loads and the shear force resulted from the plastic hinge mechanism, V_{nE} , which is given by,

$$V_{nE} = \frac{2\lambda_o M_{i,RBS}}{L_c} \quad (\text{Eqn. 2.9})$$

Therefore the ultimate shear capacity required for the connection is:

$$V_u = V_{nE} + 0.75(\gamma_D V_D + \gamma_L V_L) \quad (\text{Eqn. 2.10})$$

If a total decompression of column joint region is allowed, the friction-mobilizing normal force between end plate and column face is expected to be provided by reaction force at the edge portion of the end-plate induced by the flexural moment of beam end. According to the equilibrium condition of the end plate, this normal force can be estimated as the summation of the tension forces of all the steel rods. Thus the nominal capacity of the shear transfer mechanism corresponding to ultimate loading condition becomes:

$$V_n = 2\left(\sum_{i=1}^4 T_i\right)f \quad (\text{Eqn. 2.11})$$

where, T_i is the tensile force of each of the i -th row steel rod.

Shear Strength Check of PC Column Joint Region

The joint shear design procedure, aiming at protecting the joint concrete from any significant inelastic deformations, was based on the assumption that the post-tensioning steel has developed its over strength, $\lambda_o f_y$. For the post-tensioned connection, anchorage is not an issue since the steel rods are anchored on the opposite compression side of the column. According to Figure 2.2, the joint core horizontal shear forces for exterior and interior joints can be approximated by,

$$V_{jh} = \sum_{i=3}^4 T_i - V_{col} \quad (\text{Exterior joints}) \quad (\text{Eqn. 2.12-a})$$

$$V_{jh} = \sum_{i=1}^4 T_i - V_{col} \quad (\text{Interior joints}) \quad (\text{Eqn. 2.12-b})$$

The designation number for the rows of rods used in Eqn. 2.12 is shown in Figure 2.2.

The vertical shear force can be estimated by,

$$V_{jv} = \left(\frac{h_b}{h_c}\right)V_{jh} \quad (\text{Eqn. 2.13})$$

The total decompression of the column joint region relieves the joint from horizontal axial loading. Using the column axial force the joint normal stress in the vertical direction f_v can be estimated, and then, the joint principle compression and tensile stresses are,

$$p_c, p_t = \frac{f_h + f_v}{2} \pm \sqrt{\left(\frac{f_h - f_v}{2}\right)^2 + v_j^2} \quad (\text{Eqn. 2.14})$$

The principle stresses in the joint regions of the model subassemblies were shown to slightly exceed the cracking strength of concrete, $0.29 \sqrt{f'_c}$ MPa (or $3.5 \sqrt{f'_c}$ psi), indicating that the joints were at high possibility of cracking or minimum steel reinforcement would be sufficient to limit the growth of cracks.

2.3 Splice Design and Construction

One of the advantages of the hybrid PCS moment resisting frame system is its fast speed of construction and quality control due to the use of precast columns. Similar to the construction of steel structures, special attention must be paid to the precast column splices at levels called out. In addition, the overall performance of the hybrid system is influenced by the precast column to foundation connection details, which is a significant part of the construction procedure.

After precast concrete column has been manufactured in plant, it is shipped to the construction site and erected to form the structure. Due to the limitation of length of the transportation vehicles, the precast columns should be cut into segments so that they can be carried by the trucks. The splice connection between precast columns is usually located at place where the input load effect is small. For example, the splice point of adjoining columns is 4 feet above the floor of a 16-foot-high story every two floor levels. Figure 2.4 shows an example of the shipment and splice plan of an 8-story PCS frame. By choosing appropriate splice locations, the inelastic deformation is avoided to occur at the spliced sections. However, for the first story column, significant flexural moment demand shall be induced at the column-footing interface under earthquake loading condition.

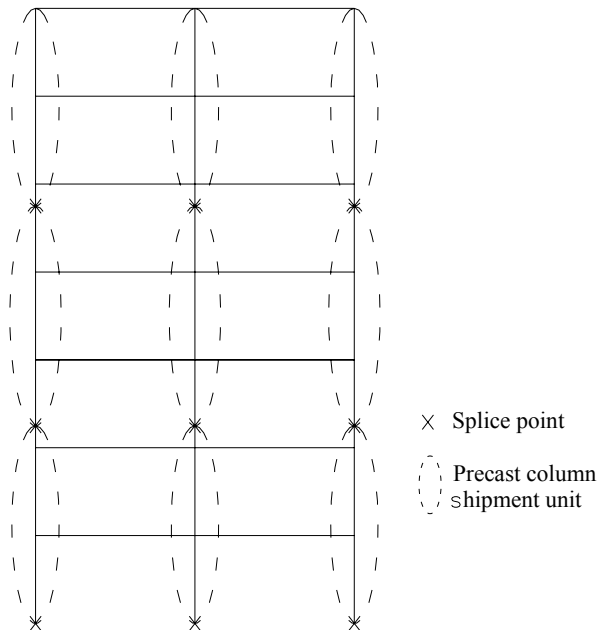


Figure 2.4: Shipment and splice plan of PCS frame

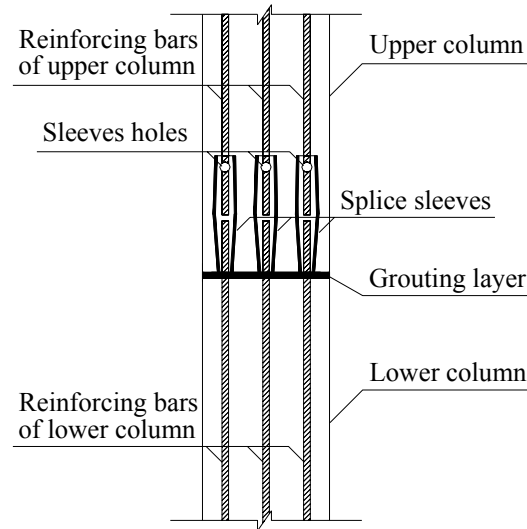


Figure 2.5: Splice of columns using embedded sleeves

According to the PCI Design Handbook of Precast and Prestressed Concrete (1999), the reinforcing bar couplers are most effective hardware to provide splice between precast columns in moment resisting frames. In a typical splice connection using reinforcing bar couplers, as shown in Figure 2.5, splice sleeve is embedded in bottom end of the column on upper side. The longitudinal reinforcing bars of the lower level column extend and insert into the embedded splice sleeves of the upper column. After the two columns are adjusted to fit each other, high strength grouting mortar is injected into the sleeves through holes.

For the time being there are not available provisions in terms of the seismic design of the connection between precast column and footing. This is mainly due to the fact that the precast seismic resisting system has not been widely accepted in the seismic regions of the United States especially in California. As a result, seismic design requirements

regarding the precast footing-footing connection have not been developed. Although a couple of precast column-footing details are suggested in the PCI Design Handbook of Precast and Prestressed Concrete, no design guidelines are presented. To adopt the PCI suggested connection details to column-footing connections in PCS special moment frames, a rational design method should be developed to check the adequacy of the connections. In this research project, a design methodology is developed and proposed in terms of two types of precast column-footing connections. According to the strength design philosophy, the design objectives of base connection can be identified as:

- (1) the base connection can develop the desired level of flexural moment transfer corresponding to levels of rotation that are compatible with story drift ratios when ultimate mechanism is developed;
- (2) the moment capacity degradation is not allowed at the base connection;
- (3) plastic behavior is preferred at the base connection.

2.3.1 Design of dowel Anchorage Base Connection

The dowel anchorage method is the way to connect precast concrete column to spread footing by inserting its reinforcing bars into the metallic conduits embedded in the footing and then filling grouting mortar into the conduits, as shown in Figure 2.6. In addition, a segment of the rebars at bottom of column is debonded from the concrete through the use of plastic tubes.

The dowel anchored precast column-footing can be designed to satisfy all design objectives if the following proposed steps are carried out:

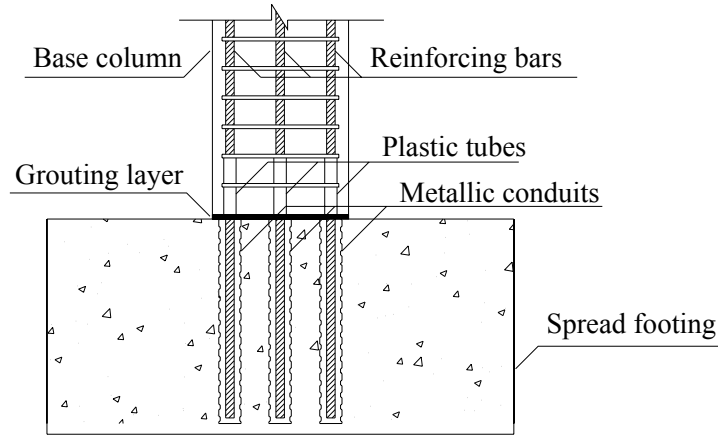


Figure 2.6: Dowel anchorage base connection

Desired levels of strengths of base connection

To ensure a ductile moment frame behavior, the plastic mechanism is considered to be developed at the ultimate condition. To determine the flexural moment demand at the column-footing connection, two sets of loading criterion must be considered. The first loading criteria is described by Eqn. 2.15, where M_1 is the moment capacity of column section based on the axial load-moment interaction relationship. P and P_n are the maximum axial force transferred to the first story column and the nominal axial load carrying capacity of column section. f_1 is the function governing the P-M relationship. Notice that the axial load P used to determine M_1 must be the maximum probable compressive axial load that may be imposed on the base column.

$$M_1 = f_1(P, P_n, M_p) \quad (\text{Eqn. 2.15})$$

The second load criteria is directly corresponding to the plastic moment capacity developed at the beam ends where plastic hinges form. Assuming the column stiffness are the same above and below the first floor, a moment demand on the column section M_2 can be calculated.

Then the flexural moment demand can be taken as the smaller one between M_1 and M_2 . The moment associated with the maximum compressive and tension axial load can be used as the capacity demand for the base column-footing connection.

Desired level of rotation capacity

The upper joint rotation associated with the plastic moments of beam ends can be estimated by

$$\theta_j = \frac{\lambda M_p L_C}{6EI} \left(\frac{L_C}{L_B} \right) \quad (\text{Eqn. 2.16})$$

where M_p is the most probable plastic moment strength at steel beam end. Note that an overstrength factor is applied to M_p . L_C and L_B represent the column and beam length respectively. The rotation of column-footing that accommodates the rotation demand is provided by the deformation of the unbonded length of column longitudinal rebars. To check the adequacy of the column-footing rotation capacity, the yield strain of the rebar is integrated along the debonded length to get the total elongation δL . Then this total elongation is divided by the neutral axis depth of column cross section. Another source of rotation of column-footing connection is the deformation of the segment of column rebars

embedded in the footing, or the so-called bond-slip, as shown in Figure 2.7. The bonding strength between rebars and footing concrete can be estimated by

$$\sigma_b = \frac{20\sqrt{f'_c}}{d_b} \leq 5.5ksi \quad (\text{Eqn. 2.17})$$

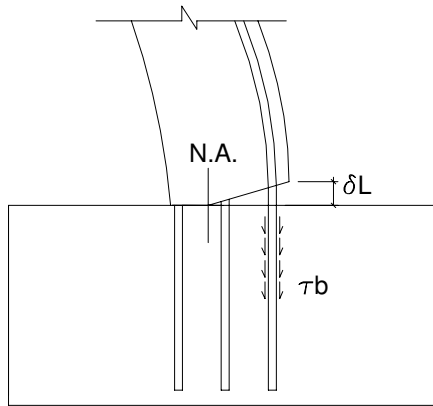


Figure 2.7: Bond slip of column rebars

The tensile stress f_s of the rebar can be found by equilibrium, or the summation of bonding stress τ_b along its distribution length. The strain of the rebar embedded in the footing then can be estimated by integration.

If the rotation of footing is also considered, the total column-footing rotation capacity can be expressed as

$$\theta_{bc} = \theta_{rb} + \theta_{bs} + \theta_f \geq \theta_j \quad (\text{Eqn. 2.18})$$

Where θ_{rb} , θ_{bs} and θ_f are the rotation contributed by the debonded rebar deformation, bond slip and footing rotation.

2.3.2 Design of Splice Sleeves Base Connection

The use of splice sleeves results in a strong connection between column bottom end and footing. The plastic deformation shall be developed outside the region where the sleeves are embedded, as shown in Figure 2.8. The critical section is on top end of the sleeves where regular concrete column section starts. The column segment where the sleeves are embedded can be considered infinitely rigid during design and analysis. This assumption is reasonable in that in addition to the size and number of steel sleeves used the grouting mortar is also high strength of up to 13 ksi minimum specified compressive strength.

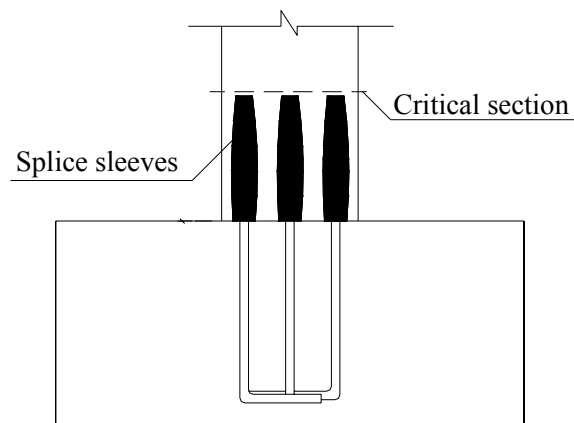


Figure 2.8: Design critical section of splice sleeve connection

Chapter 3: Experimental Program

3.1 Selection of Beam-column Connection Testing Method

Experimental study plays a significant role in the research of structural engineering. All design methods must be established and validated based on appropriate experimental study and results. Strictly speaking, it is not possible to recreate a structural model in the laboratory that reflects exactly all features of its prototype structure. However, it has been widely accepted that structural testing can be intentionally designed such that the testing of structural models can capture major features of concern of the prototype structures. In terms of seismic beam-column connections, the major features that attract the attention of researchers are:

- (1) the characteristics of load transfer between beam and column; and
- (2) the deformation of beam-column joint and its contribution to the overall lateral deflection of the structure.

Figure 3.1 to Figure 3.3 demonstrate the basis of a typical conventional beam-column moment connection experiment. Figure 3.1 shows the elevation of a moment frame under consideration before any load input and the location of beam-column subassembly to be simulated. Figure 3.2 depicts the deformed shape of the moment frame under earthquake load. The exterior beam-column subassembly is comprised of the column segment between the inflection points of the consecutive stories and the beam segment starting

from the joint and ending at the inflection point. The boundary condition of the beam-column subassembly is pin support, which is free of bending moment. Figure 3.3 shows the loading and expected deformed shape of the beam-column subassembly for the testing. This type of experiment plan is most common since the boundary conditions for all components are just simple support, which can be easily obtained in laboratory. As a result of the simple supports, the strength, stiffness and ductility of the beam-column test subassembly are mainly provided by the connection. However, this type of beam-column connection testing may have shortcoming in that the column top end is restrained from lateral displacement while the beam end moves up and down vertically during the testing. Thus the actual behavior of the frame can not be reflected. Therefore, when the overall frame behavior is the concern of research, the simple beam-column connection testing is not appropriate to study the frame behavior under earthquake loading.

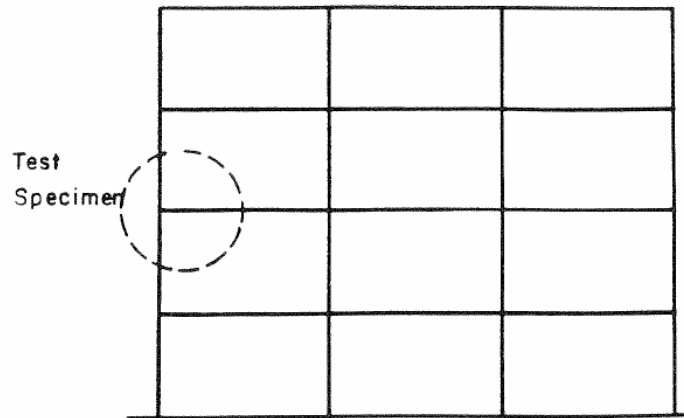


Figure 3.1: Typical beam-column connection test specimen

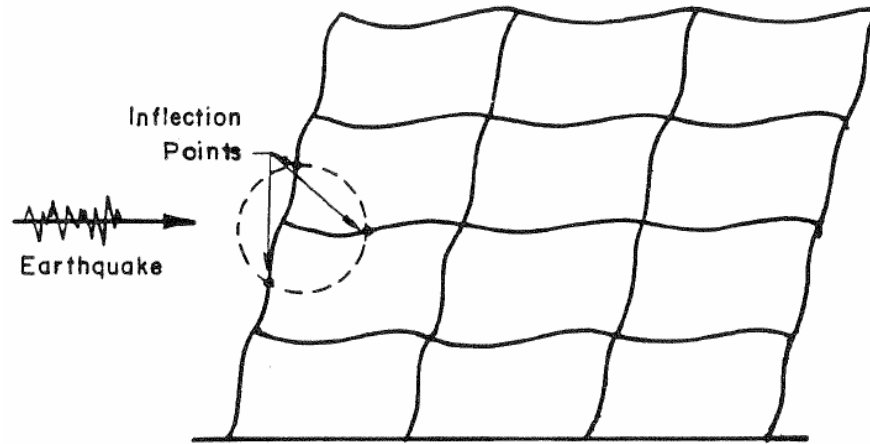


Figure 3.2: Deformed shape of test specimen

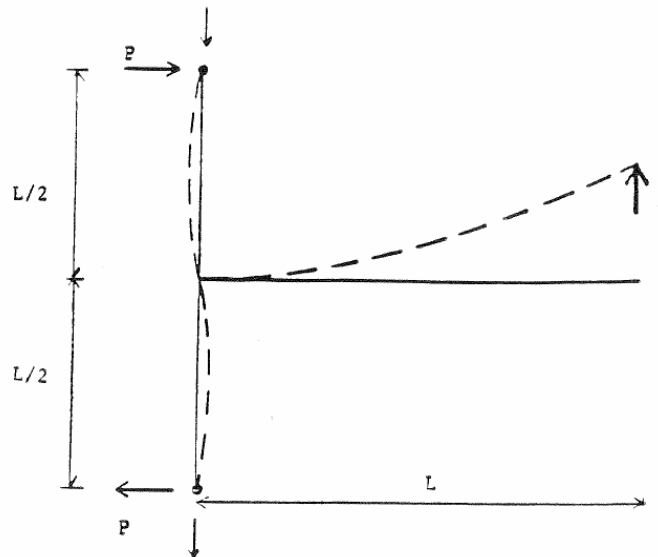


Figure 3.3: Experimental simulation of loading condition

The proposed PCS moment frame is unique in that its lateral ductility highly relies on the plastic hinge at the beam end. As for the beam-column joint region, there is not any steel-concrete bonding or anchorage issue involved since the post-tensioning rods are fully debonded from the joint concrete. To verify the proposed capacity-based design method,

it is necessary to examine the sequence of yielding of the frame components in addition to check the adequacy of strength, stiffness and ductility. Therefore, the conventional simple beam-column connection testing is not adequate to get the results for frame behavior. For the current research, a large scale beam-column-footing frame subassembly testing was developed in the structural laboratory of USC.

3.2 Objective of Experimental Program

For the special moment resisting frame located in high seismic regions, its beam-column connection plays a significant role in providing adequate lateral ductility. Current seismic provisions of building codes require a stringent detailing standard to be satisfied for the beam-column connection of special moment resisting frame. As a result, the emphasis of previous experimental research on innovative seismic resisting frame types was on the behavior of the beam-column connection. Previous experimental research on beam-column connections can be categorized into two main different fashions in terms of the way of testing and instrumentation. One way of conducting beam-column experiment is to load the beam cyclically and measure its rotational capacity. A second way of beam-column connection experiment is to construct a beam-column subassembly and cyclically load the column top laterally to examine the lateral load-lateral deflection hysteretic behavior.

For the current research, the experimental program is unique due to the uniqueness of the proposed PCS structure and the current stage of the research. Since the proposed PCS moment resisting frame combines the use of steel beam and precast column, its behavior is highly influenced by the beam-column continuity and the load transfer mechanism between steel beam and precast column. The continuity of the hybrid beam-column connection is ensured by the post-tensioning force provided by the high strength rods. The load transfer mechanism at the beam-column joint relies on the friction developed at the end-plate and column face. The system capacity hierarchy is dependent on the moment transfer mechanism. And all the above issues are covered in the design procedure. Therefore, the prime objective of the experimental program must be the verification of the design objectives.

3.3 Design of Test Models

The design of the beam-column-footing subassembly models consisted of three steps. Firstly, the sizes of the column and beam were selected so that the test models were approximately two thirds of full scales. Then the steel beams and precast reinforced concrete columns were designed respectively. The steel beam was designed and checked based on the 1997 AISC seismic provisions and FEMA350. The precast concrete columns were designed based on the ACI318-02. Finally, the connections were designed.

The prototype building of the test models was a twelve story reinforced concrete office building located in high seismic region. A typical lateral force resisting moment frame of the prototype building is shown in Figure 3.4(a). A typical test model was the exterior sub frame including the first story column and half of the second story column, half length of the beam and the foundation. Two connection details were simulated in the test models. One was the column-foundation connection, which was assumed fixed. The other was the beam-column connection.

In the prototype building, the story height was 12ft. for all stories. The center to center span length along the direction under consideration was 22ft. The exterior column had a 22in.×22in. rectangular cross section with about 2.5 percent longitudinal reinforcement ratio. The beam section was 20in. wide and 24in. deep. Based on these full scale dimensions, the test models were sized as shown in Figure 3.4(b). The precast reinforced concrete column was about 10ft. high and had a constant 14in.×14in. cross section. The steel beam length was 7ft. and W12×26 shape was selected.

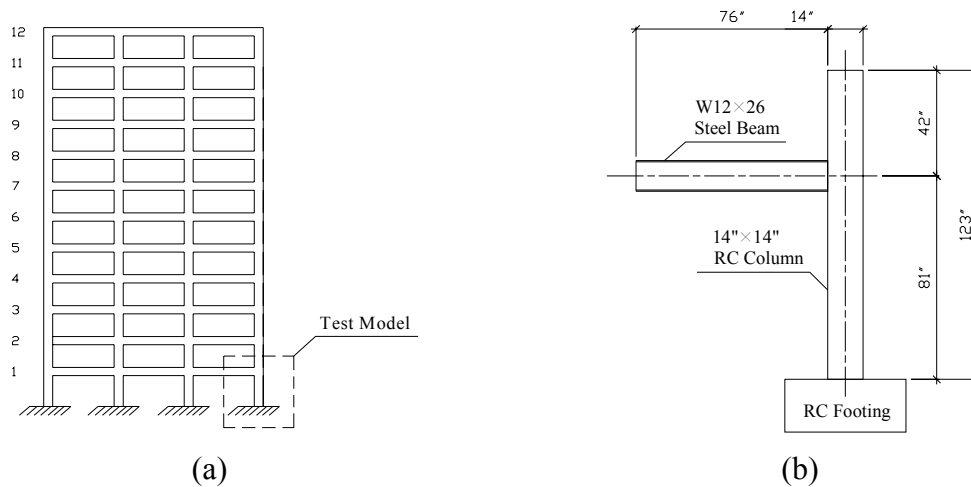


Figure 3.4: Special moment resisting frame elevation and test Model

3.3.1 Steel Beam Design

W12×26 of ASTM A992 steel material was used for the steel beam. Since the test models simulated the special moment resisting frame in region of high seismicity, the steel beams were designed and checked based on the seismic provisions for structural steel buildings published by AISC in 1997.

The first requirement was that the beam section should be seismic compact section so that the beam could withstand some plastic rotation before the onset of local buckling. The seismic compact section was ensured by limiting the width thickness ratios for both flanges and web. If the width thickness ratios for both flanges and web were less than or equal to the limiting values, which could be calculated according to the formulas given in Table I-9-1 in the 1997 AISC seismic provisions, the section was seismic compact. Table 3.1 lists the results of the comparison.

Table 3.1: Seismic compact section check for A992 W12×26

| λ | Limiting Ratios (λ_p) | Limiting Values (λ_p) | W12×26 | $\lambda < \lambda_p?$ |
|-------------------|---------------------------------|---------------------------------|--------|------------------------|
| $\frac{b_f}{t_f}$ | $\frac{52}{\sqrt{F_y}}$ | 7.35 | 8.5 | N.G. |
| $\frac{h_w}{t_w}$ | $\frac{520}{\sqrt{F_y}}$ * | 73.54 | 47.2 | O.K. |

* This formula results from the zero axial load of the steel beam.

According to Table 3.1, the beam web section was seismic compact while the flange sections were not. Thus the W12×26 section was not seismic compact as a whole. The most straightforward way of solving the section compactness problem was to reduce the

width thickness ratio of the beam flange directly. In the current study, the reduced beam sections method was used.

The determination of how much the beam flange was reduced followed the recommended procedure given in FEMA350. Basically, three dimension parameters were designated to define reduced beam sections, as shown in Figure 3.5. The three dimension parameters were: 1) the distance between column face and the initial cut section, a ; 2) the length of the beam flange segment to be cut, b and 3) the distance between the original flange edge and the most reduced section edge, c . With these three parameters known, a simple cutting procedure was conducted to make the reduced beam sections.

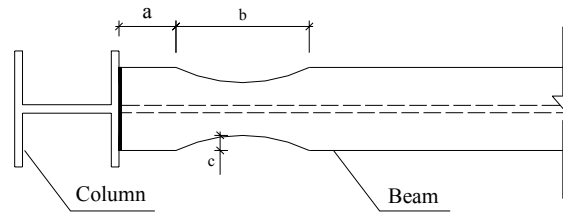


Figure 3.5: Reduced beam section parameters

The FEMA350 recommended reduced beam sections design procedure was established based on estimations of the three parameters in terms of the known beam dimensions. For example, the parameter a could be estimated to be 50 percent to 75 percent of the beam flange width. The empirical estimations should be checked later to see if certain design criterion be satisfied. For the current study, the estimated values for a , b and c were 4in., 8in. and 1.3in., respectively. The resulting flange width to thickness ratio turned out to be 5.12, which was less than the limiting ratio 7.35. Thus the beam flanges were seismic

compact after the reduced beam sections had been made. And the whole beam section became seismic compact.

The reduced beam sections shifted the location of the plastic hinge from the beam end to the most reduced beam section. The probable plastic moment capacity M_{pr} was then calculated based on the most reduced section. Equation 4.1 was used to calculate the effective plastic modulus Z_{RBS} at the most reduced section.

$$\begin{aligned} Z_{RBS} &= Z_b - 2ct_f(d - t_f) && \text{(Eqn. 3.1)} \\ &= 37.2 - 2 \times 1.3 \times 0.38 \times (12.22 - 0.38) \\ &= 25.5 \text{ in.}^3 \end{aligned}$$

where Z_b was the plastic modulus of the unreduced beam section. d was the total depth of the beam section and t_f was the flange thickness. Then the probable plastic moment M_{pr} was determined by

$$\begin{aligned} M_{pr} &= C_{pr} R_y Z_{RBS} F_y && \text{(Eqn. 3.2)} \\ &= 1.15 \times 1.1 \times 25.5 \times 50 \\ &= 1612.9 \text{ in.-kips.} \end{aligned}$$

Where C_{pr} was a factor to account for the strain hardening of the steel material in the current case and taken as 1.15. R_y was the ratio of the expected material yield strength to the specified minimum yield strength. The coefficient R_y was only used for the determination of the required strength of a connection or related member. For Grade 50 steel, R_y was taken as 1.1. To check the acceptability of the reduced beam sections, M_f , which was the bending moment at the beam end when the peak probable plastic moment M_{pr} at the most reduced beam section was developed should be calculated and compared with the probable plastic moment capacity of the beam end section. To determine M_f , the

shear force V_{RBS} , which was the shear force at the section where the plastic moment M_{pr} was developed, was calculated first. Figure 3.6 shows the bending moment and shear force developed at the plastic hinge at ultimate stage of lateral loading. When the beam self weight was ignored, V_{RBS} was calculated as

$$V_{RBS} = \frac{2M_{pr}}{L'} = \frac{2M_{pr}}{(L - 2a - b)} \quad (\text{Eqn. 3.3})$$

$$= \frac{2 \times 1613}{(76 \times 2 - 2 \times 4 - 8)} = \frac{3226}{136} = 23.8 \text{ kips}$$

where L' and L were the distance between plastic hinges and the overall beam length.

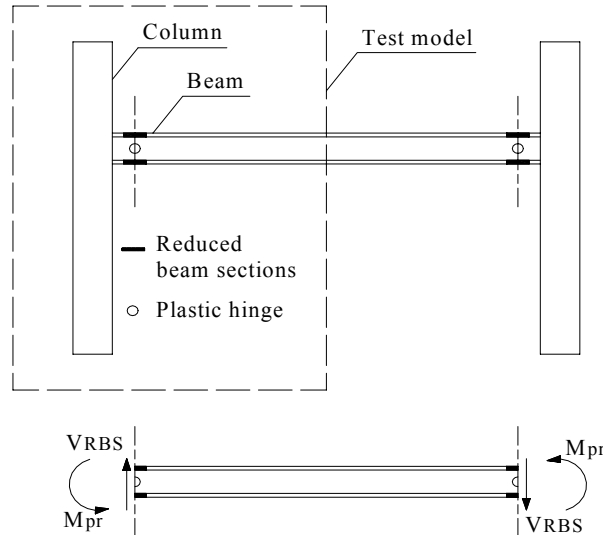


Figure 3.6: Forces developed at plastic hinges

Then the maximum moment expected at the beam end was

$$M_f = M_{RBS} + V_{RBS} \left(a + \frac{b}{2} \right) \quad (\text{Eqn. 3.4})$$

$$= 1613 + 23.8 \times \left(4 + \frac{8}{2} \right) = 1804 \text{ in.} - \text{kips}$$

The probable peak plastic moment at the beam end section was obtained by

$$\begin{aligned} M_{pe} &= R_y Z_b F_y && \text{(Eqn. 3.5)} \\ &= 1.1 \times 37.2 \times 50 = 2046 \text{in.} - \text{kips} \end{aligned}$$

The ratio of M_f to M_{pe} was about 0.88, which was acceptable since the 1997 AISC Seismic Provisions requires this ratio be somewhere between 0.85 and 1.0. Therefore, the reduced beam sections design was acceptable.

3.3.2 Precast Concrete Column Design

The specified concrete compressive strength f_c' was 5 ksi. 8 No.7 Grade 60 deformed rebars were used for the column longitudinal reinforcement, resulting in the steel reinforcement ratio of 2.45%. This reinforcement ratio was almost the same as that of columns in the prototype building. For columns in special moment frames, they are not allowed to yield prior to the beam at the beam-column joint. ACI318-02 requires that columns be designed with 20% higher flexural strength as compared to the beams meeting at the same joint. For steel special moment frames, however, flexural strengths of columns cannot be less than that of the beams meeting at the same joint according to the 1997 AISC seismic provisions. For the steel beam and reinforced concrete column composite special moment frame, a 10% increase in flexural strength of columns as compared to beams at the joint, was recommended by Xiao et al.

The flexural moment capacity of the reinforced column section was investigated with the program PCACOL3.0 without the consideration of the transverse reinforcement confinement. The axial load P vs. the bending Moment M interaction curve was shown in

Figure 3.7. From the P - M curve, the flexural moment capacity of the column section corresponding to an axial load of 98kips. was 119 ft-kips, or 1428 in.-kips. For the exterior beam-column joint, the total beam flexural strength at joint with reduced beam sections is M_f and the total column flexural strength at joint is $2M_c$. The ratio was

$$\frac{\sum M_c}{\sum M_b} = \frac{2M_c}{M_f} = \frac{2 \times 1428}{1804} = 1.58 > 1.1 \quad \text{O.K}$$

Concerns may be with the interior beam to column joints, where two beams meet at the joint. To satisfy the strong column and weak beam requirement for interior joints, larger column cross section or more reinforcement must be provided for interior columns as compared to the exterior columns.

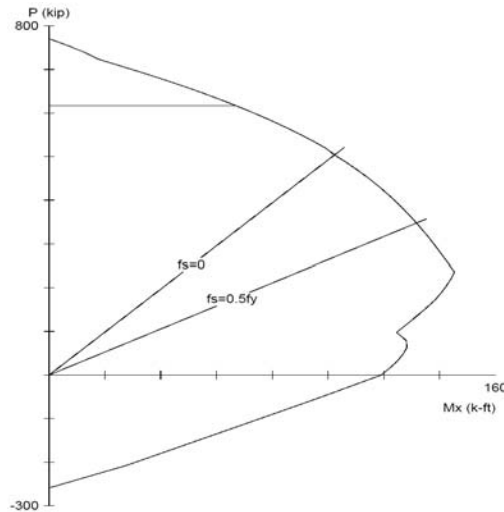


Figure 3.7: P-M Interaction curve of reinforced column section

Special transverse reinforcement for confinement was provided over a distance l_0 at column ends, where l_0 equaled the maximum values of: 1) depth of column section, 14in.; 2) one sixth of clear column height, 12.5in. and 3) 18in. The last case governed. The

maximum allowable spacing of rectangular hoops within the 18in. length shall not exceed: $0.25 \times 14 = 3.5$ in. or 4in. Conservatively, use 3in. The minimum required cross-sectional area of hoop reinforcement A_{sh} was the larger value from the following two equations:

$$A_{sh} = \frac{0.3sh_c f_c'}{f_{yh}} \left[\left(\frac{A_g}{A_{ch}} \right) - 1 \right] \quad (\text{Eqn. 3.6})$$

$$A_{sh} = \frac{0.09sh_c f}{f_{yh}} \quad (\text{Eqn. 3.7})$$

where s was the hoop spacing; h_c was cross-sectional dimension of column core measured center-to-center of confinement reinforcement, in.; A_g was gross column section area, in.²; A_{ch} was cross-sectional area of a structural member measured out-to-out of transverse reinforcement, in.² and f_{yh} was the specified yield strength of transverse reinforcement, ksi.

Using a hoop spacing of 3 in., $f_{yh} = 60$ ksi., a clear cover of 1in., and No.3 hoops, the required cross-sectional area of hoop reinforcement for the column was:

$$A_{sh} = \frac{0.3 \times 3 \times 11.625 \times 5}{60} \left[\left(\frac{196}{144} \right) - 1 \right] = 0.32 \text{in}^2 \quad (\text{Governs})$$

$$A_{sh} = \frac{0.09 \times 3 \times 11.625 \times 5}{60} = 0.26 \text{in}^2$$

Using No.3 hoops with No.3 cross ties provides $3 \times 0.11 = 0.33 \text{in}^2 > 0.32 \text{in}^2$.

The design shear force V_u was the shear force in the column when the probable flexural strength M_{pr} was developed at both column ends. To calculate M_{pr} , the tensile stress in the tensile reinforcement was taken as $1.25f_y$ to account for the strain hardening of steel material. M_{pr} turned out to be 146ft.-kips., or 1752in.-kips. Then the design shear V_u could be calculated as

$$V_u = \frac{M_{prt} + M_{prb}}{l_c} = \frac{2M_{pr}}{l_c} = \frac{2 \times 1752}{(81 - 6.1)} = 46.8 \text{ kips}$$

where M_{prt} and M_{prb} were the probable flexural strengths at top and bottom of column, in.-kips; and l_c was the clear height of the column, in. This resulting design shear force was very conservative since ACI318-02 points out that the column shear forces need not exceed those determined from joint strengths based on the probable moment strength of the beams framing into the joint. Thus the probable moment at column top section M_t could be estimated based on the maximum expected moment M_f . The distribution of beam end moment to column was in proportion of $4EI/L$ of columns above and below the joint. Since the columns were continuous, $4EI$ was constant. Moments were distributed based on $1/L$ of columns. The lower column had a height of 81in. and the upper one had a height of 42in. The lower column had a moment determined as followed at its top,

$$M_t = \left(\frac{1/81}{1/81 + 1/42} \right) \times 1804 = 616 \text{ in.-kips.}$$

$$V_u = \frac{M_t + M_{prb}}{l_c} = \frac{616 + 1752}{(81 - 6.1)} = 31.62 \text{ kips}$$

The nominal shear resistance provided by the column concrete was calculated by

$$\begin{aligned} V_c &= 2\sqrt{f_c'}b_wd && \text{(Eqn. 3.8)} \\ &= 2 \times \sqrt{5000} \times 14 \times 12.19 = 24.1kips \end{aligned}$$

Considering a strength reduction factor of $\phi = 0.85$, the ultimate shear force was:

$$\frac{V_u}{\phi} = \frac{31.6}{0.85} = 37.2kips$$

Thus the following differential shear strength should be provided by shear reinforcement.

$$V_s = \frac{V_u}{\phi} - V_c = 37.2 - 24.1 = 13.1kips$$

The required minimum shear reinforcement was determined by

$$\begin{aligned} \frac{A_v}{s} &= \frac{V_s}{f_y d} && \text{(Eqn. 3.9)} \\ &= \frac{13.1}{60 \times 12.19} = 0.0179in.^2 / in. \end{aligned}$$

If two-leg No.3 hoops plus single leg cross ties were used, the spacing would be $s = 12.29in.$ According to ACI318-02 seismic provisions, the transverse reinforcement spacing could not exceed 1) one-quarter of the minimum member dimension, which was 3.5in.; 2) six times the diameter of longitudinal reinforcement, 5.25in.; 3) $s_x = 4in.$ Thus the spacing of the transverse hoops was 3.5in.

Since the columns were designed without the consideration of axial load, shear resistance was required to check for the confined column end regions assuming $V_c = 0$. According to previous calculations, in column end regions where transverse reinforcements were provided,

$$\frac{A_v}{s} = \frac{0.33}{3} = 0.11 \text{ in.}^2 / \text{in.}$$

Then according to Eqn. 2.9, the shear resistance provided was,

$$V_s = \frac{A_v f_y d}{s} = 0.11 \times 60 \times 12.19 = 80.45 \text{ kips} > \frac{V_u}{\phi} = 37.2 \text{ kips}$$

The shear resistance was adequate.

3.3.3 Precast Reinforced Concrete Footing Design

The precast RC footings were designed to simulate the foundation of the prototype building. The precast RC columns were connected to the footing with certain details to simulate the fixed end conditions.

The two test models had different column-footing connection details, as shown in Figure 3.8, which resulted in different designs for the footings. For test model 1, the column and footing were connected through the NMB splice sleeve system. For test model 2, the column was connected to the footing through the dowel anchorage of the longitudinal bars in column. Both connection details simulated the fixed support conditions so that plastic regions could be developed at the column bottom ends.

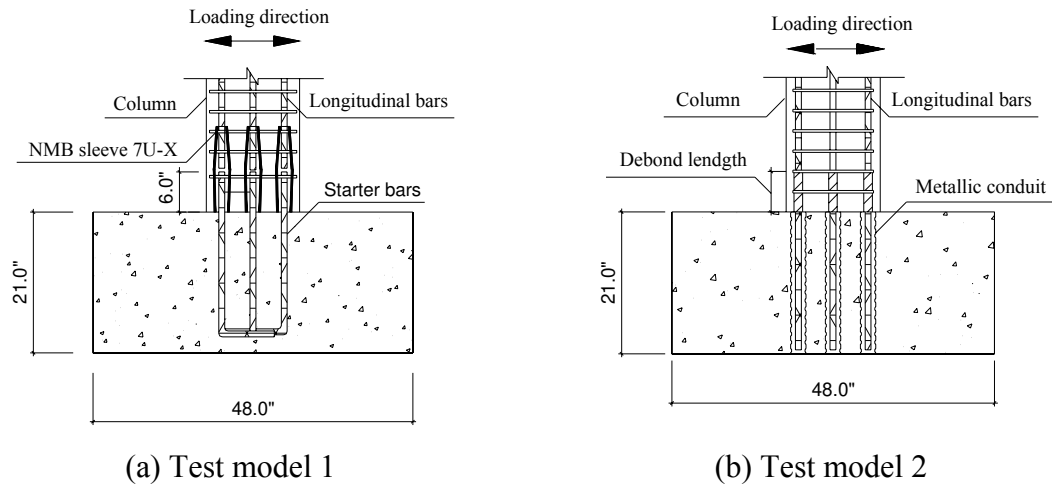


Figure 3.8: Column to footing connection details

The NMB splice sleeve system was provided by the Splice Sleeve North America, Inc. Generally the splice sleeve system was used for splicing reinforcing rebars in structural members. When using this system for column-footing connections, dowel rebars protruding from the footing should be provided first. 8 No.7 deformed rebars were used for the dowel rebars. The type of the splice sleeve was determined according to the size of the longitudinal rebars in column. For No. 7 rebars, 7U-X type sleeve was selected. The major dimensions of the 7U-X sleeve were shown in Figure 3.9. The column longitudinal rebars were inserted into the sleeve from the narrow end with an average recommended embedment length of 5.81in. The footing dowel rebars were inserted into the sleeve from the wide end of the sleeve with an average recommended embedment length of 6.11in. The grouting material for the splice sleeve system was the SS Mortar, which was a premixed formulation developed for specific use with NMB Splice Sleeve system. The minimum compressive strength of SS mortar was approximately 13ksi.

The longitudinal rebars in column of test model 2 extended beyond the column bottom surface with a length of 20in. The extending longitudinal rebars functioned as the dowel rebars for the column-footing connection of test model 2. Metallic conduits were used in the footing to form the ducts for the embedment of the dowel rebars. High strength cement was filled into the conduit to bond the dowel rebars and the footing. A 6in. long debonding region for the longitudinal rebars at column bottom end was provided so that yielding would develop at the column bottom first, where the plastic hinge would form, instead of the doweling length in the footing.

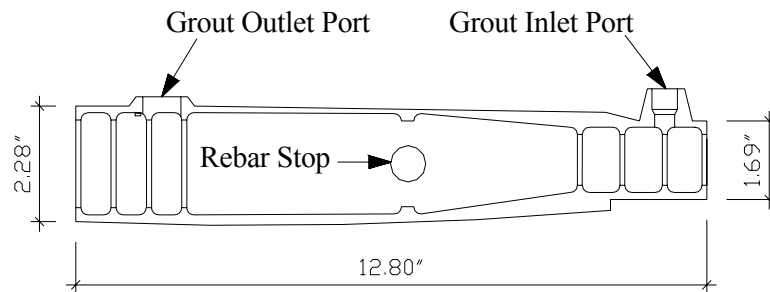


Figure 3.9: 7U-X sleeve details

The reinforcement details for the footings of test model 1 and 2 were shown in Figure 3.10 and Figure 3.11. And the final reinforcement details for columns were shown in Figure 3.12 and 3.13.

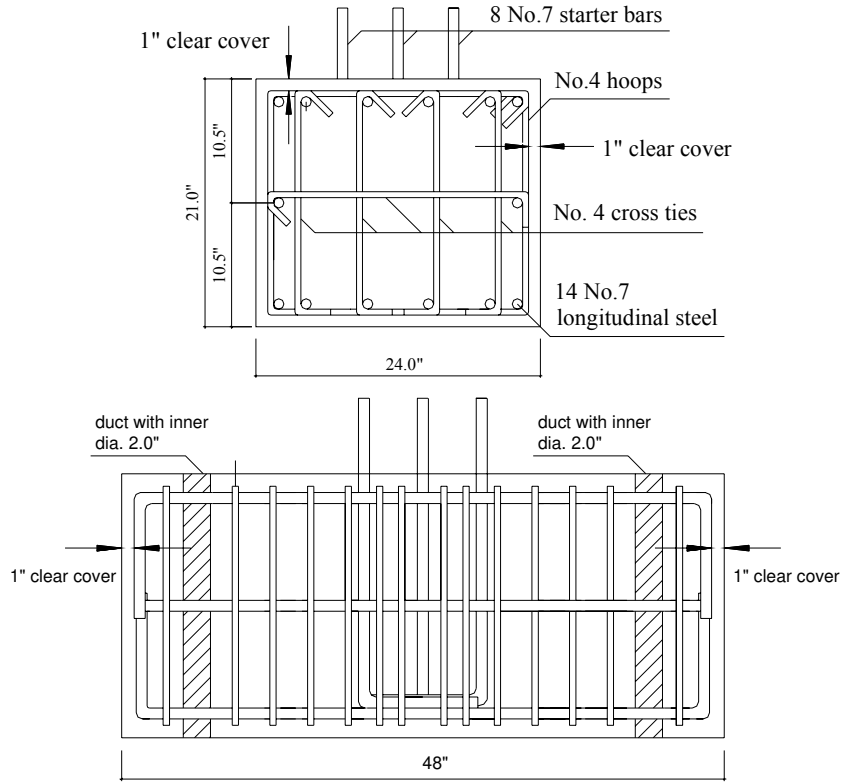


Figure 3.10: Reinforcement details of footing of test model 1

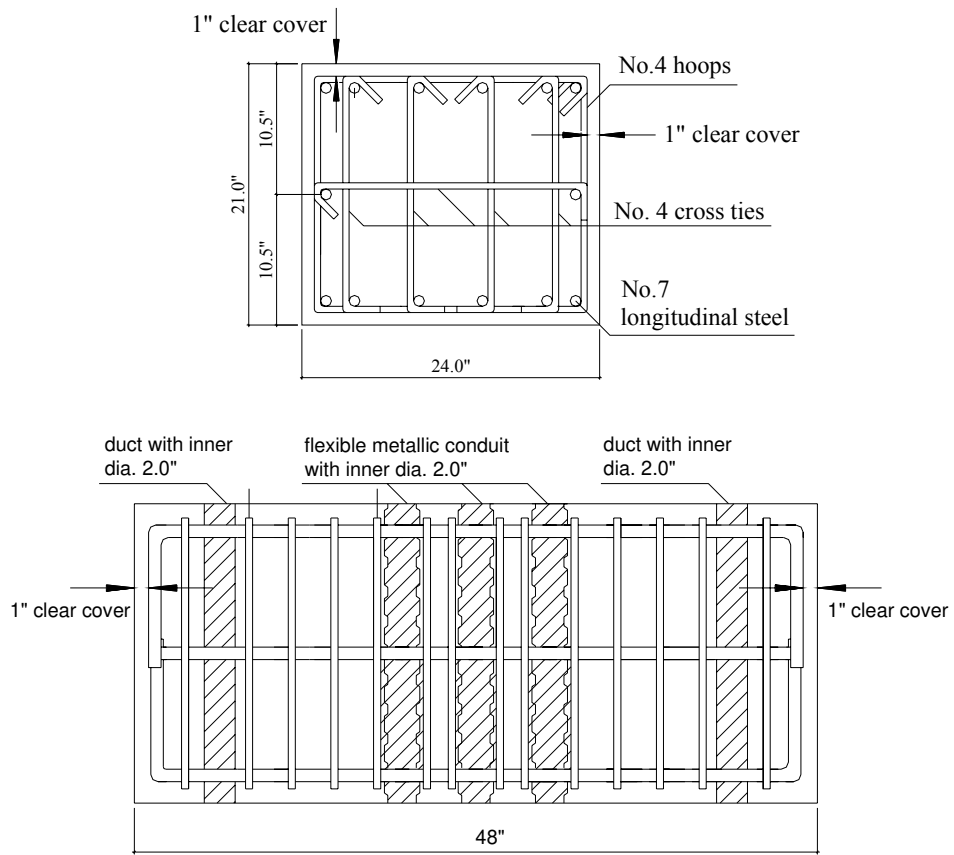
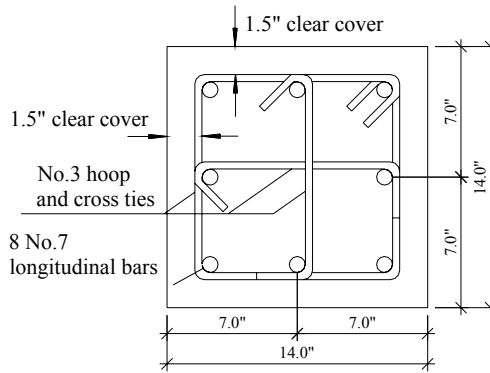
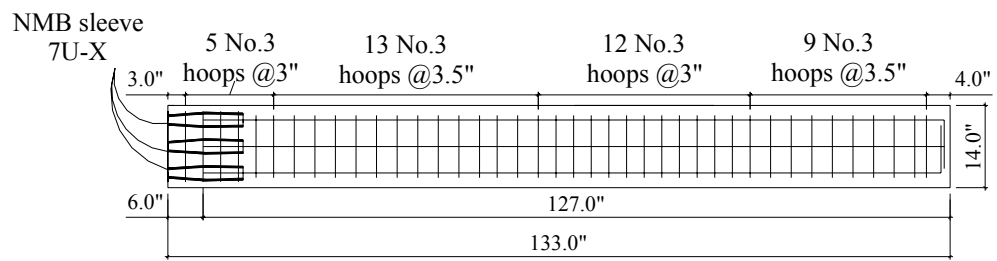


Figure 3.11: Reinforcement details of footing of test model 2

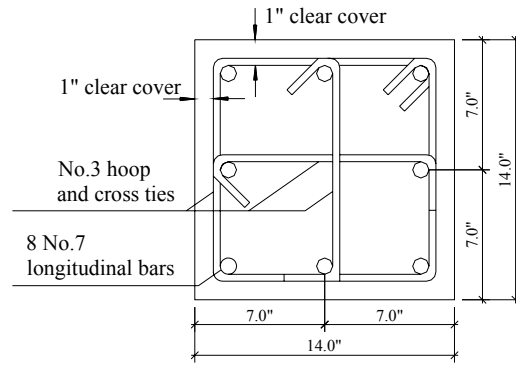


a) Cross Section details

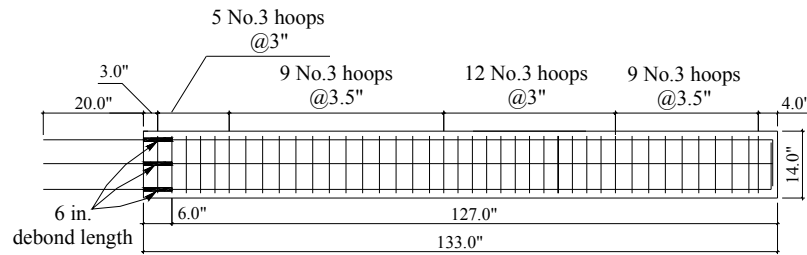


b) Overall details

Figure 3.12: Details of column in test model 1



a) Cross section details



b) Overall details

Figure 3.13: Details of column in test model 2

3.3.4 Design of Bolted Endplate Beam-Column Connection

For special moment resisting frames, the beam-column connections were of special significance since the overall integrity of the structure was dependent on the behavior of the beam to column connections. Degradation of the connection could result in large lateral deformations which could cause excessive damage or even failure. In the proposed bolted endplate connection details, the steel beam was connected to the column through post-tensioned high strength steel rods. To design the proposed connections, the flexural moments at the beam ends were resolved into a force couple consisting of a tensile force and a compressive force applied at the flanges. The tensile force was transferred to the steel rods on the tension side through the endplate and the compressive force was resisted

by the joint concrete in the compression region. At the ultimate stage, the endplate would have a relative rotation to the column surface, resulting that the endplate was in contact with the column surface at the top. The loading conditions of the connection at the ultimate stage are illustrated in Figure 3.14.

Selection of High Strength Treaded Rod

In the proposed beam-column connection details, the high strength steel rods played a significant role since they resisted the force couple transferred from the steel beam. As shown in Figure 3.14(b), the force couple used to select the high strength steel rod was based on the beam end moment M_f when the plastic hinge formed at the most reduced beam section.

$$C_f = T_f = \frac{M_f}{d - t_f} \quad (\text{Eqn. 2.10})$$

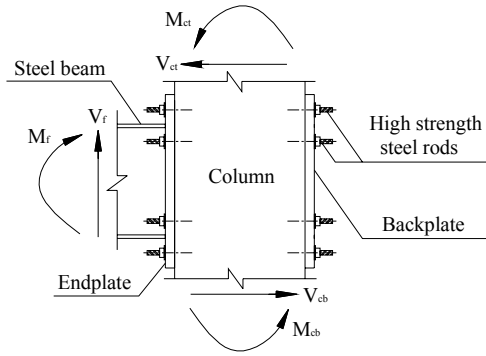
$$= \frac{1804}{12.2 - 0.38} = 152.6 \text{ kips}$$

Therefore each steel rod on the tension side resisted one fourth of T_f on conditions that all four rods yielded at the ultimate stage. The required resisting tensile force developed in each rod was

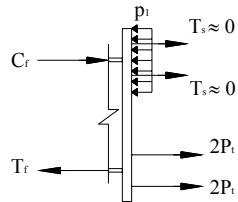
$$P_t = \frac{T_f}{4} = \frac{152.6}{4} = 38.2 \text{ kips}$$

Considering the strength reduction factor $\phi = 0.9$, the required strength for each rod was,

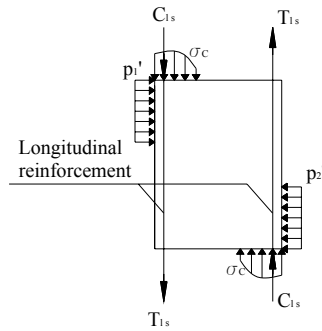
$$\frac{P_t}{\phi} = \frac{38.2}{0.9} = 42.4 \text{ kips}$$



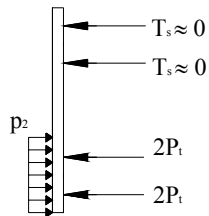
a) Beam-column joint



b) Endplate



c) Joint concrete



d) Back plate

M_f = Flexural moment at beam end at ultimate stage;

V_f = Shear force applied at beam end at ultimate stage;

M_{ct} , M_{cb} = Flexural moments at top and bottom joint column sections at ultimate stage;

V_{ct} , V_{cb} = Shear forces at top and bottom joint column sections at ultimate stage.

C_f , T_f = Equivalent compression and tension forces at beam flanges;

T_s , T_y = Tension forces in steel rods on compression region and tension sides;

N_c = Reaction force on contacting edge of endplate and column surface.

C_{ls} , T_{ls} = Compression and tensile forces in column longitudinal rebars;

σ_c = Concrete compressive stress at column section;

p_1' , p_2' = Pressure applied on the column surface by endplate and back plate.

T_s = forces in steel rods on compression side;

T_t = tensile forces in steel rods on tension side.

Figure 3.14: Models of beam-column connection for calculation

If ASTM A193 steel was used, the minimum tensile strength was 125ksi. The minimum effective tensile area could thus be calculated by

$$A_e = \frac{P_t}{\phi F_y} \quad (\text{Eqn. 3.11})$$

$$= \frac{42.4}{125} = 0.339 \text{ in}^2$$

Then the steel rod with $\frac{3}{4}$ inches nominal diameter could be used, effective tensile area of which was 0.334 in^2 . Based on this selection, the nominal bending moment capacity of the connection is

$$M_{np} = 2A_e F_t (h_0 + h_1) \quad (\text{Eqn. 3.12})$$

$$= 2 \times 0.334 \times 125 \times (10.1325 + 13.5075)$$

$$= 1973.94 \text{ in} - \text{kips}$$

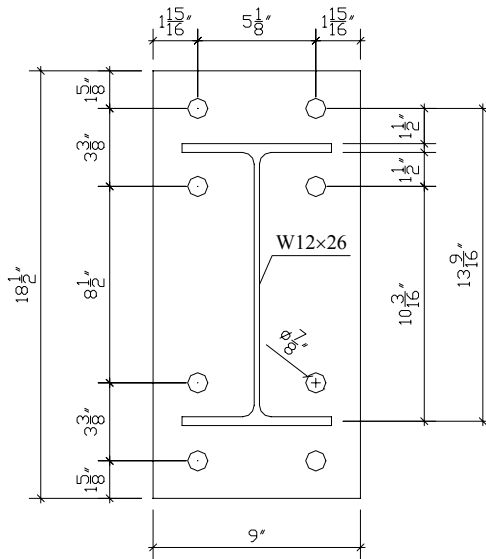


Figure 3.15: Endplate details

Design of Endplate

The design of the endplate, which was based on the yield line analysis, included the determination of endplate dimensions, especially the thickness, and the holes pattern. Previous researches on endplate connections in steel structures showed that if the endplate was not thick enough the bolts would suffer extra force caused by the so-called “prying action”. Excessive deformation of endplate was also observed along with the prying action. Thus the thick endplate was preferred so as to avoid prying action. A trial endplate holes pattern was shown in Figure 3.15.

The endplate yield line mechanism parameters were calculated as

$$s = \frac{1}{2} \sqrt{b_p g} \quad (\text{Eqn. 3.13})$$
$$= \frac{1}{2} \sqrt{9 \times 5.125} = 3.396 \text{in.}$$

$$Y_p = \frac{b_p}{2} h_1 \frac{1}{p_{fi}} + \frac{1}{s} + h_0 \frac{1}{p_{fo}} - \frac{1}{2} + \frac{2}{g} h_1 (p_{fi} + s) \quad (\text{Eqn. 3.14})$$
$$= \frac{9}{2} \times 10.1325 \times \frac{1}{1.4975} + \frac{1}{3.40} + 13.5075 \times \frac{1}{1.4975} - \frac{1}{2}$$
$$+ \frac{2}{5.125} \times 10.1325 \times (1.4975 + 3.40)$$
$$= 58.63$$

Where b_p was the width of the endplate; g was the gage distance between holes; h_0 was the distance between the centerline of inner rows of rods on tension side and the centerline of the flange in compression; h_1 was the distance between the centerline of outer row of rods on tension side and the centerline of the flange in compression; p_{fi} was the distance between the centerline of inner row of rods on compression side and the

inner edge of the flange in compression; and p_{fo} was the distance between the centerline of outer row of rods on compression side and the outer edge of the flange in compression.

Then the required endplate thickness was

$$t_{p,required} = \sqrt{\frac{1.11M_{np}}{F_{yp} Y_p}} = \sqrt{\frac{1.11 \times 1973.94}{50 \times 58.63}} = 0.87 \text{ inches}$$

Conservatively 1 in. thick endplate was used.

3.4 Construction of Test Models

The test models were built up with the following constructions and steps:

- 1) Construction of two reinforced concrete columns and two reinforced concrete footings;
- 2) Fabrication of two steel beams with welded endplates and back plates;
- 3) Connection between columns and footings;
- 4) Connection between columns and beams.

The first two steps were carried out by professional workers in factories. The last two steps were conducted by the researchers in the lab of structural engineering of USC.

3.4.1 Construction of RC Columns and Footings

The precast reinforced concrete columns were constructed at a local factory of the Pomeroy Corporation in Pomeroy. Steel pipes with 1 ½ inches inner diameter were used to make the ducts in columns. The ducts diameter was larger than that of the holes on endplates to allow for the ± ½ inch tolerances in concrete construction. The steel pipes were fixed to the steel cages by thin metal wires. For test model 1, the ends of the

longitudinal rebars were doweled into the NMB sleeves with prescribed length. Efforts were made so that the embedded rebars were not in touch with the inner surface of the sleeves. By doing so the embedded rebars would be fully covered by mortar and thus ensured the bonding. For test model 2, the longitudinal rebars extended beyond the column. Figure 3.16 shows the NMB sleeves of test model 1 and the dowel length of rebars of test model 2.



Figure 3.16: NMB splice sleeves and dowel rebars

Dowel bars with prescribed length were embedded in the footing of test model 1. these dowel bars were No.7 Grade 60 deformed rebars. When assembling test model 1, dowel bars embedded in the footing would be inserted into the NMB sleeves. Mortar was then filled into the sleeves through the inlets of the sleeves. If the sleeves were full of mortar, the extra would flow out from the outlet of the sleeves. For the footing of test model 2, ducts were made for the dowel rebars of the column with 1 ½ in. inner diameter metal conduit pipes. High strength mortar was used to bond the dowel rebars to the footing. For both footings, four pipes were put around the corners to make ducts for the sake of connection to the ground. Details of footings were shown in Figure 3.17.

The specified compressive strength of the concrete used for columns and footings construction was 5ksi. Manufactured in a local construction site in Pomeroy, all two columns and two footings were made of concrete from the same batch. Compression tests of three cylinders yielded 6.65ksi, 6.95ksi and 6.80ksi. The No.7 longitudinal reinforcement and No. 3 transverse reinforcement had specified yield strength of 60ksi.



Figure 3.17: Steel cages of footings

3.4.2 Fabrication of Steel Beams and Steel plates

The holes in the endplates had a diameter of 7/8in. The steel endplates were welded to steel beams by complete joint penetration welds. The steel endplates and the steel beams were perpendicular to each other after the welding.

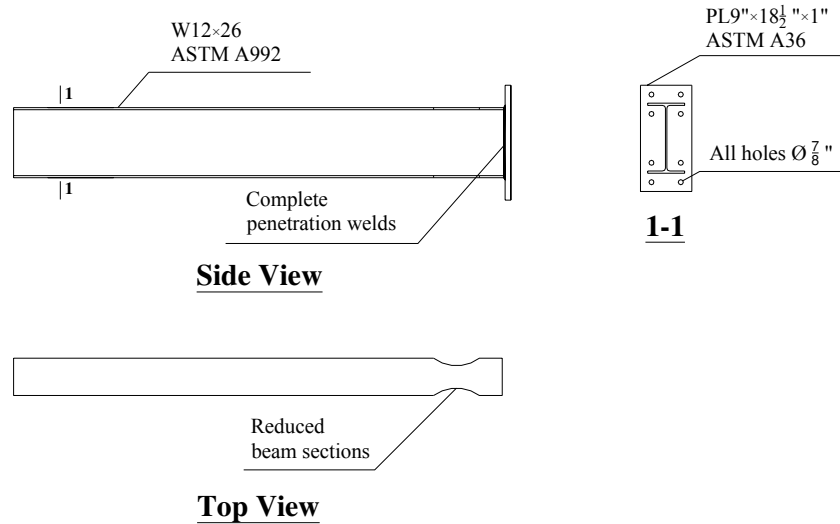


Figure 3.18: Steel beam details

3.4.3 Connection between Columns and Footings

After the columns and the footings were poured and cured at the construction site they were shipped to the structural laboratory of USC. The footing was fixed to the steel test frame by threaded rods through the ducts at the four corners of the footing, as shown in Figure 3.19. The assemblage of the test models started from the connections of columns and footings.

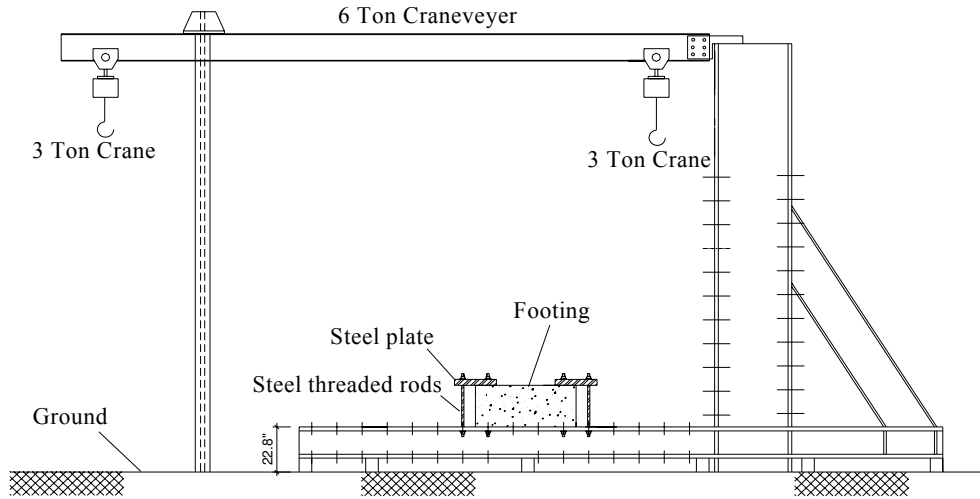


Figure 3.19: Test frame

Test Model 1

Figure 3.20 shows the footing of test model 1 was fixed to the test frame. In order to make the top surface of the footing flat, a layer of mortar was poured. The thickness of the mortar layer was around $\frac{1}{2}$ in. A small rectangular steel plate was put at the center of the footing top surface, which was aligned level. Figure 3.17 shows the moment when the column was connected to the footing. Due to the self weight of the column and the existence of the level steel plate, the mortar layer was under uniform pressure. The column was held upright with the two cranes before the splice sleeves started functioning.

Figure 3.21 demonstrates the making process of SS mortar, whose average compressive strength was 13ksi. The SS mortar was then filled into the NMB splice sleeves embedded in the column bottom end with the injecting tool, as shown in Figure 3.21. The mortar was injected into the sleeves from the inlet, which was on the bottom of the sleeve. If the sleeves were full of mortar, the extra mortar would flow out from the outlet, which was

on the top of the sleeve. Then the injection stopped and plastic plugs were used to block both the inlet and outlet. The injection process was shown in Figure 3.22.

To evaluate the tensile strengths of the NMB splice sleeve connections, three specimens were made and tested with the testing machine, as shown in Figure 3.23. The test results showed that the bonding strength between SS mortar and the steel rebars exceeded the tensile strength of the steel rebars.



Figure 3.20: Column to footing connection



Figure 3.21: SS mortar



Figure 3.22: Filling of SS mortar into sleeves



Figure 3.23: NMB splice sleeve test

Test Model 2

Due to the height limit of the test frame, the connection of the footing and column of test model 2 was done on the ground instead of on the test frame. The footing was put on the ground with a layer of mortar between them. The purpose of putting a layer of mortar was to make the footing be seated on flat and level ground. Figure 3.24 shows the connection of column to footing of TS2.

The high strength cement was filled into the metallic conduit embedded in the footing before the column was seated on top of the footing. To ensure complete bonding between column and footing, extra mortar was used so that column bottom end was seated on a layer of mortar. A small steel rectangular plate was put at the center of the footing top surface. The steel plate was aligned level.



Figure 3.24: Column-footing connection of test model 2

3.4.4 Connection between Columns and Beams

The steel beams and RC columns were connected through high strength threaded rods. The material of the steel rods was the ASTM A193. Since the connections were designed as slip critical type, preloading force up to 70 percent of the specified minimum tensile strength of the steel rod should be applied to each steel rod according to AISC specifications.

For ASTM A193 steel, the minimum specified yield and tensile strengths are 105ksi and 125ksi for steel rod of $\frac{3}{4}$ in. diameter. The effective tensile area of the steel rod of $\frac{3}{4}$ in. diameter is 0.334 in.². Thus the minimum preload F_p is

$$\begin{aligned}
 F_p &= 0.7 A_e F_t \\
 &= 0.7 \times 0.334 \times 125 \\
 &= 29.3 \text{ kips}
 \end{aligned}$$

When F_p is applied to the steel rod, the corresponding stress in the rod is 87.5 ksi, which is less than the minimum specified yield strength for ASTM A193 steel rod of $\frac{3}{4}$ in. diameter. Thus the strain in the steel rod corresponding to the preloading stress can be estimated by

$$\varepsilon_p = f_p / E$$

ε_p , σ_p and E are the preloading strain, preloading stress and Young's Modulus of the steel material. To obtain the actual Young's modulus of the steel rod, tensile tests were conducted on sample steel rods. the resulting Young's modulus were 26241ksi and 26360ksi. In estimating the applied strain to the steel rods for preloading, the Young's modulus was taken as 26000ksi. Therefore, the strain applied to the steel rods was 0.0034. Calibrated torch wrench was used to preload the steel rods.

3.5 Test Setup

The test setup is shown in Figure 3.25. The test models were loaded at the column top with the horizontal actuator, which was attached to the vertical reaction frame. To keep the load applying actuator horizontal during test process, it was held by the crane with steel chain. The steel beam end was supported by the vertical actuator to simulate a roller support condition. The horizontal actuator has a stroke of ± 10 in. The stroke of the vertical actuator is ± 5 in.

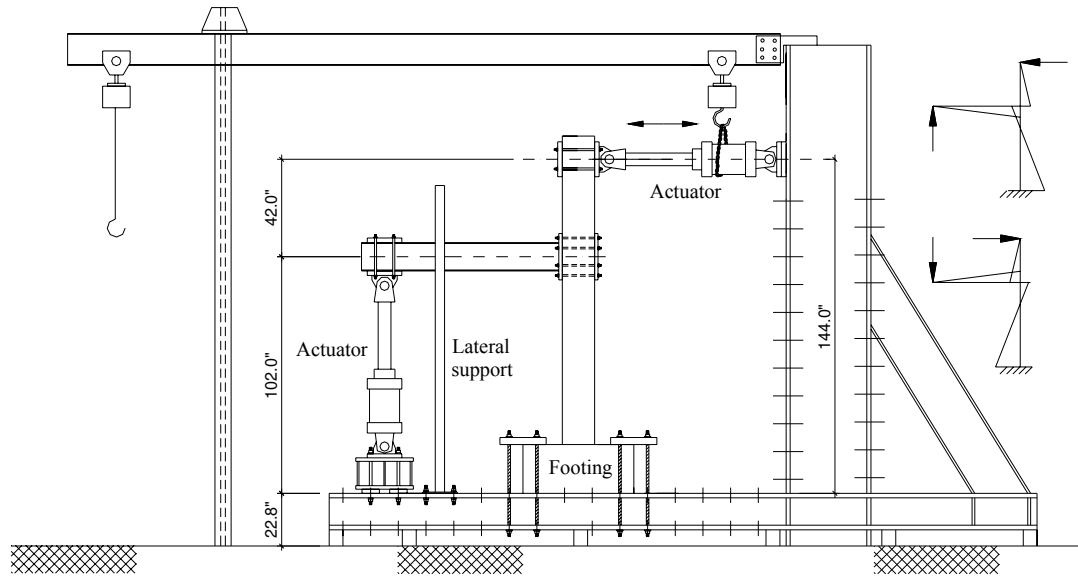


Figure 3.25: Test setup

Horizontal movement of the footings during loading was restrained by the friction force between the footings and the mortar. Pressure was applied to the footings by the steel plates, which were connected to the test floor by 7/8in. diameter post tensioned high strength threaded rods. The footing rotations were also restrained by the two steel plates.

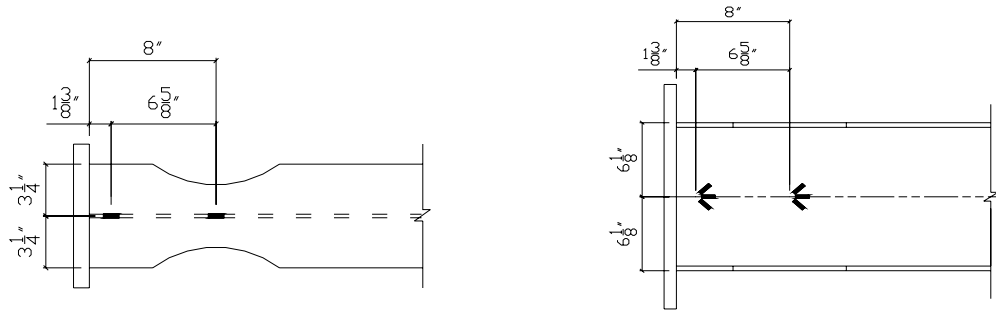
To prevent the steel beams from lateral torsional buckling, lateral supports were provided on both sides of beam at two thirds of the beam length from endplate. Teflon pads were attached on the lateral supports in the contact regions with the beam flanges to ensure the steel beam can slide freely along the loading directions. Axial load was not applied to the columns of the two test models.

3.6 Instrumentation

The applied horizontal force was measured by calibrated load cell. Displacements at the point of horizontal force application were measured by a ± 10 in. stroke linear potentiometer. Horizontal displacements at the column joint region were measured by a ± 5 in. linear potentiometer. Linear ports were employed to measure column curvatures with potential plastic hinge region.

In an actual moment resisting frame, the first story column height starts to vary when cracks forms in the column concrete, which causes the variation in the floor height. Therefore during the model testing process the steel beam end position was adjusted by applying vertical displacements to the beam end by the vertical actuator. The vertical displacements at the column joint and at the beam end were measured by ± 0.5 in. linear ports.

Strain gages were mounted at critical positions on the steel beam to measure the strain history during the test. The first critical section was the most reduced beam section and the second one was the beam end section, which was 1.375 in. away from the nearest surface of the endplates. Unidirectional strain gages were attached on top and bottom flanges at these sections. On the beam web, three unidirectional strain gages were used together to measure strains at critical sections along three different directions, as shown in Figure 3.26. The two angles between the three strain gages were -45° and $+45^\circ$, respectively.



(a) Strain gages on top and bottom flanges

(b) Strain gages on web

Figure 3.26: Instrumentation for steel beam

Instrumentations were provided at the beam-column joint to monitor the joint behavior during the test. Strain gages were used to measure the strains in high strength steel rods, as shown in Figure 3.27(a). Besides measuring strains in steel rods during the test, the strain gages were also used for preloading the steel rods. To measure the rotation of the steel endplate relative to column surface, two linear ports were used in such a way as shown in Figure 3.27(b). The rotation of the steel endplate was measured by the inclinometer made by the researchers. The joint concrete deformation was measured with linear ports. As shown in Figure 3.27(b), the solid circles represent the embedded expansion bolts. The solid lines indicate the linear ports. The instrumentation for column base is shown in Figure 3.28.

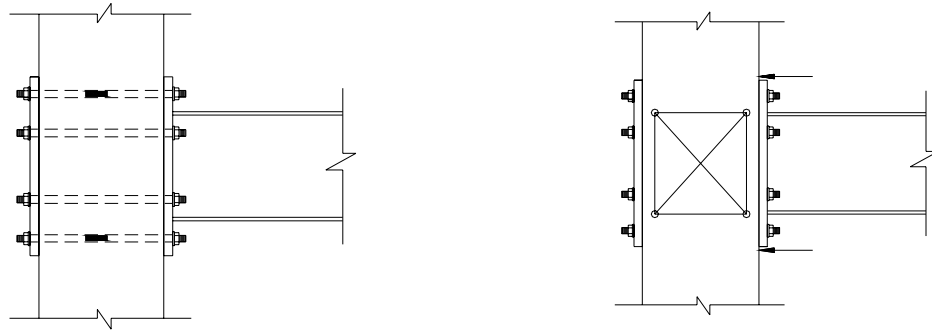


Figure 3.27: Instrumentation for beam-column Joint

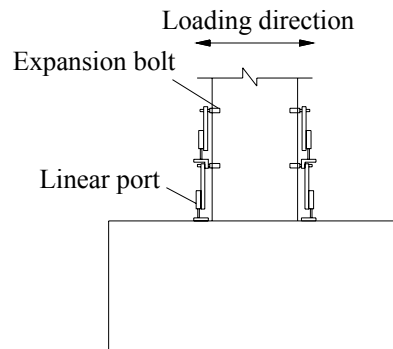


Figure 3.28: Instrumentation for curvature at column plastic hinge

3.7 Test Regimen

The loading program was designed to subject the concrete column to cyclic horizontal forces at the top end. The beam tip, to which a vertical actuator was attached, was kept at the same level as that of the beam-column joint. This was to account for the column height changes due to the variation of neutral axis. The horizontal forces were applied by the ± 9 in. stroke horizontal actuator. The vertical actuator had a ± 4.5 in. stroke.

For test model 1, the lateral loading sequence was controlled by force for the initial loading cycles till the reduced beam section was observed starting to yield. This observation was accomplished by monitoring the reaction forces of the vertical actuator, which were measured by the load cell. If F_{by} was used to indicate the vertical actuator reaction force when the reduced beam section started to yield, the first three cycles was controlled by the peak reaction force $0.5F_{by}$ and the second three cycles by $0.75F_{by}$. After another three cycles controlled by $1.0F_{by}$, the loading sequence was controlled by displacement. Let Δ_y denote the horizontal displacement of the column top end when the reduced beam section arrived at its yielding moment, then two complete loading cycles were performed at peak displacements equal to $2.0\Delta_y$, $3.0\Delta_y$, $4.0\Delta_y$, etc. until the reduced beam section buckled. During the test, the potential plastic hinge region at column base was monitored so that if it lost moment capacity the test would be stopped.

For test model 2, the lateral loading sequence was controlled by the interstory drift from the very beginning of the test. The interstory drift was defined as

$$\delta = \frac{\Delta_l}{H_l}$$

where δ is the interstory drift used to control the lateral loading; Δ_l is the lateral displacement measured at the centerline of the joint; and H_l is the column height measured from the base of column to the centerline of the joint, where Δ_l is measured. Figure 3.29 depicts the interstory drift of the test models. The peak interstory drift for the first three cycles was about 1.05%. Followed was another two cycles with peak interstory

drift of 1.1%. Then the controlling drifts for the rest of test were 1.5%, 2%, 3%, 4% and 6%. Two cycles were applied for each controlling interstory drifts.

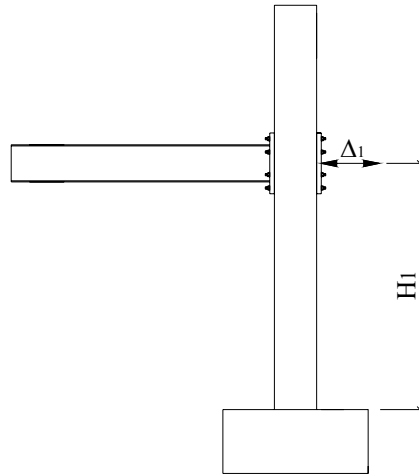


Figure 3.29: Interstory drift

3.8 Experimental Results and Discussions

3.8.1 General Observations

Both TS1 and TS2 developed ductile and stable responses during the testing. Inelastic deformation occurred first at column bottom end initiated by the cracking of cover concrete. Then the reduced section of steel beam started to yield until plastic hinge formed. Diagonal shear cracks of beam-column joint concrete were mainly developed during loading cycles corresponding to low lateral drifts, indicating that inelastic deformation of joint concrete was effectively limited. Even upon the ultimate loading stage, no severe loading capacity degradations were observed in both subassemblies, reflecting their good stiffness and strength retention capacity. Testing of both

subassemblies stopped shortly after the web and flanges of steel beam at reduced beam section buckled. Both subassemblies had similar ultimate condition patterns for the steel beam and the beam-column joint. The ultimate buckling condition of beam end of TS1 and ultimate cracking pattern of column joint region of TS2 are shown in Figure 3.30 and Figure 3.31, respectively. The ultimate cracking conditions of the PC columns of both subassemblies are shown in Figure 3.32 and Figure 3.33.



Figure 3.30: Buckling of steel beam RBS of TS1



Figure 3.31: Cracking of beam-column joint of TS2



Figure 3.32: Cracking of column of TS1

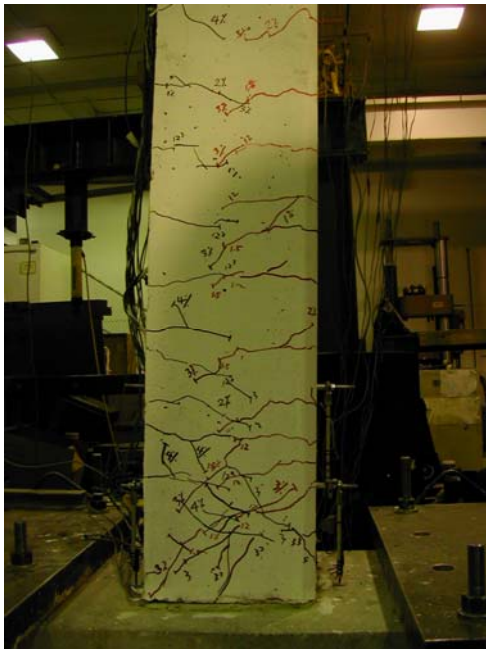


Figure 3.33: Cracking of column of TS2

In TS1, the PC column was connected to footing through embedded splice sleeves. Due to the use of high strength grouting mortar ($f_c' = 90$ MPa), the dowel bars of the footing were strongly bonded to the column. At the initial loading stages, flexural cracking was dominant at column base. At a horizontal load of 108 kN, which was the calculated first yield strength, the corresponding first-story drift ratio θ was 1.3%. Thus 1.3% was defined as the yield first-story drift ratio for TS1. During loading cycles corresponding to peak ductility factor $\mu = 1$ ($\theta = 1.3\%$), the flexural cracks started to bend indicating the influence of shear. During the second cycle corresponding to peak ductility factor $\mu = 2.0$ ($\theta = 2.6\%$), severe flexural cracking leading to cover concrete spalling was developed at the column bottom end. The beam flanges at RBS started to yield during cycles of peak ductility factor $\mu = 0.9$ ($\theta = 1.0\%$) judging by the spalling of the white limestone coating. Severe concrete crush finally occurred at PC column bottom end during loading cycles corresponding to peak ductility factor $\mu = 4.0$ ($\theta = 5.0\%$). The flanges and web of RBS buckled after the peak ductility factor $\mu = 4.0$ was exceeded. Throughout the whole testing process the precast concrete footing stayed uncracked. PC column of TS2 was connected to foundation by dowel anchorages. The overall response of TS2 was very similar to but even better than that of TS1. The calculated horizontal load causing the first yield of the system was 97.4 kN, corresponding to a first-story drift ratio of 1.0%. The first yielding of TS2 was earlier than TS1 because of the debonded length of dowel bars of TS2. In addition, due to the use of the 152 mm debonded length for the dowel bars at the column-footing interface, much energy was absorbed and dissipated by the inelastic deformation of the debonded segment of longitudinal bars at the column bottom end. As

a result, the crushing of concrete at column bottom region in TS2 was less severe than that in TS1.

For both test subassemblies, the end plate stayed in elastic range, judging by the fact that there was no spalling of the white limestone paint on the plate.

3.8.2 Horizontal Force – Displacement Response

The relationships of applied horizontal force V at column upper end and the resulting first-story drift ratio are shown in Figure 3.34 and Figure 3.35 for model subassemblies TS1 and TS2, respectively. It can be seen that hysteretic responses of both subassemblies are stable and ductile. However, for cycles where peak displacements exceeded 2% of first-story drift ratio, the responses varied between TS1 and TS2. Pinching of the hysteresis loops at low lateral displacements was obvious for TS1, primarily due to the severe concrete cracking and crushing at column bottom region. For TS2, however, stable hysteresis loops with good energy dissipation capacity were developed for loading cycles even at large peak displacements, indicating the fact that the debonding of the longitudinal bars at the column end enabled the full formation of the plastic hinge. Figure 3.36 compares the different hysteretic loops of TS1 and TS2 corresponding to the peak first-story drift ratio of 4%.

The theoretical flexural strength V_{if} of test subassemblies was estimated corresponding to the formations of most probable plastic moments at the reduced beam section and at the column bottom section. The theoretical first yield strength of test subassemblies V_{iy} was developed when the outermost longitudinal rebars at the column bottom section started to yield. The calculated first yield strength V_{iy} for TS2 is smaller than that of TS1 due to the consideration of the debonded longitudinal bars at column base in TS2. The calculated values of V_{iy} and V_{if} are shown in Figure 3.34 and Figure 3.35. Both model subassemblies developed the calculated theoretical flexural strength, V_{if} .

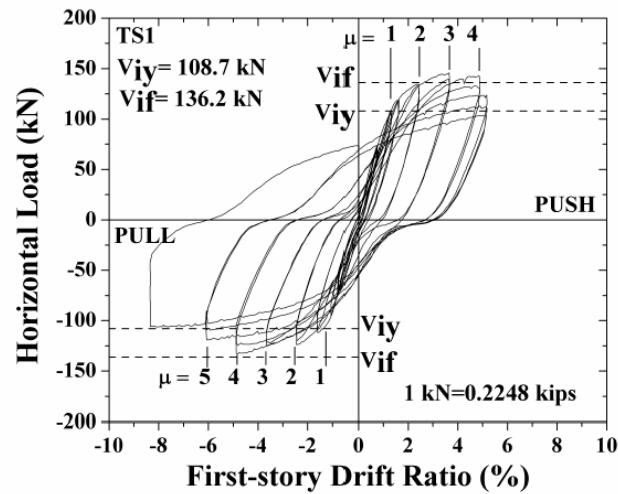


Figure 3.34: Horizontal force-drift ratio relationship of TS1

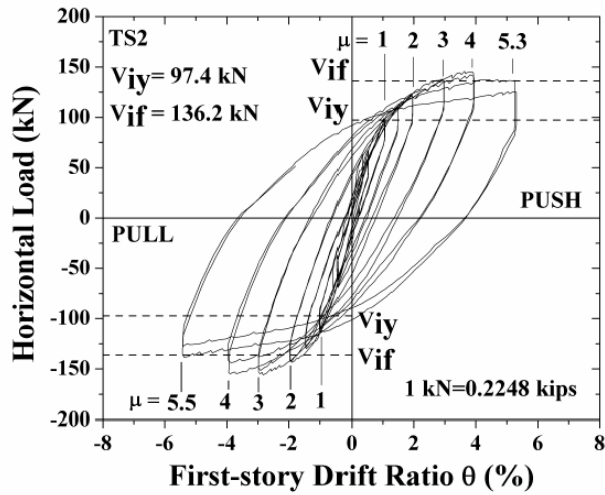


Figure 3.35: Horizontal force-drift ratio relationship of TS2

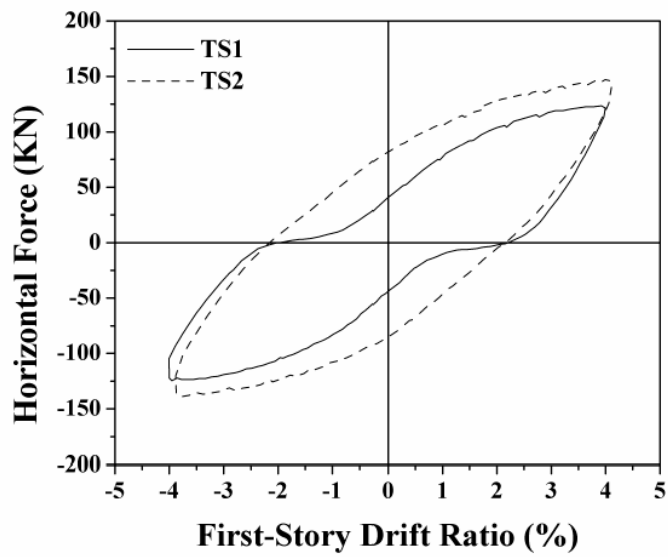


Figure 3.36: Typical hysteresis hoop of TS1 and TS2

3.8.3 Overstrength of RBS

According to AISC seismic provisions (2005), the maximum expected plastic moment $M_{pr,RBS}$ and ideal plastic flexural capacity $M_{i,RBS}$ at the reduced beam section (RBS) are related by,

$$M_{pr,RBS} = 1.15R_y Z_{RBS} F_y = 1.15R_y M_{i,RBS} \quad (\text{Eqn. 3.14})$$

where, R_y , is the ratio of beam expected yield strength to the specified minimum yield strength; Z_{RBS} is the plastic sectional modulus at the RBS section; and F_y is the nominal yield strength of steel. For A992 Grade 50 steel, R_y is equal to 1.1. Thus the nominal over-strength of RBS is 1.265. Figure 10 shows the measured relationship of curvature of RBS and the corresponding normalized flexural moment in terms of $M_{i,RBS}$, or the over-strength, for TS1 and TS2, respectively. The two dashed lines in Figure 3.35 represent the over strength factors of 1.0 and 1.265. For both test subassemblies, the actual maximum over-strength developed at RBS reached 1.50. Thus the nominal over-strength factor $\lambda_o=1.265$ is underestimated and may be increased in actual design. Figure 3.37 and Figure 3.38 also indicate that even after the buckling of the flanges and web of RBS, the section flexural capacity remained almost unchanged.

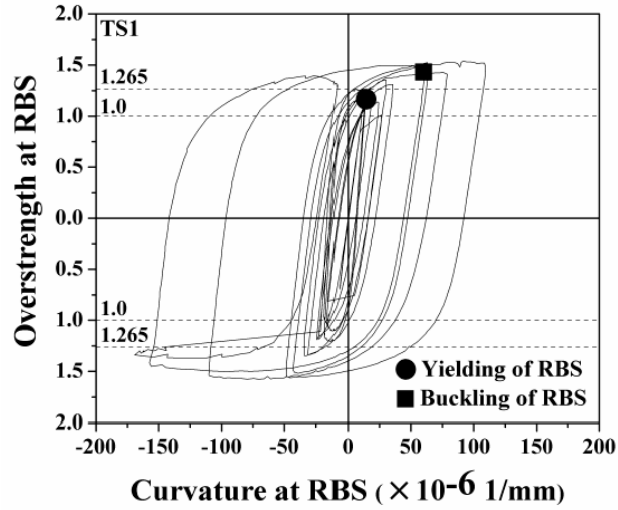


Figure 3.37: Overstrength of RBS of TS1

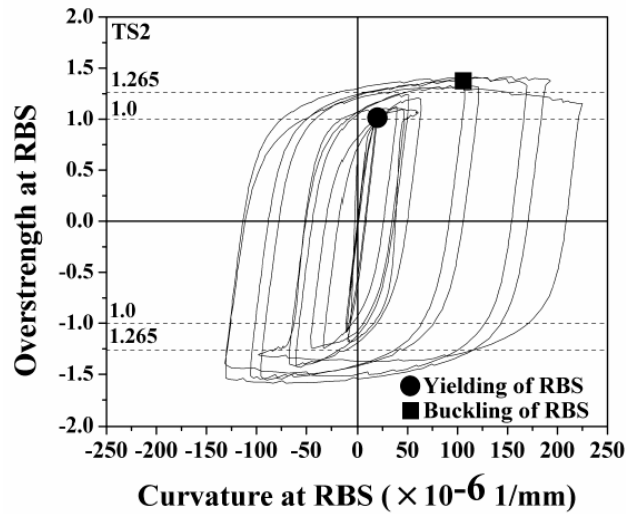


Figure 3.38: Overstrength of RBS of TS2

3.8.4 Post-tensioning Steel Rods

The stress-strain relationship of the Grade A193 high strength steel rod was obtained through tensile tests of sample rod coupons using universal testing machine. The typical first yield strength and tensile strength of the rod are 148 kN and 193 kN, respectively.

During testing, the tension force in each rod could be approximated by resolving the bending moment at beam end into equal compression and tension forces and then assigning to each row based on the strain compatibility analysis. Figure 3.37 shows the experimental relationship of strain and corresponding approximated tension force of a rod at the outermost row. In Figure 3.39, F_0 and ε_0 represent the effective pretension and the resulting initial strain in the steel rod under consideration. The dashed line defines the boundary between gap opening and closing. Below this boundary line, the gap is closed and the tension force in the steel rod remains the value corresponding to the closing point. Above the boundary line, additional tension force is induced, resulting in additional tensile strain in the rod that caused the gap opening. The shape of the boundary line also indicates the gradual loss of prestressing force in the steel rod due to the accumulation of inelastic deformation of the rod.

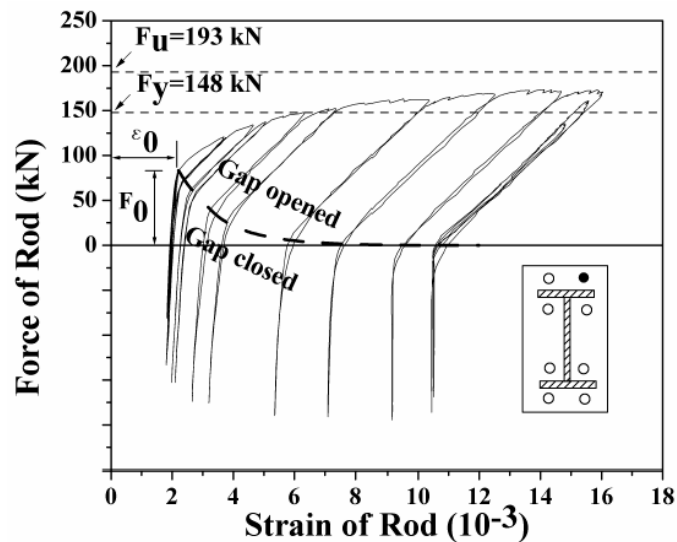


Figure 3.39: Deformation-force relationship of post-tensioning rod

3.8.5 Beam-column Joint Region

For both TS1 and TS2, the diagonal cracks of joint concrete were observed to develop mainly during the loading cycles corresponding to peak first story drifts of 1%, 1.5% and 2%. However during loading cycles corresponding to high peak lateral drift ratios, neither additional diagonal cracks appeared, nor the existing diagonal cracks widened. This indicated that the formation of the plastic hinge at the beam end and the inelastic deformation of column base effectively prevented the further damage to the beam-column joint region. Post-tensioning of steel beam end plate to the PC column also contributed to the reduction of the principal tensile stress in the joint region.

3.8.6 PC Column Base

The PC column base of TS1 refers to the column bottom segment where the splice sleeves are embedded. Thus the column base length of TS1 is equal to the length of the splice sleeve, which is 325 mm measured from the column-footing interface. Test results indicated that the use of splice sleeves resulted in a rigid column core confined by hoops at the column base region. As a result and also due to the much larger diameter of the sleeves, the cover concrete at the column base region cracked severely and spalled during early loading stage. Following the total spalling of cover concrete, a major crack was developed right above the splice sleeves. The width of this major crack varied in accordance with the applied lateral drift, indicating its contribution to the flexural rotation

capacity of the column bottom end. In TS2, the 153 mm length of PC column segment measured from the column-footing interface where the longitudinal bars were debonded from concrete is regarded as the column base region. It was observed that diagonal cracks dominated at the base region while the first flexural crack occurred in the vicinity of the section where longitudinal bars started to be bonded to concrete. Only very minor cover concrete crushing was observed throughout the testing.

Figure 3.38 and Figure 3.39 show the experimental relationships of the measured average curvature of column base and moment at column bottom section of TS1 and TS2, respectively. The theoretical yield strength M_y and flexural strength M_p based on sectional moment-curvature analysis are also given in these two figures. It is obvious that the theoretical strengths agreed well with the experimental results for TS2. For TS1, due to the severe cover concrete crushing at base region, the experimental strengths are less than theoretical predictions. Although the conventional methods are not valid for the analysis of column base sections of TS1 and TS2 due to the splice sleeves in TS1 and the debonded lengths of longitudinal rebars in TS2, the overall behavior can still be approximated using the sectional analysis. Figure 3.40 and Figure 3.41 show the experimental relationships of first-story drift ratio and average curvature of column base of TS1 and TS2, respectively.

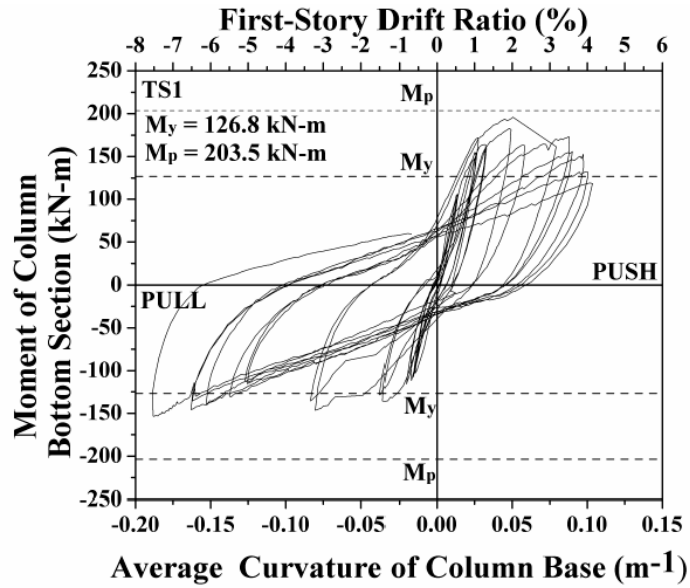


Figure 3.40: Curvature-moment relationship of TS1

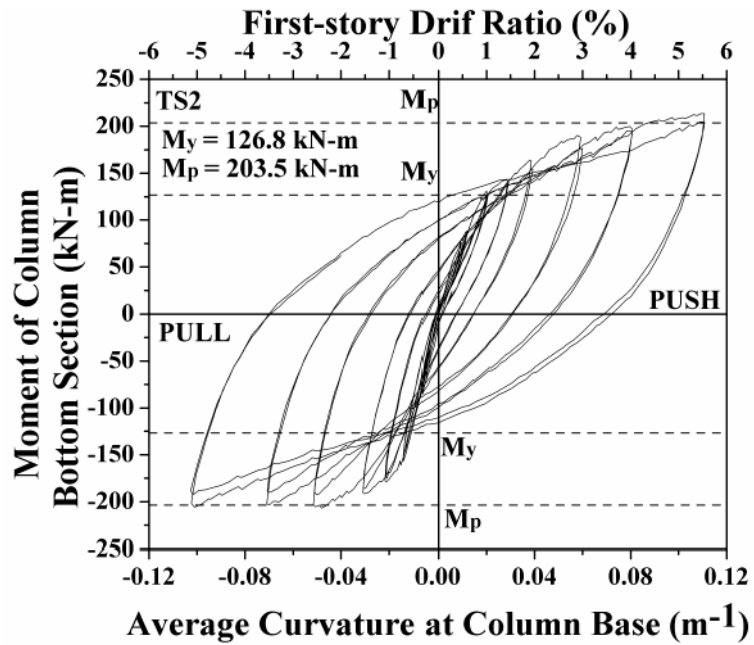


Figure 3.41: Curvature-moment relationship of TS2

3.8.7 Yield Sequence of Test Subassembly Components

The yielding sequence of the test subassembly components reflects how a PCS frame behaves during an earthquake. For a rational seismic design of a structural system, the post-yield deformation capacity of the system is expected to be provided by the plastic hinges formed at the RBSs of the steel beams and the column bases. This mechanism is ensured by designing other system components based on the most probable plastic strength of RBS amplified with appropriate over strength factor. This desired system capacity hierarchy can be verified by examining the yielding sequence of the test subassembly components based on the test results. Figure 3.42 and Figure 3.43 shows the first story drift ratio-horizontal force envelope curves of TS1 and TS2 in the push loading direction only. The yielding events of critical sections are marked on the curves. It can be seen that the design objectives are well realized. In most cases, the effectiveness of a design of composite PCS moment structure can only be evaluated using analytical procedures that are developed based on appropriate modeling assumptions and techniques for PCS structure.

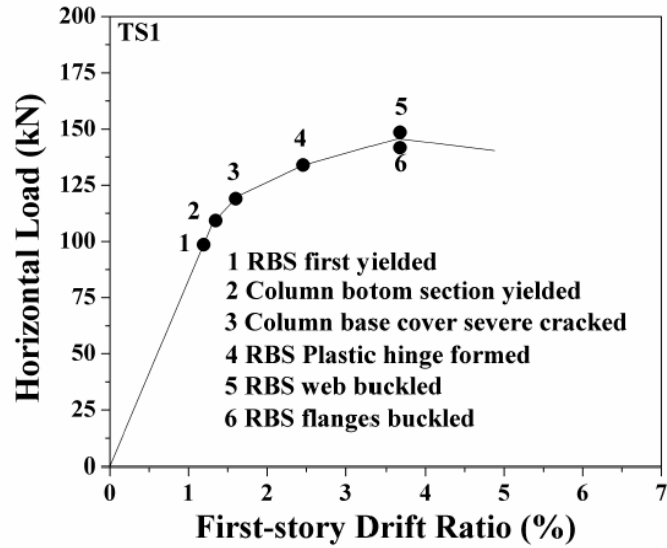


Figure 3.42: Yield sequence of TS1

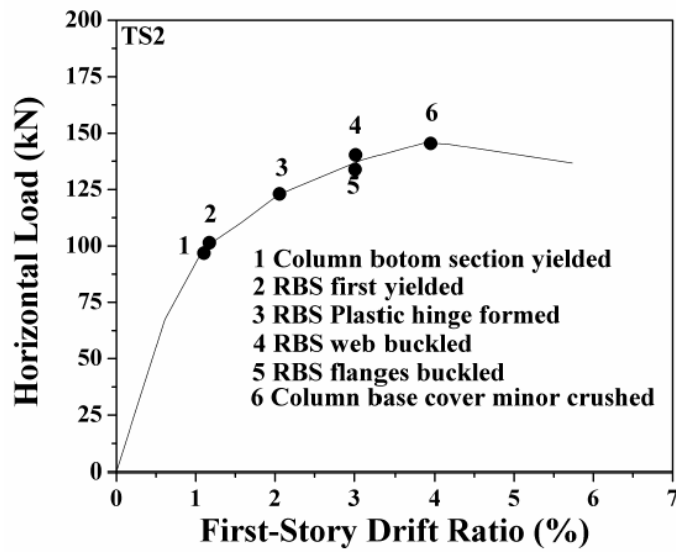


Figure 3.43: Yield sequence of TS2

3.9 Conclusions

In this experimental research program, two steel beam-PC column and footing subassembly modules were tested under reversed cyclic loading to simulate the seismic

behavior of the composite PCS moment resisting frame for the use in high seismic region. Responses of the test subassemblies were examined to investigate the effectiveness of the design method aiming at providing rational strength hierarchy and sufficient post-yield deformation capacity. The following conclusions can be drawn based on the experimental observations, discussions and analyses presented in this paper:

- (1) The ASTM A192 high strength steel rod can be used to post-tension the steel beam to PC column. It is rational to design the composite post-tensioned endplate connection as a partial prestressed system that allows a total decompression for reasons of cost effectiveness and ease of construction.
- (2) The reduced beam section (RBS) of steel beam is effective in relocating the plastic hinge away from beam end and in dissipating most of seismic-induced inelastic energy at system post-yield stage.
- (3) The two types of column to footing connection resulted into different hysteretic behaviors, though both were sufficient in supporting the formation of a ductile system behavior. The use of splice sleeves may lead to a relatively rigid core at PC column base and shift the concrete crushing above the splice region, leading to early severe cracking and spalling of cover concrete. By anchoring the longitudinal bars of the PC column to the conduits embedded in the footing and by debonding a certain length of

the longitudinal bars at the column end not only secured the moment connection but also enabled the full formation of the plastic hinge at the column end.

(4) According to test results, when the first story drift ductility reached about 5.0, the system still exhibited excellent strength and stiffness retention capacity. The composite PCS moment frames can be designed to possess adequate lateral force resistance capacity, ductility and energy dissipation capacity for buildings located in regions of high seismicity.

(5) The structural failure of the PC column joint region is less likely to occur than conventional monolithic RC joint since the post-tensioning rods running through the column enable a favorable joint shear resisting mechanism.

Chapter 4: Comparative Study of RC, S and PCS Building

Design

4.1 Introduction

In Chapter 3, the experimental program has verified the effectiveness of the proposed design procedure, which ensures a reasonable strength hierarchy among components of the hybrid structural system. The system post-yield deformation capacity and inelastic energy dissipation capacity are mainly provided by the reduced beam section (RBS) at steel beam ends. It must be pointed out that the use of RBS as the structural fuse is only one option out of several others for the hybrid PCS system. For example, another option is also acceptable where a post-tensioning tendon is used at the center of the end-plate to provide continuity and shear resistance and mild steel is used at the flange areas to provide energy dissipation capacity. Due to the use of steel beam and the composite metal deck slab system the shear demand is much reduced compared with the use of concrete beam. Therefore, the reduced beam section is considered the most economic choice.

In this chapter, three similar prototype structures are designed based on current building codes and the proposed design procedure. These three prototype buildings include one conventional reinforced concrete office building, one conventional steel office building

and one proposed hybrid PCS office building. The lateral force resisting systems of these three prototype buildings are all special moment resisting frames since they are located in high seismic region. The three prototype buildings are designed to be similar to each other so that they are comparative. The prototype buildings are considered similar to each other in that their lateral force resisting systems are intentionally designed to obtain the same flexural stiffness.

4.2 Prototype Buildings

It is intended to make the comparative study of RC, S and hybrid PCS buildings as realistic as possible. To do this, a well-known existing 13-story steel building is selected as the basis for design of the other two prototype buildings. In other words, the conventional RC building and the hybrid PCS building are designed to be similar to the existing steel building. The reinforced concrete building is preliminarily designed by substituting the steel members of the steel building with reinforced concrete members of equivalent flexural stiffness. The PCS building is preliminarily designed by substituting the steel columns of the steel building with reinforced concrete columns. The detailed design of the three prototype buildings are given in Appendix A. The plan view and the moment frame plan of each prototype building is shown in Figure 4.1 to Figure 4.3. Notice that the lateral force resisting frames are arranged along the perimeter of the building while the interior beams and columns are only for gravity load bearing.

The three prototype buildings have the same loading criteria. Due to the use of steel beam in S and PCS buildings, composite slab system can be used, as shown in Figure4.4. However, the slab system of RC prototype building is composed of only concrete. The superimposed dead loads and live loads for the three buildings are exactly the same.

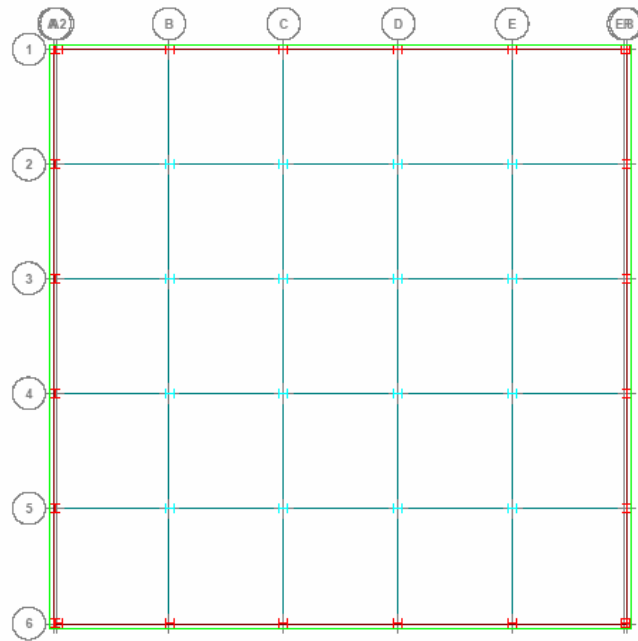


Figure 4.1: Typical floor plan of Steel building

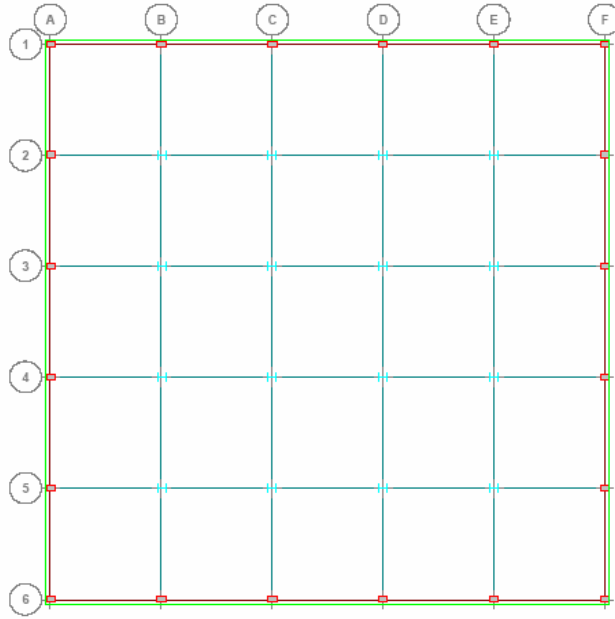


Figure 4.2: Typical floor plan of PCS building

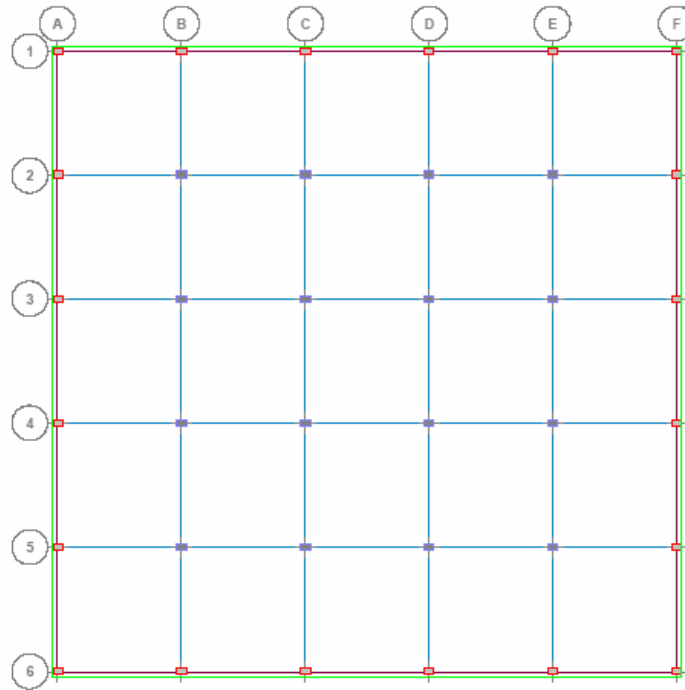


Figure 4.3: Typical floor plan of RC building

4.3 Characteristics of Seismic Design of Prototype Buildings

The seismic design of prototype buildings is based on the provisions of ASCE 7-05, which has been mostly adopted by the 2007 California Building Code (CBC 2007). Due to the regularity of the prototype buildings, the ASCE 7-05 equivalent lateral force procedure can be used to conduct the seismic analysis of the prototype buildings.

4.3.1 Building Period T_a

The building periods of S, PCS and RC buildings are listed in Table 4.1.

Table 4.1: Fundamental period of prototype building

| | C_t | x | h_n (ft.) | $T_a=C_t h_n^x$ (sec.) |
|-----|-------|------|-------------|------------------------|
| S | 0.028 | 0.8 | 186.5 | 1.835 |
| PCS | 0.022 | 0.85 | 186.5 | 1.873 |
| RC | 0.016 | 0.9 | 186.5 | 1.769 |

It is noted that PCS and RC buildings have the longest and shortest fundamental periods respectively.

4.3.2 Seismic Weight W

The seismic weight of building for design base shear calculation is usually the self-weight of the building plus 25% of live load when applicable. It is easy to conclude that the RC building has the highest seismic weight among the three prototype buildings. According to estimation of Appendix A, the total seismic weights of S, PCS and RC

prototype buildings are 18628 kips, 21072 kips and 39085 kips. Figure 4.4 shows the comparison of the seismic weights of the three buildings. It is obvious that the total weights of steel and PCS buildings are very close to each other. The sharp increase of self weight of RC building is largely due to the different slab systems used with steel beams and concrete beams.

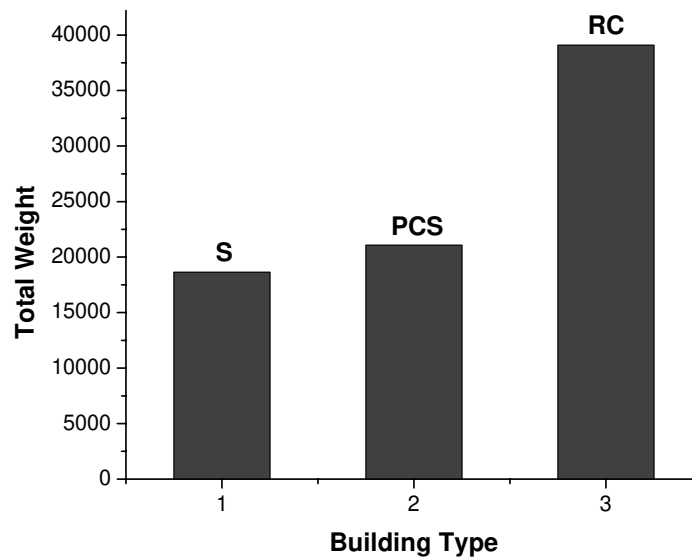


Figure 4.4: Seismic weight comparison

4.3.3 Design Base Shear V

The design base shear forces of the prototype buildings are determined according to equivalent lateral force procedure of ASCE 7-2005. For reinforced concrete special moment frame and steel special moment frame, the response modification factor R is taken as 8. This indicates that no matter what material is used, the special moment frame

system shall be design to obtain the same level of ductility. Therefore, R factor for the hybrid PCS SMRF is also 8. Figure 4.5 compares the design base shears of the three prototype buildings. The RC building has to be designed to resist the highest level of base shear. Base shear of PCS building is very close to that of steel building.

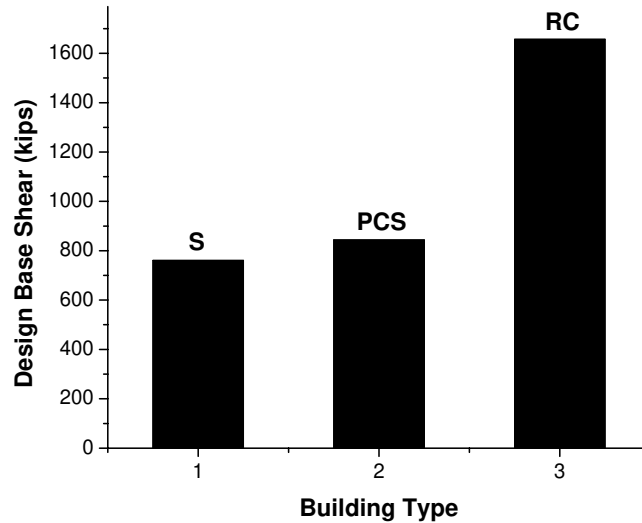


Figure 4.5: Design base shear of prototype buildings

4.3.4 Vertical Distribution of Design Base Shear V

Figure 4.6 and Figure 4.7 depict the vertical distribution of design base shear and story shear in S, PCS and RC buildings. It can be seen that the RC shear distribution exceeds the other two by a relatively large amount.

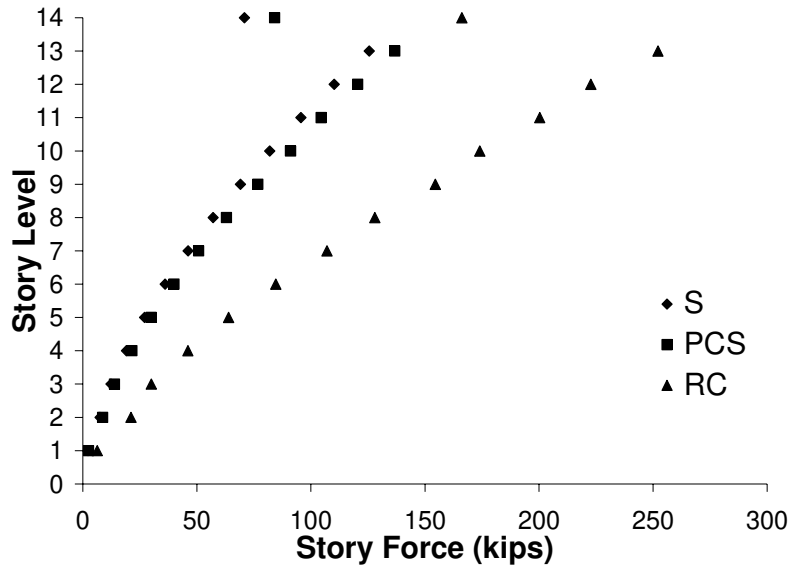


Figure 4.6: Vertical distribution of design base shear

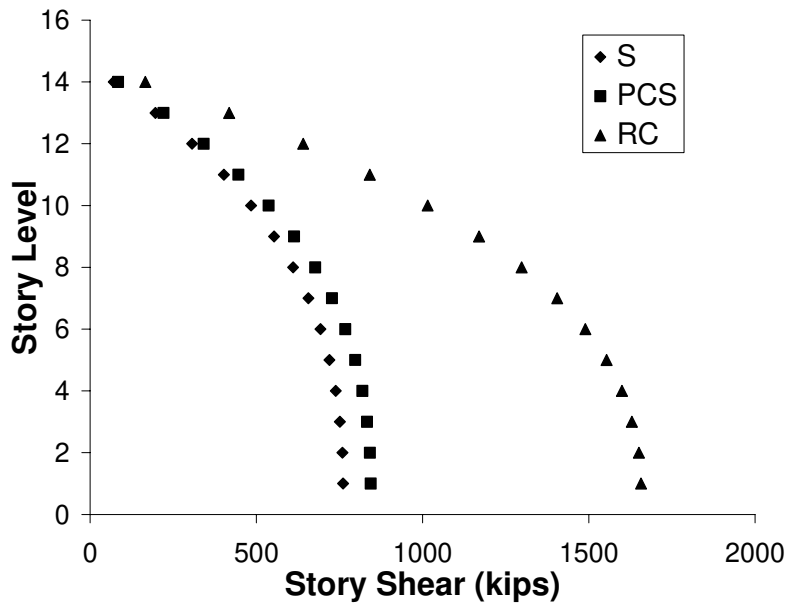


Figure 4.7: Story shear of prototype buildings

4.3.5 Lateral Displacement and Inter-story Drifts

Figure 4.8 and Figure 4.9 show the lateral displacement and interstory drift of the three prototype buildings. The results of S and PCS are very close to each other, indicating that the lateral behavior of PCS can be designed to be similar to that of steel structure under static analysis.

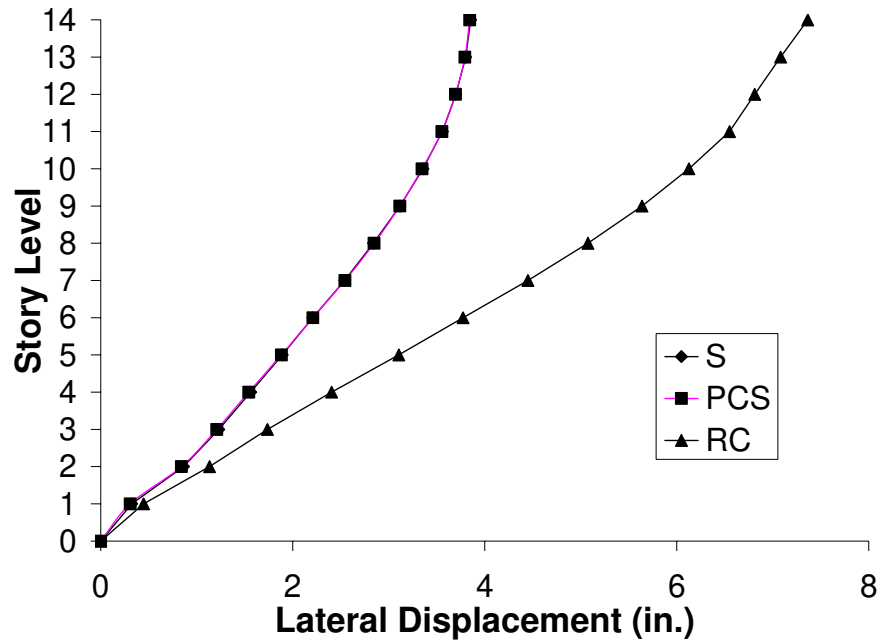


Figure 4.8: Lateral Displacement of Prototype Buildings

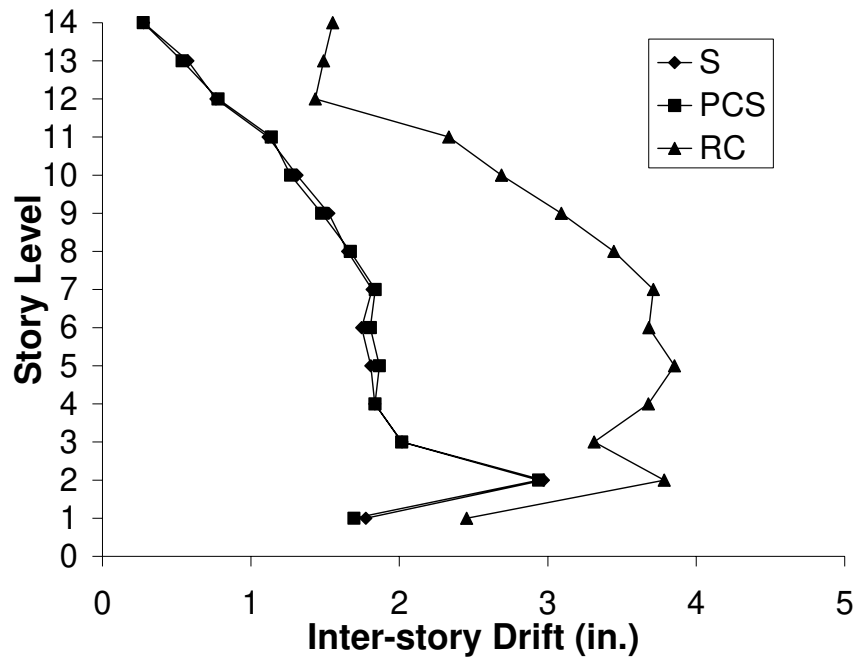


Figure 4.9: Inter-story Drift of Prototype Buildings

Chapter 5: Nonlinear Modeling of Hybrid PCS Beam-column Connection

In the previous chapters, the capacity-based design methodology of hybrid PCS moment resisting frame is introduced and applied to the design of a prototype building. As indicated in Chapter 2, the objective of the proposed capacity-based design is to provide the PCS system with adequate strength and energy dissipation capacity by ensuring a reasonable strength hierarchy and by selecting an efficient energy dissipating mechanism. The results of the experimental program then validated the effectiveness of the design method. In order to further reveal the characteristics of the proposed hybrid PCS frame system, the behavior of the post-tensioned beam-column connection of hybrid PCS frame is discussed and efforts are made to introduce a nonlinear model which can capture the major characteristics of the hybrid PCS beam-column connection. It is believed that the proposed nonlinear PCS beam-column connection model can found a sound basis for future study of the PCS system.

5.1 Modeling Philosophy

The hybrid steel beam-concrete column is very unique in that it is an assemblage of steel beam and precast column connected by post-tensioning rods without any bonding. The continuity and toughness of the beam-column frame system is provided effectively by the

post-tensioning force of the steel rods. As a result, the first issue to concern is the residual post-tensioning force of steel rods. The second issue to consider is the rotational capacity of the beam-column joint. In design of conventional steel ductile frame system, the rotational capacity of the joint is a significant source of lateral ductility. The more ductility is expected the higher rotational capacity is required for the joint. Therefore, in AISC Seismic Provisions, the rotational capacities for special moment resisting frame and intermedium moment resisting frame are 0.03 rad and 0.02 rad, respectively. The rotation of hybrid steel beam-precast column comes from two sources. The first source is the rotation of column joint and the second source is the gap opening between end-plate and column surface due to the elongation of post-tensioning rods.

5.2 Rotation of Hybrid PCS Beam-column Connection

The rotational behavior of the steel beam under earthquake-induced moment can be described by Figure 5.1.

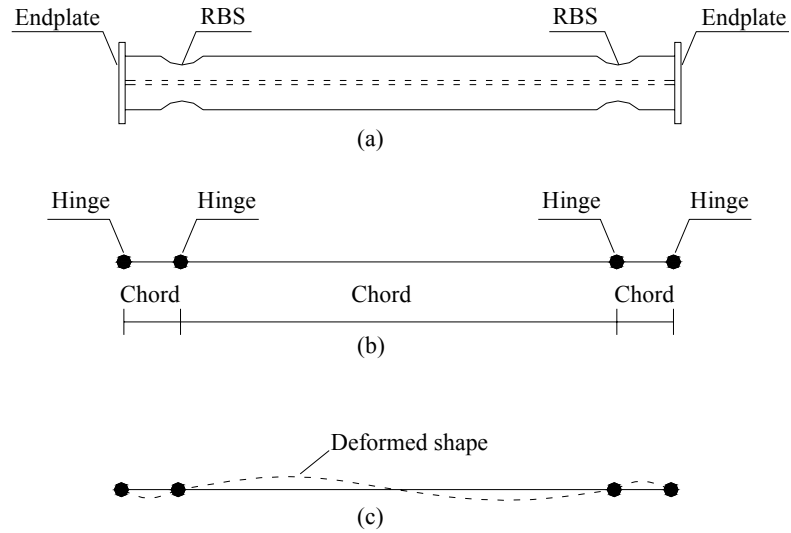


Figure 5.1: Chord-hinge model of steel beam

Figure 5(a) is a top view of the steel beam, including the reduced beam location and steel end-plate welded at beam ends. Figure 5(b) shows the chord-hinge model of the steel beam including the beam-column connection. Figure 5(c) is the side view of the model, depicting of the deformed shape of the entire beam under earthquake load after both hinges form. The reduced beam section can be regarded as a hinge since it is much weakened compared with the rest of beam segments. The beam-column connections are also treated as hinges to account for the rotational behavior contributed by the post-tensioning rods. The moment-rotation characteristics of the RBS-type hinge and the post-tensioning-type hinge can both be depicted as in Figure 5.2.

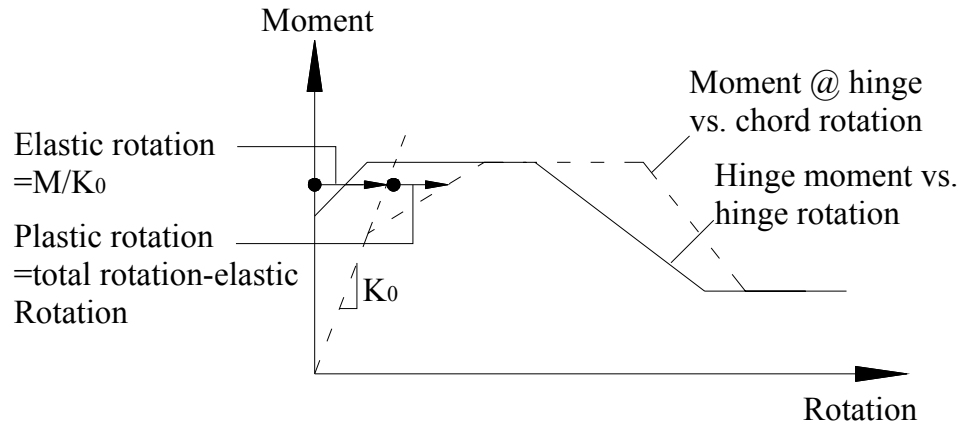


Figure 5.2: Hinge moment rotation relationship

Note that the deformed shape shown in Figure 5.1(c) is the situation after both the hinges at RBS and at connection form. However the two hinges usually won't form at the same time. Before we start to discuss the sequence of formation of plastic hinge at RBS and connection, it is worthwhile to identify the different mechanisms causing the hinge behavior at RBS and at connection.

As discussed in Chapter 2, the steel rods that connect steel beam to precast column are pre-tensioned during construction. This is to create the post-tensioning force that provides system continuity and toughness for the PCS frame. According to AISC specification, the pre-tension force is usually up to 70 percent of the tensile strength of the steel rod. As a result, when the pre-tension force is applied, the steel rod is close to yield or even already yielded. This is definitely unlike the RBS. At the RBS section, the plastic hinge forms when the entire section reaches the yield strength. Therefore, for the beam-column connection hinge, the elastic segment of moment-rotation relationship is not provided by the elasticity of steel rods.

The un-overcome post-tensioning force of steel rods provides the elastic rotational capacity for the beam-column connection. More specifically, the plastic hinge at the beam-column connection will not form until when the input earthquake-induced moment at the beam-column connection M is large enough, or

$$M \geq 4P_0d \quad (\text{Eqn. 5.1})$$

where P_0 is the total residual pretension force of rods on one flange and d is the distance between the centerlines of top and bottom flanges of steel beam. It is easy to understand that the elastic rotation of the beam-column connection can be estimated as the shear strain γ of the joint concrete region, or

$$\gamma = \frac{v_c}{G} \frac{1}{\rho_{\text{mod}}} \quad (\text{Eqn.5.2})$$

where v_c is the shear stress at the column joint region; G is the shear modulus of concrete and ρ_{mod} is a modification factor for the effect of the presence of reinforcing steel on the shear strain of the cracked joint.

$$\rho_{\text{mod}} = \frac{\sum A_s}{D_b D_c} \frac{E_s}{E_c} \quad (\text{Eqn.5.3})$$

In (Eqn.5.3), $\sum A_s$ is the total shear reinforcement area; D_b and b_c are the depth of beam and width of the column. It should be pointed out that shear deformation γ of column joint region is the measure of the joint rotation only before the post-tensioning force of steel rods is overcome. When the post-tensioning force is overcome, the total rotation of the beam-column joint becomes the summation of column joint rotation plus the extra

rotation of steel end-plate caused by extra elongation of steel rods. The total rotation α (rad) can be estimated by

$$\alpha = \gamma + \theta \quad (\text{Eqn.5.4})$$

$$\theta = \frac{\Delta M L_{rod}}{4 A_{rod} d^2 E_s} \quad (\text{Eqn.5.5})$$

In (Eqn.5.5), ΔM is the increment of earthquake-induced moment at beam end compared with the minimum moment that causes the overcome of post-tensioning force; A_{rod} is the cross-sectional area of each post-tensioning rod; L_{rod} is the effective length of each steel rod. It can be seen from (Eqn.5.5) that the calculation of rotation θ is still based on elastic property of steel rod even though the steel rod has yielded. And the resulting rotation is regarded as plastic compared with the rotation contributed by the column joint region.

Figure 5.1(b) also indicates that the steel beam segments between the hinges are treated as elastic chord. This assumption is very realistic in terms of the beam segment between RBS hinges, according the test results. For the beam segment between the RBS and its immediate beam end, however, the elastic chord assumption is just approximate. This is mainly due to the stress concentrated at the beam end where the end-plate is welded to the steel beam end. According to the test results, beam sections close to the beam end-endplate interface yielded. However, compared with the deformation of steel rods, the rotation contributed by the beam-end-endplate interface is very small. Thus it is still believed to be reasonable to ignore that rotation and treat the beam segment between RBS and beam end as elastic chord.

In Figure 5.2, the solid line represents the moment-rotation relationship of hinge rotation and hinge moment. This is a typical rigid-plastic relationship, meaning before the hinge forms the hinge segment has infinitely large stiffness in terms of plastic rotation. Thus the initial segment of the solid line is along the Moment axis. Both rotation vs. moment relationships of RBS hinge and beam end hinge can be described by this solid line. For the RBS plastic hinge, the solid line curve starts to be sloped at the point where the section of RBS starts to yield. For the beam end hinge, the solid line curve starts to be sloped when the post-tensioning force is overcome. When the entire RBS yields the plastic hinge forms and the solid line becomes flat until it drops. The beam end hinge forms when all of the post-tensioning rods on the tension side of beam flange yield and the solid line becomes flat indicating the entrance to the yield plateau.

In Figure 5.2 the dashed line represents the relationship between the bending moment and the total rotation of the beam segment under consideration. For the RBS segment, a tributary length should be assigned to the hinge so that the total rotation can be obtained by integrating the beam curvature along this tributary length. Then the plastic hinge rotation can be got by subtracting the elastic beam rotation, which is ML/EI , from the total rotation. For the beam end hinge, the elastic rotation is contributed by the column joint region.

Chapter 6: Conclusions and Future Research

In this research project, the behavior of hybrid PCS special moment frame is studied experimentally and theoretically. The experimental program validated that the hybrid PCS frame can be designed with adequate strength, stiffness and energy-dissipation capacity for seismic resistance. The design of hybrid PCS building was carried out and compared with the design of conventional types of structures. In addition, the nonlinear modeling of hybrid beam-column connection is discussed and compared with the characteristics of common type plastic hinge.

6.1 Conclusions

- (1) The ASTM A192 high strength steel rod can be used to post-tension the steel beam to PC column. It is rational to design the composite post-tensioned endplate connection as a partial prestressed system that allows a total decompression for reasons of cost effectiveness and ease of construction.
- (2) The reduced beam section (RBS) of steel beam is effective in relocating the plastic hinge away from beam end and in dissipating most of seismic-induced inelastic energy at system post-yield stage.
- (3) The two types of column to footing connection resulted into different hysteretic behaviors, though both were sufficient in supporting the formation of a ductile system

behavior. The use of splice sleeves may lead to a relatively rigid core at PC column base and shift the concrete crushing above the splice region, leading to early severe cracking and spalling of cover concrete. By anchoring the longitudinal bars of the PC column to the conduits embedded in the footing and by debonding a certain length of the longitudinal bars at the column end not only secured the moment connection but also enabled the full formation of the plastic hinge at the column end.

- (4) According to test results, when the first story drift ductility reached about 5.0, the system still exhibited excellent strength and stiffness retention capacity. The composite PCS moment frames can be designed to possess adequate lateral force resistance capacity, ductility and energy dissipation capacity for buildings located in regions of high seismicity.
- (5) The structural failure of the PC column joint region is less likely to occur than conventional monolithic RC joint since the post-tensioning rods running through the column enable a favorable joint shear resisting mechanism.
- (6) The hybrid PCS moment frame and steel moment frame have similar design base shear and lateral displacement in seismic design. But PCS frame is more economical than steel frame due to the use of precast column.

(7) Compared with RC frame, the hybrid PCS moment frame is much lighter, more economical and faster for construction speed.

(8) The modeling of hybrid PCS beam-column connection is easier than the monolithic RCS moment connection where the steel beam and cast-in-place RC column are completely bonded together.

6.2 Future Research

The current research is in terms of the overall behavior of hybrid PCS moment frame structure. The suggested future research focuses on the local behavior of the hybrid PCS beam-column connection. A suggested test setup is shown in Figure 6.1.

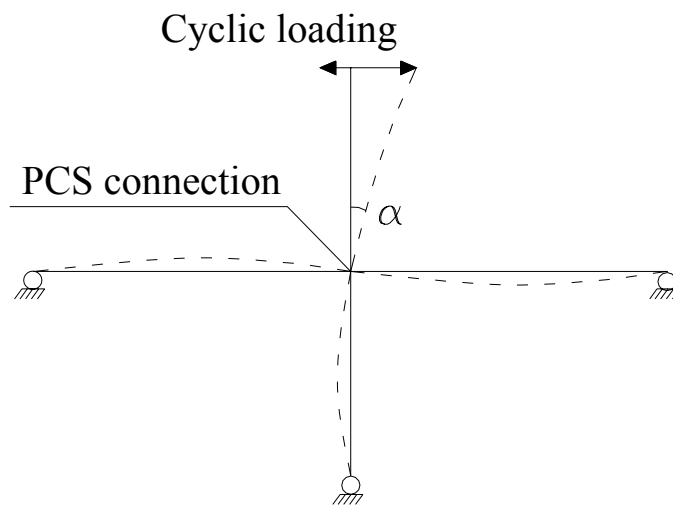


Figure 6.1: Suggested test setup

The test setup is an interior beam-column subassembly consisting of steel beams and PC columns. The beam-column joint is the target of the test. Since the beam ends and column ends are free of rotation, the overall deflection angle α is contributed by the beam-column joint. Then instrumentation shall be provided at column joint region and the shear deformation of the column joint is measured. By this way the rotation of the rigid-plastic beam-column hinge can be determined.

The modeling of beam-column hinge can be used for the development of performance-based design methodology, which requires an accurate nonlinear modeling of structural components.

Notation

The following symbols are used in this paper:

- M_{ct}, M_{cb} = bending moment at top and bottom sections of joint region;
- V_{ct}, V_{cb} = Shear force at top and bottom sections of joint region;
- P_{col} = column axial load;
- $M_{lbo},$
 M_{rbo} = beam overstrengthened end moment at left and right side of joint region;
- V_{lb}, V_{rb} = beam shear force at left and right side of joint region;
- N_{pl} = normal force between endplate and column face due to compression;
- T_{st}, T_{sb} = steel tension force at top and bottom section of joint region;
- C_{ct}, C_{cb} = internal concrete compression force at top and bottom of joint region;
- $M_{i,RBS}$ = ideal plastic moment at reduced beam section;
- Z_{RBS} = plastic sectional modulus at reduced beam section;
- F_y = specified yield strength of steel beam material;
- M_{BE} = flexural moment at beam end section;
- L_c = span length between reduced beam sections;
- L' = distance between reduced beam section and adjacent column face;
- $M_{pr,BE}$ = most probable plastic moment at beam end section;
- λ_o = overstrength factor;
- M_{PL} = ideal flexural strength of end-plate;
- F_{py} = specified yield strength of end-plate material;
- t_p = end-plate thickness;

- Y = parameter reflecting yield mechanism of end-plate;
- b_p = width of end-plate;
- h_i, h_o = end-plate geometric parameters as shown in Fig. 3;
- g, s = end-plate geometric parameters as shown in Fig. 3;
- p_{fo}, p_{fi} = end-plate geometric parameters as shown in Fig. 3;
- t_f = thickness of beam flange;
- ϕ_{pl}, ϕ_r = strength reduction factors for end-plate and steel rods;
- F_b, f_t = specified tensile strength of post-tensioning rod;
- M_R = Moment strength provided by the end-plate and steel rods;
- d_i = Distance from center line of the i th row steel rods to end-plate edge;
- D = nominal diameter of steel rods;
- V_D, V_L = shear due to dead and live loads, respectively;
- P_{pre} = pretension force for each steel rod;
- γ_D, γ_L = Load combination factors for dead and live loads;
- f = friction coefficient;
- V_{nE} = nominal shear demand due to seismic load;
- V_u = factored shear demand;
- V_n = nominal shear capacity;
- T_i = Tension force of each of i th row steel rods;
- V_{jh}, V_{jv} = horizontal and vertical shear forces at middle section of joint region;
- V_{col} = horizontal shear load transferred to joint region;
- h_b, h_c = effective depths of beam and column, respectively;

p_c, p_t = principle stresses;

f_h, f_v = horizontal and vertical normal stresses of joint center;

θ, θ_y = first-story drift ratio and first-story drift ratio corresponding to first yield;

H_l = first story height;

Δ_l = lateral displacement of first story;

μ = drift ductility.

V_{iy}, V_{if} = System lateral yield strength and flexural strength.

Bibliography

1. ACI. (1999). Building code requirements for reinforced concrete. *ACI 318-99*, Farmington Hills, Michigan.
2. AISC. (1997). *Seismic provisions for structural steel buildings*. Chicago.
3. AISC. (2001). *Manual of steel construction-load and resistance factor design*, 3rd Ed., Chicago.
4. Chou C.C, Uang C.M. (1998), “Experimental and analytical studies of two types of moment connections for composite special moment frames.” Report No. SSRP 98-12, San Diego, La Jolla, CA, Department of Structural Engineering, University of California.
5. Deierlein, G.G., and Noguchi, H., (2004), “Overview of U.S.-Japan research on the seismic design of composite reinforced concrete and steel moment frame structures.” *J. of Struc. Eng.*, 130(2), 361-367.
6. Englekirk R.E. (1994), *Steel structures: controlling behavior through design*, 1st Edition, John Wiley & Sons, Inc., New York.
7. Griffis, L. G. (1992). “Composite frame construction.” *Constructional steel design—An Int. guide*, P. Dowling, J. Harding, and R. Bjorhovde, eds., Elsevier Applied Science, New York, 523–554.
8. Kurama, Y.C., Pessiki, S., Sause, R., and Lu, L.W. (1999), “seismic Behavior and Design of Unbonded Post-Tensioned Precast Concrete Walls”, *PCI Journal*, Precast/Prestressed Concrete Institute, 44(3), 72-89.
9. Li, X.; Wu, Y.T.; Mao, W.F.; Xiao, Y.; Anderson, J.C.; Guo, Y.R., (2006) “Bolted End Plate Connections for Steel Reinforced Concrete Composite Structures,” *Journal of Structural Engineering and Mechanics*, Vol. 24, No.3, October, pp.291-306.
10. Murray, T.M.; Sumner E.A., (2004), *Extended End-Plate Moment Connections*, American Institute of Steel Construction, Inc., 2004.
11. PCI. (1999). *PCI design handbook*, 5th Edition, Precast/Prestressed Concrete Institute, Chicago.

12. Sheikh, T. M., Deierlein, G. G., Yura, J. A., and Jirsa, J. O. (1989), "Beam-column moment connections for composite frames: Part 1." *J. Struct. Eng.*, 115(11), 2858–2876.

13. Stone, W.C., Cheok, G.S., and Stanton, J.F. (1995). "Performance of hybrid moment-resisting precast beam-column concrete connections subjected to cyclic loading." *ACI struct. J.*, 91(2), 229-249.

14. Xiao, Y.; J. C. Anderson, and Wu, Y.T. (2003) "Development of Bolted End Plate Connections for Steel Reinforced Concrete Composite Structures," *Advances in Structures Steel, Concrete, Composite and Aluminum*, ASSCCA 2003, Sidney, Australia, June 23-25.

Appendix A: Structural Design of Prototype Buildings

A.1 Building Codes and Computer Programs

The design of the prototype buildings follows relevant provisions of IBC2000. Specifically, design of reinforced concrete and steel members of gravity system follows ACI318-02 and AISC 360-05 LRFD, respectively. The live loads reduction follows the alternate method of IBC2000. The seismic load analysis follows provisions in ASCE 7-05.

The gravity system design of the prototype buildings is conducted using the computer program RAM Version 11.3.1. For the lateral force resisting system design, the computer program ETABS Nonlinear Version 8 is used.

A.2 Existing Steel Office Building

The 13-story steel office building is located in South Fernando Valley about 5 km southwest of the Northridge epicenter. It is composed of one basement floor and 13 floors above ground. The footprint of the 13-story building is 160 feet by 160 feet. The exterior frames of the structure are the moment resisting frames while the interior frames are gravity load carrying only. The foundation consists of piles, pile caps and grade beams. The floor plan view of the perimeter frames and a typical elevation of one of these frames

are shown in Figure A.1 and Figure A.2. The member sizes are given in Table A.1. The typical floor system consists of about 2.5 in. of concrete fill over 3 in. 20-gage steel decking. The roof system is lighter with 2.25 in. of vermiculite fill on 3-in. 20-gage steel decking. 3 ksi concrete was specified for all deck fill. Exterior walls are composed of 6-in. 22-gage steel studs with 0.25 in. opaque glass and 2-in. precast panels. A total uniform load of 102.5 psf was used to calculate the building mass properties and axial load on columns.

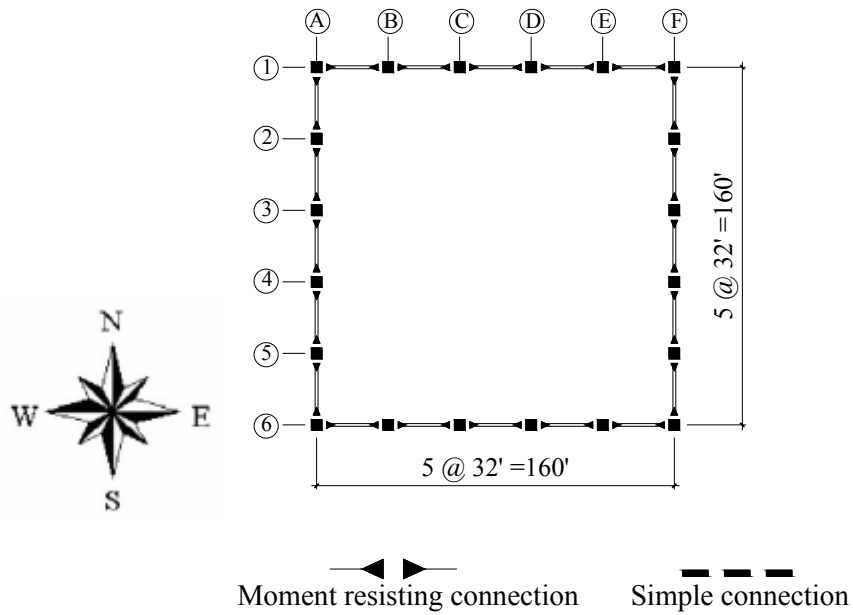


Figure A.1: Plan view of perimeter frames

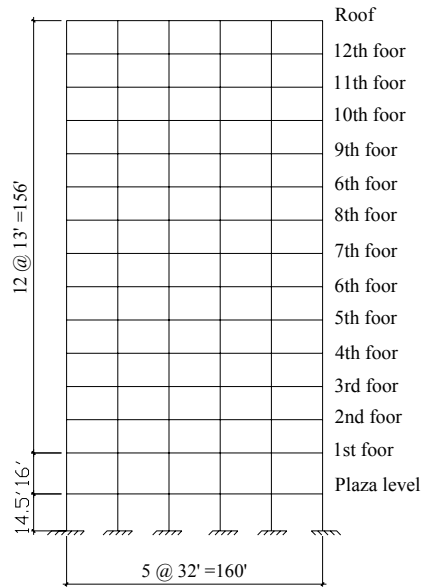


Figure A.2: Elevation of perimeter frame

Table A.1: Member sizes of 13-story steel prototype building

| COLUMNS | | | | | | |
|---------|---------|---------|---------|---------|---------|---------|
| Story | A | B | C | D | E | F |
| Plaza | W14×500 | W14×500 | W14×500 | W14×500 | W14×500 | W14×500 |
| 1 | W14×500 | W14×500 | W14×500 | W14×500 | W14×500 | W14×500 |
| 2-3 | W14×426 | W14×426 | W14×426 | W14×426 | W14×426 | W14×426 |
| 4-5 | W14×398 | W14×398 | W14×398 | W14×398 | W14×398 | W14×398 |
| 6-7 | W14×311 | W14×311 | W14×311 | W14×311 | W14×311 | W14×311 |
| 8-9 | W14×283 | W14×283 | W14×283 | W14×283 | W14×283 | W14×283 |
| 10-11 | W14×257 | W14×257 | W14×257 | W14×257 | W14×257 | W14×257 |
| 12-13 | W14×176 | W14×176 | W14×176 | W14×176 | W14×176 | W14×176 |
| BEAMS | | | | | | |
| Story | A-B | B-C | C-D | D-E | E-F | - |
| Plaza | W33×201 | W33×201 | W33×201 | W33×201 | W33×201 | - |
| 1 | W36×232 | W36×232 | W36×232 | W36×232 | W36×232 | - |
| 2-6 | W33×152 | W33×152 | W33×152 | W33×152 | W33×152 | - |
| 7-8 | W33×141 | W33×141 | W33×141 | W33×141 | W33×141 | - |
| 9-10 | W33×130 | W33×130 | W33×130 | W33×130 | W33×130 | - |
| 11-12 | W33×118 | W33×118 | W33×118 | W33×118 | W33×118 | - |
| Roof | W27×84 | W27×84 | W27×84 | W27×84 | W27×84 | - |

A.3 Equivalent RC Members

In order to carry out the design procedure for the hybrid PCS and RC buildings out of the existing prototype steel building, the equivalent RC member sizes are determined first.

The equivalency of steel member and RC member is based on two criteria:

1) Flexural stiffness of the cross section. Note that the cracking of concrete section is considered for RC beam and RC column, respectively.

$$0.35E_cI_g = E_sI_s \quad \text{for RC beam;}$$

$$0.70E_cI_g = E_sI_s \quad \text{for RC column}$$

Where E_c and E_s are the Young's modulus of concrete and steel material; I_g and I_s are the moment of inertia of the gross concrete column section and steel column section.

$$E_c = 57000\sqrt{f'_c} \text{ in psi and } E_s = 29,000,000 \text{ psi}$$

2) Strong column-weak beam relationship

The strong column-weak beam is a fundamental principle for design of special moment resisting frame. After a preliminary selection of RC member sizes according to the flexural stiffness, the moment strength between steel beam and RC column in PCS frame and the moment strength between RC beam and RC column must be checked to see if the strong column-weak beam relationship can be satisfied.

Table A.2 lists the equivalent concrete section sizes. Notice that the RC columns are all square. For the equivalent RC beams, the depths are maintained similar to those of steel beams in order to keep the same clear story height.

Table A.2: Equivalent concrete column sizes

| Level | Steel column | | | RC column | | |
|-------|--------------|-------|-----------|-----------|----------------------|---------------------|
| | Shape | I_s | $E_s I_s$ | I_g | h_{nominal} | H_{design} |
| Roof | W14X176 | 2140 | 62060000 | 21997 | 23 | 24 |
| 12 | W14X176 | 2140 | 62060000 | 21997 | 23 | 24 |
| 11 | W14X257 | 3400 | 98600000 | 34948 | 25 | 26 |
| 10 | W14X257 | 3400 | 98600000 | 34948 | 25 | 26 |
| 9 | W14X283 | 3840 | 111360000 | 39470 | 26 | 28 |
| 8 | W14X283 | 3840 | 111360000 | 39470 | 26 | 28 |
| 7 | W14X311 | 4330 | 125570000 | 44507 | 27 | 28 |
| 6 | W14X311 | 4330 | 125570000 | 44507 | 27 | 28 |
| 5 | W14X398 | 6000 | 174000000 | 61672 | 29 | 30 |
| 4 | W14X398 | 6000 | 174000000 | 61672 | 29 | 30 |
| 3 | W14X426 | 6600 | 191400000 | 67840 | 30 | 32 |
| 2 | W14X426 | 6600 | 191400000 | 67840 | 30 | 32 |
| 1 | W14X500 | 8210 | 238090000 | 84388 | 32 | 34 |
| Plaza | W14X500 | 8210 | 238090000 | 84388 | 32 | 34 |

Table A.3: Equivalent concrete beam sizes

| Level | Steel beam | | | | RC beam | | |
|-------|------------|-------|-----------|------|---------|-----|-----|
| | Shape | I_s | $E_s I_s$ | d | I_g | h | b |
| Roof | W27X84 | 2850 | 82650000 | 26.7 | 58589 | 28 | 32 |
| 12 | W33X118 | 5900 | 171100000 | 32.9 | 121289 | 34 | 38 |
| 11 | W33X118 | 5900 | 171100000 | 32.9 | 121289 | 34 | 38 |
| 10 | W33X130 | 6710 | 194590000 | 33.1 | 137941 | 34 | 42 |
| 9 | W33X130 | 6710 | 194590000 | 33.1 | 137941 | 34 | 42 |
| 8 | W33X141 | 7450 | 216050000 | 33.3 | 153153 | 34 | 48 |
| 7 | W33X141 | 7450 | 216050000 | 33.3 | 153153 | 34 | 48 |
| 6 | W33X152 | 8160 | 236640000 | 33.5 | 167749 | 34 | 52 |
| 5 | W33X152 | 8160 | 236640000 | 33.5 | 167749 | 34 | 52 |
| 4 | W33X152 | 8160 | 236640000 | 33.5 | 167749 | 34 | 52 |
| 3 | W33X152 | 8160 | 236640000 | 33.5 | 167749 | 34 | 52 |
| 2 | W33X152 | 8160 | 236640000 | 33.5 | 167749 | 34 | 52 |
| 1 | W36X232 | 15000 | 435000000 | 37.1 | 308362 | 38 | 68 |
| Plaza | W33X201 | 11600 | 336400000 | 33.7 | 238467 | 34 | 74 |

According to Table A.2 and Table A.3, the preliminary member sizes for the conventional RC frame and hybrid PCS frame can be summarized as shown in Table A.4 and Table A.5.

Table A.4: Member sizes of 13-story RC prototype frame

| COLUMNS | | | | | | |
|---------|-------|-------|-------|-------|-------|-------|
| Story | A | B | C | D | E | F |
| 12-13 | 24×24 | 24×24 | 24×24 | 24×24 | 24×24 | 24×24 |
| 10-11 | 26×26 | 26×26 | 26×26 | 26×26 | 26×26 | 26×26 |
| 8-9 | 28×28 | 28×28 | 28×28 | 28×28 | 28×28 | 28×28 |
| 6-7 | 28×28 | 28×28 | 28×28 | 28×28 | 28×28 | 28×28 |
| 4-5 | 30×30 | 30×30 | 30×30 | 30×30 | 30×30 | 30×30 |
| 2-3 | 32×32 | 32×32 | 32×32 | 32×32 | 32×32 | 32×32 |
| 1 | 34×34 | 34×34 | 34×34 | 34×34 | 34×34 | 34×34 |
| Plaza | 34×34 | 34×34 | 34×34 | 34×34 | 34×34 | 34×34 |
| BEAMS | | | | | | |
| Story | A-B | B-C | C-D | D-E | E-F | - |
| Roof | 32×28 | 32×28 | 32×28 | 32×28 | 32×28 | - |
| 11-12 | 38×34 | 38×34 | 38×34 | 38×34 | 38×34 | - |
| 9-10 | 42×34 | 42×34 | 42×34 | 42×34 | 42×34 | - |
| 7-8 | 48×34 | 48×34 | 48×34 | 48×34 | 48×34 | - |
| 2-6 | 52×34 | 52×34 | 52×34 | 52×34 | 52×34 | - |
| 1 | 68×38 | 68×38 | 68×38 | 68×38 | 68×38 | - |
| Plaza | 74×34 | 74×34 | 74×34 | 74×34 | 74×34 | - |

Table A.5: Member sizes of 13-story PCS prototype frame

| COLUMNS | | | | | | |
|---------|---------|---------|---------|---------|---------|-------|
| Story | A | B | C | D | E | F |
| 12-13 | 24×24 | 24×24 | 24×24 | 24×24 | 24×24 | 24×24 |
| 10-11 | 26×26 | 26×26 | 26×26 | 26×26 | 26×26 | 26×26 |
| 8-9 | 28×28 | 28×28 | 28×28 | 28×28 | 28×28 | 28×28 |
| 6-7 | 28×28 | 28×28 | 28×28 | 28×28 | 28×28 | 28×28 |
| 4-5 | 30×30 | 30×30 | 30×30 | 30×30 | 30×30 | 30×30 |
| 2-3 | 32×32 | 32×32 | 32×32 | 32×32 | 32×32 | 32×32 |
| 1 | 34×34 | 34×34 | 34×34 | 34×34 | 34×34 | 34×34 |
| Plaza | 34×34 | 34×34 | 34×34 | 34×34 | 34×34 | 34×34 |
| BEAMS | | | | | | |
| Story | A-B | B-C | C-D | D-E | E-F | - |
| Roof | W33×201 | W33×201 | W33×201 | W33×201 | W33×201 | - |
| 11-12 | W36×232 | W36×232 | W36×232 | W36×232 | W36×232 | - |
| 9-10 | W33×152 | W33×152 | W33×152 | W33×152 | W33×152 | - |
| 7-8 | W33×141 | W33×141 | W33×141 | W33×141 | W33×141 | - |
| 2-6 | W33×130 | W33×130 | W33×130 | W33×130 | W33×130 | - |
| 1 | W33×118 | W33×118 | W33×118 | W33×118 | W33×118 | - |
| Plaza | W27×84 | W27×84 | W27×84 | W27×84 | W27×84 | - |

It must be pointed out that the equivalent RC beam sizes shown in Table A.4 are not realistic since beam width rarely exceeds depth in actual RC beam design. The RC beam sizes based on the flexural stiffness listed in Table A.4 are accepted in that the beam depths maintain the same story clear height as those of the prototype steel building.

A.4 Seismic Load Analysis

A.4.1 Approximate fundamental period T_a

Equation 9.5.5.3.2-1 of ASCE 7-05 is used to compute the fundamental period (T_a) of the prototype structure.

$$T_a = C_t h_n^x \quad (\text{Eqn. 4.1})$$

Where h_n is the building height in ft above the base to the highest level of the structure and the numerical coefficients C_t and x are determined from the type of structural system. Since hybrid PCS system combines the reinforced concrete and steel moment resisting frame, its coefficients C_t and x can be taken as the average values of those for conventional RC and conventional steel moment frames. As a result, C_t and x are taken as 0.022 and 0.85 for the PCS moment frames. The approximate fundamental periods for the S, PCS and RC prototype buildings are 1.835 sec., 1.873 sec. and 1.769 sec. respectively.

A.4.2 Seismic weight W

The seismic weight of the prototype buildings consists of all material weight and superimposed dead load.

Table A.6: Seismic weight of prototype buildings(kips)

| Story Level | Steel | PCS | RC |
|-------------|-------|-------|-------|
| Roof | 676 | 808 | 1484 |
| 12 | 1352 | 1485 | 2534 |
| 11 | 1352 | 1492 | 2542 |
| 10 | 1352 | 1492 | 2625 |
| 9 | 1352 | 1519 | 2652 |
| 8 | 1352 | 1519 | 2781 |
| 7 | 1352 | 1510 | 2772 |
| 6 | 1352 | 1510 | 2855 |
| 5 | 1352 | 1521 | 2866 |
| 4 | 1352 | 1521 | 2866 |
| 3 | 1352 | 1552 | 2898 |
| 2 | 1352 | 1552 | 2898 |
| 1 | 1503 | 1773 | 3641 |
| Plaza | 1573 | 1818 | 3673 |
| Σ | 18628 | 21072 | 39085 |

A.4.3 Seismic design base shear V

The seismic design base shears are calculated using the spreadsheets shown below.

BASE SHEAR OF STEEL BUILDING 2007 CBC / ASCE 7-05 Equivalent Lateral Force Procedure

Building Data

Occupancy Category = **I** Table 1604.5, 2007 CBC Importance Factor, $I = 1.00$ Table 11.5-1

Seismic Ground Motion Values Section 11.4

| | | | | | |
|--------------|--------------|----------------------------------|--------------------------|--------------|--------------|
| $S_S =$ | 1.500 | From geotech or Figs. 22-1 to 14 | $F_a =$ | 1.00 | Table 11.4-1 |
| $S_1 =$ | 0.600 | From geotech or Figs. 22-1 to 14 | $F_v =$ | 1.50 | Table 11.4-2 |
| Site Class = | D | From geotech or Table 20.3-1 | $S_{MS} = F_a S_S =$ | 1.500 | Eq. 11.4-1 |
| $T_L =$ | 8 sec | Figs. 22-15 to 20 | $S_{M1} = F_v S_1 =$ | 0.900 | Eq. 11.4-2 |
| | | | $S_{DS} = (2/3)S_{MS} =$ | 1.000 | Eq. 11.4-3 |
| | | | $S_{D1} = (2/3)S_{M1} =$ | 0.600 | Eq. 11.4-4 |

Seismic Design Category **D** Tables 11.6-1 & 2

Building Period Section 12.8.2

| | | | | | |
|---------|------------------|---|--------------------------|------------------|----------------|
| $C_t =$ | 0.028 | Table 12.8-2 | $T_a = C_t h_n^x =$ | 1.835 sec | Eq. 12.8-7 |
| $x =$ | 0.8 | Table 12.8-2 | $C_u =$ | 1.40 | Table 12.8-1 |
| $h_n =$ | 186.50 ft | Height of Building | $T_{a, max} = C_u T_a =$ | 2.569 sec | Section 12.8.2 |
| $T_b =$ | 0.000 sec | From Analysis (Input zero to use T_a) | | | |

Period = 1.835 sec <-- used for design
1.835 sec <-- used for drift
Section 12.8.6.2

Base Shear Section 12.8

| | | |
|---------|--------------------|------------------------|
| $W =$ | 18,628 kips | Total Structure Weight |
| $R =$ | 8 | Table 12.2-1 |
| $C_d =$ | 5.5 | Table 12.2-1 |

For Design Only

| | | |
|----------------|----------------------------------|--------------------------------|
| $C_{s, max} =$ | $S_{DS} / (R/I) = 0.125$ | Eq. 12.8-2 |
| $C_s =$ | $S_{D1} / [T (R/I)] = 0.041$ | Eq. 12.8-3, for $T \leq T_L$ |
| $C_s =$ | $S_{D1} T_L / [T^2 (R/I)] = N/A$ | Eq. 12.8-4, for $T > T_L$ |
| $C_{s, min} =$ | 0.01 | Eq. 12.8-5 |
| $C_{s, min} =$ | $0.5S_1 / (R/I) = 0.038$ | Eq. 12.8-6, if $S_1 \geq 0.6g$ |

Use, $C_s = 0.041$

$V_{design} = C_s W = 761$ kips Eq. 12.8-1

For Drift Only

| | |
|----------------|-------|
| $C_{s, max} =$ | 0.125 |
| $C_s =$ | 0.041 |
| $C_s =$ | N/A |
| $C_{s, min} =$ | 0.01 |
| $C_{s, min} =$ | 0.038 |

Use, $C_s = 0.041$

$V_{drift} = C_s W = 761$ kips
Allowable Drift = **0.025 h_{sx}**
Table 12.12-1

* Note: All references are from ASCE 7-05 unless noted otherwise.

BASE SHEAR OF PCS BUILDING

2007 CBC / ASCE 7-05 Equivalent Lateral Force Procedure

Building Data

Occupancy Category = **I** Table 1604.5, 2007 CBC Importance Factor, I = **1.00** Table 11.5-1

Seismic Ground Motion Values Section 11.4

| | | | | | |
|--------------|--------------|----------------------------------|--------------------------|--------------|--------------|
| $S_S =$ | 1.500 | From geotech or Figs. 22-1 to 14 | $F_a =$ | 1.00 | Table 11.4-1 |
| $S_1 =$ | 0.600 | From geotech or Figs. 22-1 to 14 | $F_v =$ | 1.50 | Table 11.4-2 |
| Site Class = | D | From geotech or Table 20.3-1 | $S_{MS} = F_a S_S =$ | 1.500 | Eq. 11.4-1 |
| $T_L =$ | 8 sec | Figs. 22-15 to 20 | $S_{M1} = F_v S_1 =$ | 0.900 | Eq. 11.4-2 |
| | | | $S_{DS} = (2/3)S_{MS} =$ | 1.000 | Eq. 11.4-3 |
| | | | $S_{D1} = (2/3)S_{M1} =$ | 0.600 | Eq. 11.4-4 |

Seismic Design Category **D** Tables 11.6-1 & 2

Building Period Section 12.8.2

| | | | | | |
|---------|------------------|---|--------------------------|------------------|-----------------|
| $C_t =$ | 0.022 | Table 12.8-2 | $T_a = C_t h_n^x =$ | 1.873 sec | Eq. 12.8-7 |
| $x =$ | 0.85 | Table 12.8-2 | $C_u =$ | 1.40 | Table 12.8-1 |
| $h_n =$ | 186.50 ft | Height of Building | $T_{a, max} = C_u T_a =$ | 2.622 sec | Section. 12.8.2 |
| $T_b =$ | 0.000 sec | From Analysis (Input zero to use T_a) | | | |

Period = 1.873 sec <-- used for design
1.873 sec <-- used for drift
 Section. 12.8.6.2

Base Shear Section 12.8

| | | |
|---------|--------------------|------------------------|
| $W =$ | 21,072 kips | Total Structure Weight |
| $R =$ | 8 | Table 12.2-1 |
| $C_d =$ | 5.5 | Table 12.2-1 |

For Design Only

| | | |
|----------------|----------------------------------|--------------------------------|
| $C_{s, max} =$ | $S_{DS} / (R/I) = 0.125$ | Eq. 12.8-2 |
| $C_s =$ | $S_{D1} / [T (R/I)] = 0.040$ | Eq. 12.8-3, for $T \leq T_L$ |
| $C_s =$ | $S_{D1} T_L / [T^2 (R/I)] = N/A$ | Eq. 12.8-4, for $T > T_L$ |
| $C_{s, min} =$ | 0.01 | Eq. 12.8-5 |
| $C_{s, min} =$ | $0.5S_1 / (R/I) = 0.038$ | Eq. 12.8-6, if $S_1 \geq 0.6g$ |

Use, $C_s = 0.040$

$V_{design} = C_s W = 844 \text{ kips}$ Eq. 12.8-1

For Drift Only

| | |
|----------------|-------|
| $C_{s, max} =$ | 0.125 |
| $C_s =$ | 0.040 |
| $C_s =$ | N/A |
| $C_{s, min} =$ | 0.01 |
| $C_{s, min} =$ | 0.038 |

Use, $C_s = 0.040$

$V_{drift} = C_s W = 844 \text{ kips}$
Allowable Drift = 0.025 h_{sx}
 Table 12.12-1

* Note : All references are from ASCE 7-05 unless noted otherwise.

BASE SHEAR OF RC BUILDING ASCE 7-05 Equivalent Lateral Force Procedure

Building Data

Occupancy Category = **I** Table 1604.5, 2007 CBC Importance Factor, $I = 1.00$ Table 11.5-1

Seismic Ground Motion Values Section 11.4

| | | | |
|-----------------------|----------------------------------|---------------------------------|--------------|
| $S_S = 1.500$ | From geotech or Figs. 22-1 to 14 | $F_a = 1.00$ | Table 11.4-1 |
| $S_1 = 0.600$ | From geotech or Figs. 22-1 to 14 | $F_v = 1.50$ | Table 11.4-2 |
| Site Class = D | From geotech or Table 20.3-1 | $S_{MS} = F_a S_S = 1.500$ | Eq. 11.4-1 |
| $T_L = 8 \text{ sec}$ | Figs. 22-15 to 20 | $S_{M1} = F_v S_1 = 0.900$ | Eq. 11.4-2 |
| | | $S_{DS} = (2/3) S_{MS} = 1.000$ | Eq. 11.4-3 |
| | | $S_{D1} = (2/3) S_{M1} = 0.600$ | Eq. 11.4-4 |

Seismic Design Category

D Tables 11.6-1 & 2

Building Period Section 12.8.2

| | | | |
|---------------------------|---|---|----------------|
| $C_t = 0.016$ | Table 12.8-2 | $T_a = C_t h_n^x = 1.769 \text{ sec}$ | Eq. 12.8-7 |
| $x = 0.9$ | Table 12.8-2 | $C_u = 1.40$ | Table 12.8-1 |
| $h_n = 186.50 \text{ ft}$ | Height of Building | $T_{a, \text{max}} = C_u T_a = 2.477 \text{ sec}$ | Section 12.8.2 |
| $T_b = 0.000 \text{ sec}$ | From Analysis (Input zero to use T_a) | | |

Period = 1.769 sec «-- used for design
1.769 sec «-- used for drift
Section 12.8.6.2

Base Shear Section 12.8

$W = 39,085 \text{ kips}$ Total Structure Weight
 $R = 8$ Table 12.2-1
 $C_d = 5.5$ Table 12.2-1

For Design Only

| | | |
|-----------------------|---|--------------------------------|
| $C_{s, \text{max}} =$ | $S_{DS} / (R/I) = 0.125$ | Eq. 12.8-2 |
| $C_s =$ | $S_{D1} / [T (R/I)] = 0.042$ | Eq. 12.8-3, for $T \leq T_L$ |
| $C_s =$ | $S_{D1} T_L / [T^2 (R/I)] = \text{N/A}$ | Eq. 12.8-4, for $T > T_L$ |
| $C_{s, \text{min}} =$ | 0.01 | Eq. 12.8-5 |
| $C_{s, \text{min}} =$ | $0.5 S_I / (R/I) = 0.038$ | Eq. 12.8-6, if $S_I \geq 0.6g$ |

Use, $C_s = 0.042$

$V_{\text{design}} = C_s W = 1,657 \text{ kips}$ Eq. 12.8-1

For Drift Only

| | |
|-----------------------|-------|
| $C_{s, \text{max}} =$ | 0.125 |
| $C_s =$ | 0.042 |
| $C_s =$ | N/A |
| $C_{s, \text{min}} =$ | 0.01 |
| $C_{s, \text{min}} =$ | 0.038 |

Use, $C_s = 0.042$

$V_{\text{drift}} = C_s W = 1,657 \text{ kips}$
Allowable Drift = 0.025 h_{sx}
Table 12.12-1

* Note: All references are from ASCE 7-05 unless noted otherwise.

A.4.4 Vertical distribution of design base shear F_x

The base shear is distributed over the height of the building. According to Eq. 9.5.5.4-1 and Eq. 9.5.5.4-1, the lateral force induced at each level can be calculated by,

$$F_x = C_{vx} V$$

and

$$C_{vx} = \frac{w_x h_x^k}{\sum_{i=1}^n w_i h_i^k}$$

The coefficient k is computed according to the fundamental period T . For structures having a period of 0.5 sec or less, k equals 1.0. For structures having a period of 2.5 sec or more, k equals 2.0. For structures having a period between 0.5 sec and 2.5 sec, k can be determined by linear interpolation between 1 and 2.

Table A.7: Seismic forces and story shears of steel building ($V = 761$ kips)

| Level | Story weight w_x (kips) | Height (ft) | $w_x h_x^k$ ($k=1.677$) | Lateral force F_x (kips) | Story shear V_x (kips) |
|----------|------------------------------|----------------|------------------------------|-------------------------------|-----------------------------|
| 14 | 676 | 186.5 | 4343853 | 71 | 71 |
| 13 | 1352 | 173.5 | 7696299 | 126 | 196 |
| 12 | 1352 | 160.5 | 6753958 | 110 | 307 |
| 11 | 1352 | 147.5 | 5861934 | 96 | 402 |
| 10 | 1352 | 134.5 | 5021621 | 82 | 484 |
| 9 | 1352 | 121.5 | 4234587 | 69 | 553 |
| 8 | 1352 | 108.5 | 3502615 | 57 | 610 |
| 7 | 1352 | 95.5 | 2827759 | 46 | 657 |
| 6 | 1352 | 82.5 | 2212432 | 36 | 693 |
| 5 | 1352 | 69.5 | 1659530 | 27 | 720 |
| 4 | 1352 | 56.5 | 1172633 | 19 | 739 |
| 3 | 1352 | 43.5 | 756350.6 | 12 | 751 |
| 2 | 1503 | 30.5 | 463585.5 | 8 | 759 |
| 1 | 1573 | 14.5 | 139425.7 | 2 | 761 |
| Σ | | | 46646582 | | |

Table A.8: Seismic forces and story shears of PCS building (V = 844 kips)

| Level | Story weight w_x (kips) | Height (ft) | $w_x h_x^k$ ($k=1.687$) | Lateral force F_x (kips) | Story shear V_x (kips) |
|----------|------------------------------|----------------|------------------------------|-------------------------------|-----------------------------|
| 14 | 808 | 186.5 | 5470746 | 84 | 84 |
| 13 | 1485 | 173.5 | 8900710 | 137 | 221 |
| 12 | 1492 | 160.5 | 7841609 | 121 | 341 |
| 11 | 1492 | 147.5 | 6800189 | 105 | 446 |
| 10 | 1519 | 134.5 | 5925326 | 91 | 537 |
| 9 | 1519 | 121.5 | 4991579 | 77 | 614 |
| 8 | 1510 | 108.5 | 4099651 | 63 | 677 |
| 7 | 1510 | 95.5 | 3305542 | 51 | 727 |
| 6 | 1521 | 82.5 | 2601280 | 40 | 767 |
| 5 | 1521 | 69.5 | 1947859 | 30 | 797 |
| 4 | 1552 | 56.5 | 1401514 | 22 | 819 |
| 3 | 1552 | 43.5 | 901619.1 | 14 | 833 |
| 2 | 1773 | 30.5 | 565877.7 | 9 | 841 |
| 1 | 1818 | 14.5 | 165509 | 3 | 844 |
| Σ | | | 54919012 | | |

Table A.9: Seismic forces and story shears of RC building (V = 1657 kips)

| Level | Story weight w_x (kips) | Height (ft) | $w_x h_x^k$ ($k=1.635$) | Lateral force F_x (kips) | Story shear V_x (kips) |
|----------|------------------------------|----------------|------------------------------|-------------------------------|-----------------------------|
| 14 | 1484 | 186.5 | 7655857 | 166 | 166 |
| 13 | 2534 | 173.5 | 11616125 | 252 | 418 |
| 12 | 2542 | 160.5 | 10259524 | 223 | 641 |
| 11 | 2625 | 147.5 | 9227929 | 200 | 841 |
| 10 | 2652 | 134.5 | 8017417 | 174 | 1015 |
| 9 | 2781 | 121.5 | 7120053 | 155 | 1170 |
| 8 | 2772 | 108.5 | 5898218 | 128 | 1298 |
| 7 | 2855 | 95.5 | 4930735 | 107 | 1405 |
| 6 | 2866 | 82.5 | 3896533 | 85 | 1489 |
| 5 | 2866 | 69.5 | 2943888 | 64 | 1553 |
| 4 | 2898 | 56.5 | 2121767 | 46 | 1599 |
| 3 | 2898 | 43.5 | 1383657 | 30 | 1629 |
| 2 | 3641 | 30.5 | 972861.3 | 21 | 1650 |
| 1 | 3673 | 14.5 | 290976.3 | 6 | 1657 |
| Σ | | | 76335540 | | |

A.5 Three-dimensional Linear Static Analysis of Prototype Buildings

A.5.1 Modeling of prototype buildings for linear static analysis with ETABS

Three-dimensional analysis of the building was performed for the seismic forces listed in Table A.7 through Table A.9, using ETABS V8. In the models, rigid diaphragms were assigned at each floor level, and rigid end offsets were defined at the ends of each horizontal member of the moment resisting frames so that results were automatically obtained at the faces of each support. The interior gravity load carrying frames are not included in the ETABS models of each prototype building. For the steel beams of perimeter moment resisting frames, the reduction of flexural stiffness due to the reduced beam section was considered since ETABS provides the modeling of RBS in steel beam types. The post-tensioned beam-column connection was assumed rigid. This assumption is only valid for the linear static analysis. For the nonlinear static and nonlinear dynamic analyses of the perimeter moment resisting frames, which are conducted in chapter 5, the post-tensioned beam-column connections and the reduced beam sections are simulated with reasonable models that can capture their major inelastic behaviors. For the steel beams, the portion of the adjoining composite slab was not included in the analysis as part of the beam. For the reinforced concrete columns, the stiffness properties were input assuming cracked sections. It was taken as $0.70I_g$ for the column cross sections, where I_g is the moment of inertia of the gross section.

The mass at each level was assumed to be displaced from the calculated center of mass a distance equal to 5 percent of the building dimension at that level perpendicular to the direction of the force under consideration.

A.5.2 Lateral Drifts and Inter-story Drifts

Table A.10 summarizes the lateral displacements and drifts of each floor of each prototype building due to seismic forces. δ_{xe} is the lateral deflection determined by the three-dimensional elastic analysis. δ_x is the lateral deflection amplified by the deflection amplification factor C_d . it is computed by

$$\delta_x = \frac{C_d \delta_{xe}}{I}$$

Where I is the importance factor and C_d is shown in Table 9.5.2.2 of ASCE 7-05. Since the amplification factors for both steel special moment frames and special reinforced concrete frames are 5.5, C_d for the hybrid PCS moment frame is also 5.5.

According to 9.5.5.7.1 of ASCE 7-05, the calculated story drifts using δ_x shall not exceed 0.025 times the story height for structures having a fundamental period of 0.7 sec or greater. The use of 0.025 instead of 0.020 is because the prototype buildings are located in seismic design category D, which leads to the stringent requirement that every structural component not included in the lateral force resisting system in the direction under consideration shall be designed to be adequate for the gravity load effects and the seismic forces resulting from displacements to the design story drift determined above. For the 13 feet, 16 feet and 14.5 feet story heights, the maximum drifts are equal to 3.9

in., 4.8 in. and 4.35 in. It is clear from Table A.10 that for all stories of the prototype buildings the lateral drifts obtained from the prescribed lateral forces are less than the limiting values.

Table A.10: Lateral displacements and drifts of prototype buildings (in.)

| Level | S | | | PCS | | | RC | | |
|-------|---------------|------------|----------|---------------|------------|----------|---------------|------------|----------|
| | δ_{xe} | δ_x | Δ | δ_{xe} | δ_x | Δ | δ_{xe} | δ_x | Δ |
| 14 | 3.853 | 21.192 | 0.278 | 3.843 | 21.138 | 0.275 | 7.364 | 40.502 | 1.551 |
| 13 | 3.802 | 20.914 | 0.576 | 3.793 | 20.863 | 0.537 | 7.082 | 38.951 | 1.49 |
| 12 | 3.698 | 20.337 | 0.765 | 3.696 | 20.325 | 0.779 | 6.811 | 37.461 | 1.434 |
| 11 | 3.559 | 19.572 | 1.116 | 3.554 | 19.546 | 1.138 | 6.550 | 36.026 | 2.333 |
| 10 | 3.356 | 18.456 | 1.311 | 3.347 | 18.408 | 1.268 | 6.126 | 33.693 | 2.688 |
| 9 | 3.117 | 17.146 | 1.525 | 3.116 | 17.140 | 1.477 | 5.637 | 31.005 | 3.091 |
| 8 | 2.840 | 15.620 | 1.652 | 2.848 | 15.663 | 1.670 | 5.075 | 27.914 | 3.445 |
| 7 | 2.540 | 13.968 | 1.816 | 2.544 | 13.993 | 1.838 | 4.449 | 24.469 | 3.711 |
| 6 | 2.209 | 12.152 | 1.746 | 2.210 | 12.155 | 1.805 | 3.774 | 20.758 | 3.680 |
| 5 | 1.892 | 10.406 | 1.808 | 1.882 | 10.350 | 1.866 | 3.105 | 17.079 | 3.853 |
| 4 | 1.563 | 8.598 | 1.835 | 1.542 | 8.484 | 1.836 | 2.405 | 13.226 | 3.677 |
| 3 | 1.230 | 6.763 | 2.018 | 1.209 | 6.648 | 2.016 | 1.736 | 9.549 | 3.312 |
| 2 | 0.863 | 4.745 | 2.971 | 0.842 | 4.632 | 2.938 | 1.134 | 6.237 | 3.784 |
| 1 | 0.323 | 1.774 | 1.774 | 0.308 | 1.694 | 1.694 | 0.446 | 2.453 | 2.453 |

A.5.3 P-Δ Effect Check

ASCE 7-05 requires that the P-Δ effects on story shears and moments, the resulting member forces and moments, and the story drifts need not to be considered when the stability coefficient θ as determined by the following equation is equal to or less than 1.0,

$$\theta = \frac{P_x \Delta}{V_x h_{sx} C_d}$$

Where P_x is the total vertical service load at and above level x ; Δ is the design story drift listed in Table A.10 for level x ; V_x is the seismic shear force acting between levels x and $x-1$ and h_{sx} is the story height below level x .

A.6 Member Design for PCS Building

The steel beams of PCS frame are designed according to ASIC LRFD method and AISC Seismic Provisions. The RC columns are designed following ACI 318-05 code. The load effects are determined based on the elastic static analysis.

A.6.1 Load combinations

The basic load combinations for the strength design are shown below:

- (1) $1.4D$
- (2) $1.2D + 1.6L + 0.5L_r$
- (3) $1.2D + 1.0L + 1.0E$
- (4) $0.9D + 1.0E$

Where E is the effect of horizontal and vertical earthquake-induced forces, which can be computed by

$$E = \rho Q_E + 0.2S_{DS}D \text{ for combination (3), and}$$

$$E = \rho Q_E - 0.2S_{DS}D \text{ for combination (4)}$$

Where ρ is the reliability factor; S_{DS} is the design spectral response acceleration at short periods and D is the effect of dead load. The reliability factor ρ is 1.0. For the 13-story PCS prototype building the load combinations are:

(1) $1.4D$

(2) $1.2D + 1.6L + 0.5L_r$

(3) $1.4D + 1.0L + 1.427E$

(4) $0.7D + 1.427E$

A.6.2 Design of Beam-column Connections

The hybrid beam-column connection design includes the design of end-plate and selection of post-tensioning rods. The flexural strength of end-plate is predicted with the yield line theory. Previous research has indicated that the flexural strength of the end-plate is controlled by the yield line pattern and the thickness of end-plate. Two issues need to be considered in terms of the end-plate design. Firstly, the flexural rigidity controlled by the thickness may have influence on the load transferred to the post-tensioning rods. According to previous research, additional load can be induced to the steel rods when the end-plate is not thick enough. This additional load induced due to the inadequate flexural rigidity of end-plate is called the prying force. Secondly, if the flexural stiffness of the end-plate is not great enough, the deformation of the end-plate caused by the seismic-induced bending moment at beam end may cause additional rotation of beam end, leading to a further reduced beam-column joint. Therefore, it is

worthwhile to create a design that results in a relatively thick end-plate and smaller diameter post-tensioning rods. This design philosophy is usually governed by the rupture of steel rods. However, for the hybrid PCS beam-column connection, the rupture of steel rods is avoided by designing the rods according to a targeted strength amplified by overstrength factor. Another benefit of adopting such a design philosophy is in terms of the simulating the behavior of the end-plate connection. The design procedure is summarized as follows:

(1) Determine the required rod diameter assuming no prying force,

$$d_{R,reqd} = \sqrt{\frac{2\lambda_p M_f}{\pi\phi F_{yR} (\sum d_n)}}$$

where,

$\phi = 0.75$ (adopted from Murray, etc, 2002);

F_{yR} = steel rod material yield strength.

M_f = flexural strength at beam end corresponding to plastic hinge formation at RBS

λ_p = overstrength factor

d_n = distance measured from the center line of the n^{th} tension rod row to the center of the compression flange.

After the diameter of post-tensioning rod has been determined, the nominal flexural moment capacity of the rod group can be computed by

$$M_{np} = 2P_t \sum d_n$$

Where M_{np} is the nominal moment capacity of steel rod group; P_i is yield strength of each rod and

$$P_i = \frac{\pi d_b^2}{4} F_{yR}$$

(2) Solve for the required end-plate thickness, $t_{p,reqd}$

$$t_{p,reqd} = \sqrt{\frac{\lambda_{ep} \phi M_{np}}{\phi_b F_{pY} Y}}$$

Where

$$\phi_b = 0.9$$

λ_{ep} = overstrength factor

F_{pY} = end-plate material yield strength

Y = yield line mechanism parameter

ϕM_{np} = connection strength with post-tensioning steel rod yield limit state and no prying action.

In this design procedure, two overstrength factors are used for the design of rod and end-plate. The overstrength factor λ_p for the post-tensioning rod design mainly accounts for the increase of rod load due to the prying action of end-plate. The overstrength factor λ_{ep} for the end-plate design mainly accounts for the strain hardening of the post-tensioning rods. Therefore the value of λ_{ep} is recommended to be 1.15.

The high strength post-tensioning rods are pre-tensioned during the construction as the beam-column connections are slip-critical. Considering the current practice of bolt fastening, it is recommended that the rod diameter be 1 in. at most. When the rod diameter is larger than 1 in., it will not be economical to provide the code required pretension.

A.6.3 Design of reduced beam section (RBS)

The design of reduced beam section (RBS) is according to the Recommended Seismic Design Criteria for New Steel moment-Frame Buildings (FEMA 350, 2000). The design parameters are shown in Figure 3.5. According to the recommended procedure, these parameters can be estimated by

$$a = (0.5\sim 0.75) b_f$$

$$b = (0.65\sim 0.85) d$$

$$c = 0.2 b_f$$

where d and b_f are the overall depth and flange width of the steel beam under consideration.

The flexural moment capacity of the reduced beam section M_{RBS} are computed using the following formula:

$$Z_{RBS} = Z_b - 2ct_f(d-t_f)$$

$$F_{ye} = R_y F_y$$

$$M_{RBS} = 1.15 Z_{RBS} F_{ye}$$

where Z_{RBS} is the plastic modulus of the most reduced section; Z_b is the original plastic modulus of the beam section; t_f is the thickness of flange; R_y is the strength increase factor accounting for the strain hardening effect of steel material; F_y is the yield strength of steel beam material.

The flexural moment M_f of the beam end section corresponding to M_{RBS} is then calculated by

$$M_f = M_{RBS} + V_{RBS} (a+b/2)$$

$$V_{RBS} = \frac{2M_{RBS} + PL' + WL'^2 / 2}{L'}$$

V_{RBS} is the shear force at the reduced beam section where M_{RBS} is developed. P and W are the concentrated load and uniformly distributed load acting upon the beam under consideration. L' is the beam length measured between the reduced beam section at each end of the beam.

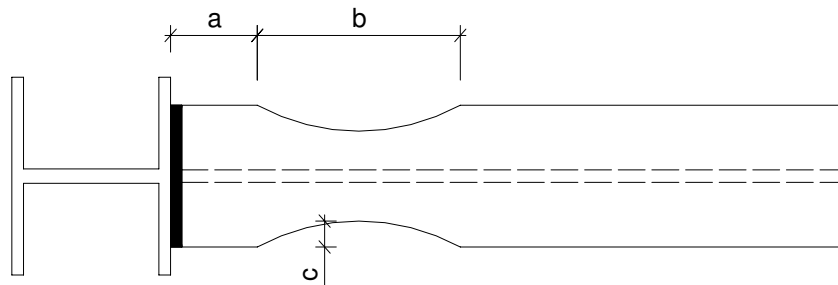


Figure A.3: Geometrical parameters of reduced beam section

The last step of the RBS design is to check the efficiency of design. This check is done by comparing M_f with the most probable flexural strength M_{pe} of the uncut beam section. If the ratio of M_f to M_{pe} is larger than 0.85, the reduced beam design is acceptable since the reduction doesn't cause much loss of flexural strength at beam end. It is also possible that this ratio exceeds 1.0, which may be due to the inadequate beam size. Table A.11 shows the results of RBS design based on the recommended procedure.

Table A.11: Reduced beam design results

| Story | Beam | a | b | c | M_{RBS} | M_f | M_{pe} | M_f / M_{pe} |
|-------|---------|---|----|-----|-----------|---------|----------|----------------|
| Plaza | W33×201 | 8 | 22 | 3 ¼ | 33503 | 37663.3 | 42515 | 0.89 |
| 1 | W36×230 | 9 | 24 | 3 ½ | 40320 | 45927.8 | 51865 | 0.89 |
| 2-3 | W33×152 | 6 | 22 | 2 ½ | 24482 | 27150.0 | 30745 | 0.88 |
| 4-6 | W33×152 | 6 | 22 | 2 ½ | 24482 | 27133.0 | 30745 | 0.88 |
| 7-8 | W33×141 | 6 | 22 | 2 ½ | 22692 | 25133.6 | 28270 | 0.89 |
| 9-10 | W33×130 | 6 | 22 | 2 ½ | 20819 | 23058.9 | 25685 | 0.90 |
| 11-12 | W33×118 | 6 | 22 | 2 ½ | 18723 | 20724.3 | 22825 | 0.91 |
| Roof | W27×84 | 5 | 18 | 2 | 11213 | 12182.4 | 13420 | 0.91 |

A.6.4 Strong Column-Weak Beam Check

The strong column-weak beam philosophy must be followed in the capacity-based design methodology. Current building codes have different specifications on steel moment resisting frames and reinforced concrete column moment resisting frames. In general, it must be satisfied that,

$$\frac{\sum M_{pc}}{\sum M_b} \geq \alpha$$

Where M_{pc} is the probable flexural strength of column section below and above the beam-column joint; M_b is the probable flexural moment of the beam end section left and right to the beam-column joint; α is a factor dependent on type of the moment frame. For steel moment frame and reinforced concrete moment frame, α is taken as 1.0 and 1.2. For the hybrid precast concrete and steel moment resisting frame, it is suggested to take 1.1 for the factor α . The sum of the expected flexural moment strength $\sum M_b$ can be obtained using the values of M_f shown in Table A.11. To calculate the sum of nominal flexural strength of column sections below and above the beam-column joint, it is necessary to determine the service axial load caused by dead and live loads for each column. Then the nominal flexural strength of column section is obtained from the P-M interaction diagram. Table A.11 and Table A.12 list the axial load for each edge and the corner column for the PCS building.

Table A.12: Service dead and live load axial forces for an edge column

| Story | Dead Load (psf) | Live Load (psf) | Supported Area (ft ²) | Reduced Live Load (psf) | Live Load (kips) | Cumulative Dead Load (kips) | Cumulative Live Load (kips) |
|-------|-----------------|-----------------|-----------------------------------|-------------------------|------------------|-----------------------------|-----------------------------|
| Plaza | 97 | 50 | 7168 | 20 | 10.24 | 543.2 | 142.8 |
| 1 | 93 | 50 | 6656 | 20 | 10.24 | 493.6 | 132.6 |
| 2 | 80 | 50 | 6144 | 20 | 10.24 | 446 | 122.4 |
| 3 | 80 | 50 | 5632 | 20 | 10.24 | 405 | 112.1 |
| 4 | 78 | 50 | 5120 | 20 | 10.24 | 364 | 101.9 |
| 5 | 78 | 50 | 4608 | 20 | 10.24 | 324.1 | 91.6 |
| 6 | 75 | 50 | 4096 | 20 | 10.24 | 284.2 | 81.4 |
| 7 | 75 | 50 | 3584 | 20 | 10.24 | 245.8 | 71.2 |
| 8 | 75 | 50 | 3072 | 20 | 10.24 | 207.4 | 60.9 |
| 9 | 75 | 50 | 2560 | 20 | 10.19 | 169 | 50.7 |
| 10 | 73 | 50 | 2048 | 21 | 10.64 | 130.6 | 40.5 |
| 11 | 73 | 50 | 1536 | 22 | 11.30 | 93.2 | 29.8 |
| 12 | 73 | 50 | 1024 | 24 | 12.40 | 55.8 | 18.5 |
| 13 | 36 | 20 | 512 | 12 | 6.14 | 18.4 | 6.14 |

Table A.13: Service dead and live load axial forces for a corner column

| Story | Dead Load (psf) | Live Load (psf) | Supported Area (ft ²) | Reduced Live Load (psf) | Live Load (kips) | Cumulative Dead Load (kips) | Cumulative Live Load (kips) |
|-------|-----------------|-----------------|-----------------------------------|-------------------------|------------------|-----------------------------|-----------------------------|
| Plaza | 97 | 50 | 3584 | 20 | 5.1 | 271.6 | 71.4 |
| 1 | 93 | 50 | 3328 | 20 | 5.1 | 246.8 | 66.3 |
| 2 | 80 | 50 | 3072 | 20 | 5.1 | 223.0 | 61.2 |
| 3 | 80 | 50 | 2816 | 20 | 5.1 | 202.5 | 56.1 |
| 4 | 78 | 50 | 2560 | 20 | 5.1 | 182.0 | 50.9 |
| 5 | 78 | 50 | 2304 | 20 | 5.1 | 162.0 | 45.8 |
| 6 | 75 | 50 | 2048 | 20 | 5.1 | 142.1 | 40.7 |
| 7 | 75 | 50 | 1792 | 20 | 5.1 | 122.9 | 35.6 |
| 8 | 75 | 50 | 1536 | 20 | 5.1 | 103.7 | 30.5 |
| 9 | 75 | 50 | 1280 | 20 | 5.1 | 84.5 | 25.3 |
| 10 | 73 | 50 | 1024 | 21 | 5.4 | 65.3 | 20.2 |
| 11 | 73 | 50 | 768 | 22 | 5.6 | 46.6 | 14.8 |
| 12 | 73 | 50 | 512 | 24 | 6.1 | 27.9 | 9.2 |
| 13 | 36 | 20 | 256 | 12 | 3.1 | 9.2 | 3.1 |

Table A.14: Longitudinal reinforcement for PCS building

| Story | Column Size | Longitudinal Reinforcement | ρ | P (kips) | M_n |
|-------|-------------|----------------------------|--------|----------|-------|
| Plaza | 34×34 | 12 NO.18 | 3% | 440.2 | 3452 |
| 1 | 34×34 | 12 NO.18 | 4% | 402.2 | 4210 |
| 2 | 32×32 | 12 NO.14 | 2.49% | 365.5 | 2489 |
| 3 | 32×32 | 12 NO.14 | 2.49% | 332.8 | 2489 |
| 4 | 30×30 | 12 NO.14 | 3.09% | 299.8 | 2487 |
| 5 | 30×30 | 12 NO.14 | 3.09% | 267.7 | 2487 |
| 6 | 28×28 | 12 NO.14 | 3.46% | 235.6 | 2487 |
| 7 | 28×28 | 12 NO.14 | 3.46% | 204.4 | 2304 |
| 8 | 28×28 | 12 NO.14 | 3.46% | 173.2 | 2304 |
| 9 | 28×28 | 12 NO.14 | 3.11% | 141.9 | 2114 |
| 10 | 26×26 | 12 NO.14 | 3.91% | 110.7 | 2114 |
| 11 | 26×26 | 12 NO.14 | 3.52% | 79.6 | 1900 |
| 12 | 24×24 | 8 NO.14 | 3.52% | 48.2 | 1900 |
| 13 | 24×24 | 8 NO.11 | 2.20% | 16.0 | 1117 |

A.6.5 Steel Beam Local Stability Check

Since the two prototype steel buildings were designed and constructed in the 1970s', it is necessary to check the steel beam local stability according to the current seismic specifications for steel structure design. The AISC seismic provisions (2005) require the width-to-thickness ratios of flange and web satisfy:

$$\frac{b_f}{2t_f} \leq 0.3 \sqrt{\frac{E}{F_y}} \quad (\text{flange})$$

$$\frac{h_c}{t_w} \leq 3.76 \sqrt{\frac{E}{F_y}} \quad (\text{web})$$

Where b_f and t_f are the width and thickness of beam flanges; h_c and t_w are the depth and thickness of the beam web; E and F_y are the Young's modulus and specified yield strength of the beam material. If both requirements are satisfied, the steel beam section can be categorized as seismic compact beam section. Otherwise, measures must be taken to avoid the use of non-compact section in high seismic region. One of the effective measures is the use of reduced beam section.

A.6.6 Composite Slab system of PCS Building

Figure A.4 and Figure A.5 depict the composite slab system used for PCS building. The composite slab system is much lighter than traditional reinforced concrete slab system.

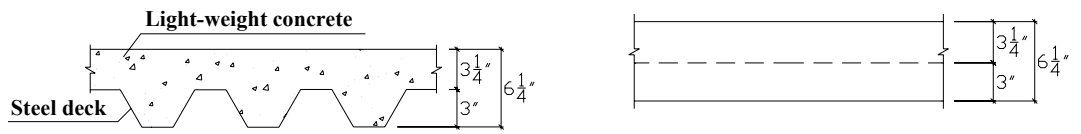


Figure A.4: Light-weight concrete floor slab system

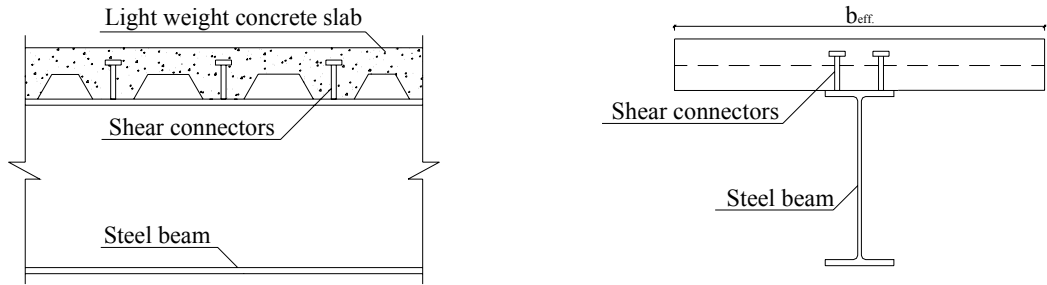


Figure A.5: Composite beam section

Appendix B: Testing Data

In the appendix chapter all the recorded data were plotted. The interstory drift was used as the horizontal axis and other data was the vertical axis.

B.1 Testing Data of Test Model 1

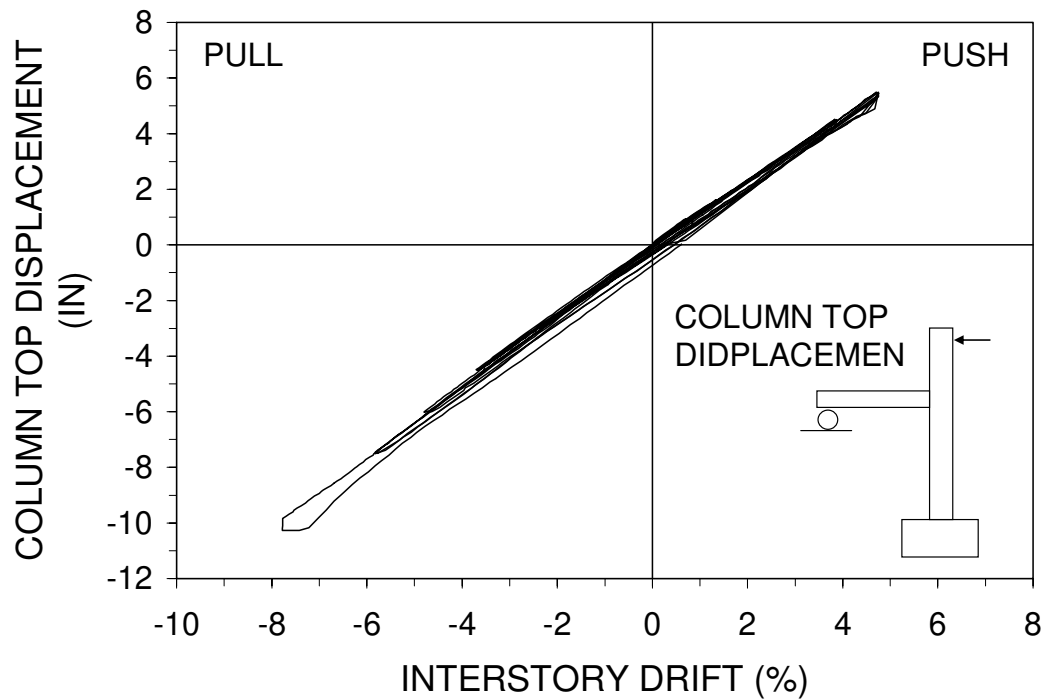


Figure B.1: Interstory drift vs. column top displacement

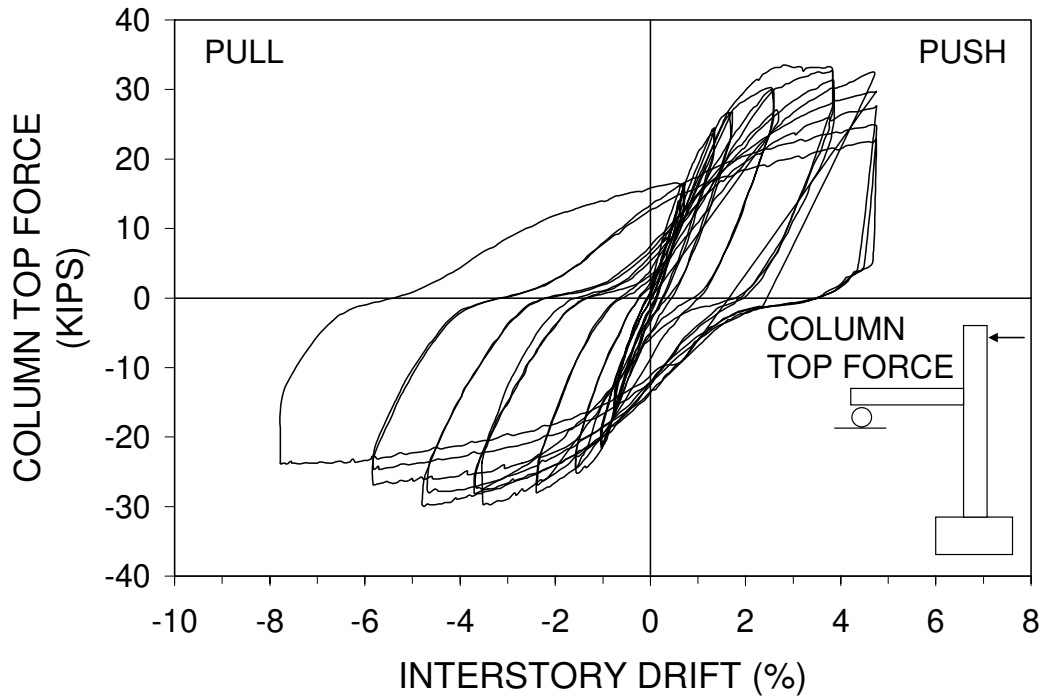


Figure B.1, continued: Interstory drift vs. column top force

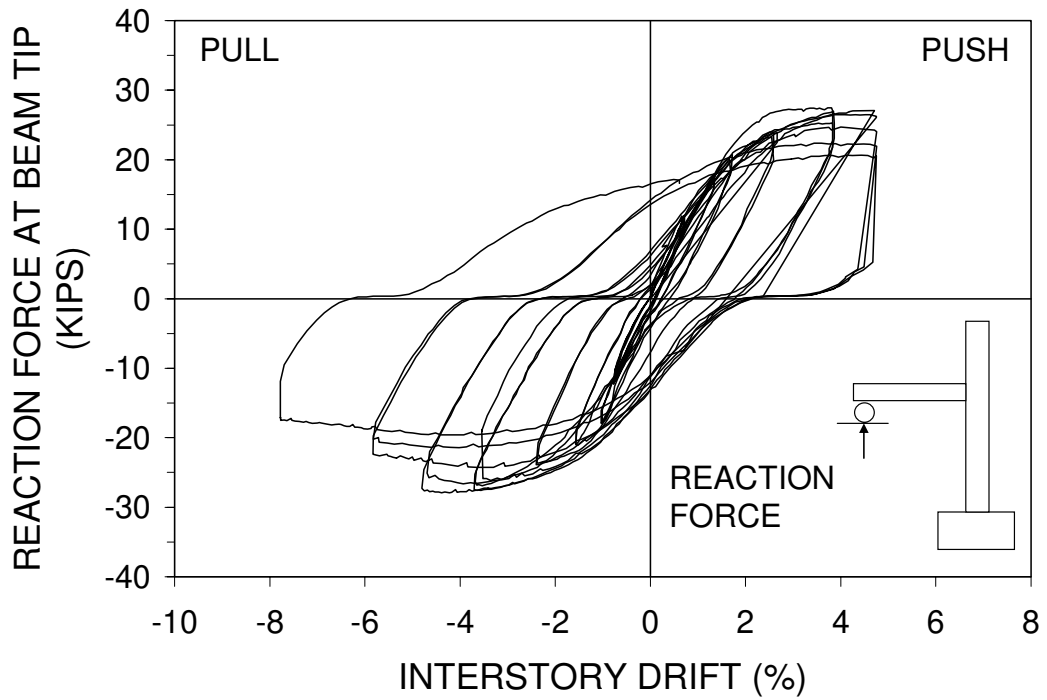


Figure B.1, continued: Interstory drift vs. reaction force at beam tip

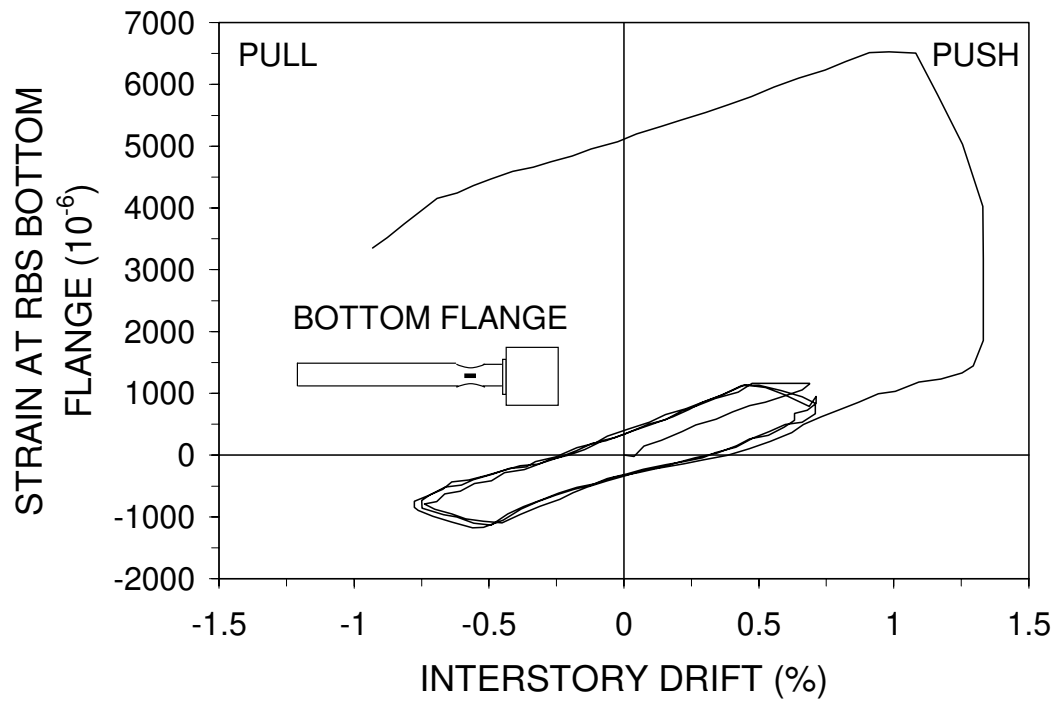


Figure B.1, continued: Interstory drift vs. strain at RBS bottom flange

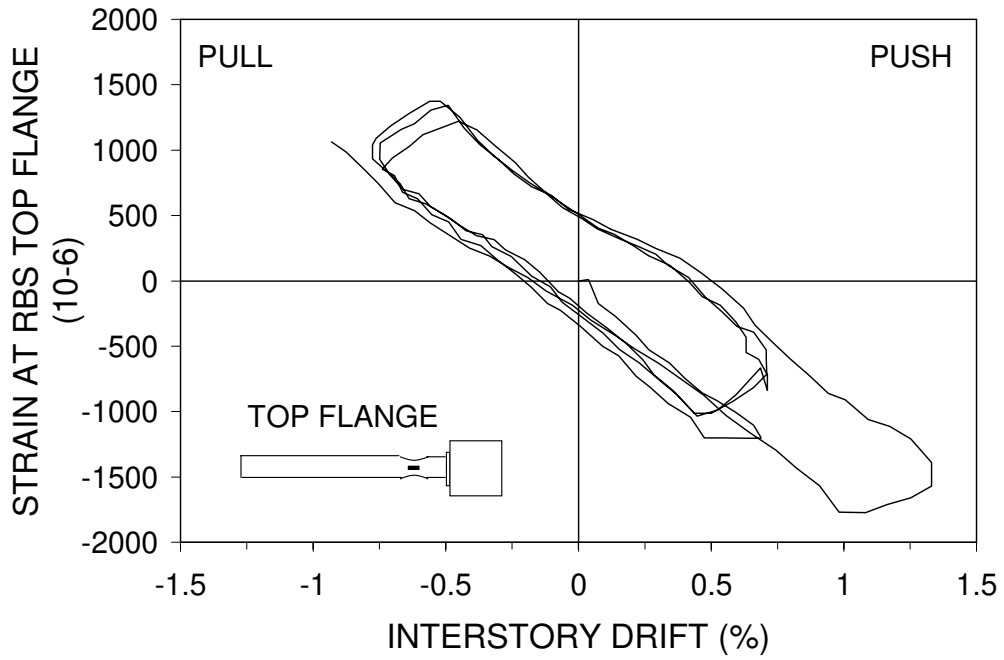


Figure B.1, continued: Interstory drift vs. strain at RBS top flange

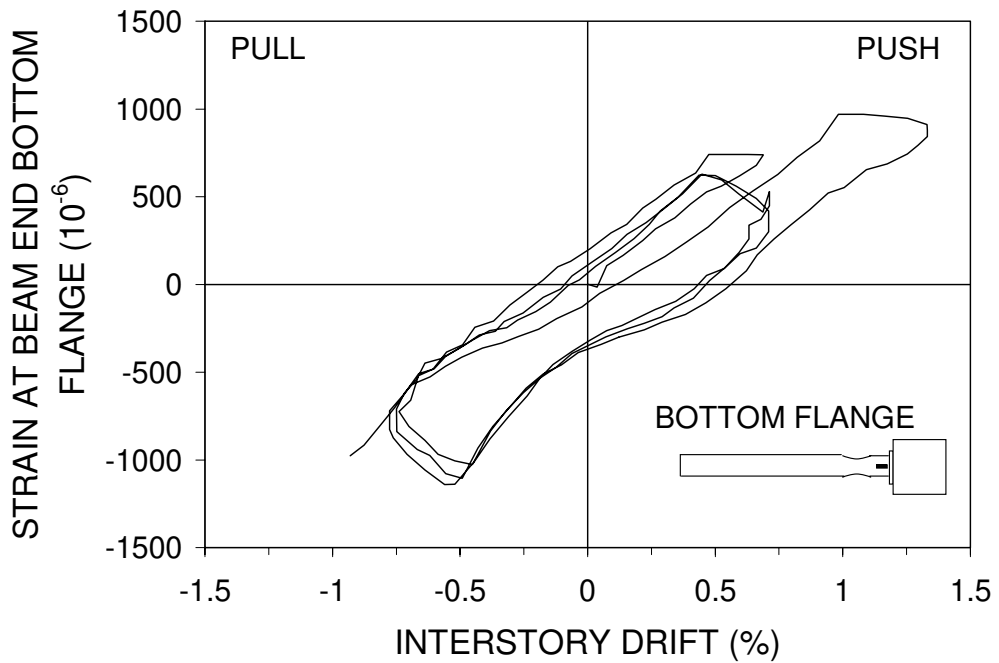


Figure B.1, continued: Interstory drift vs. strain at beam end bottom flange

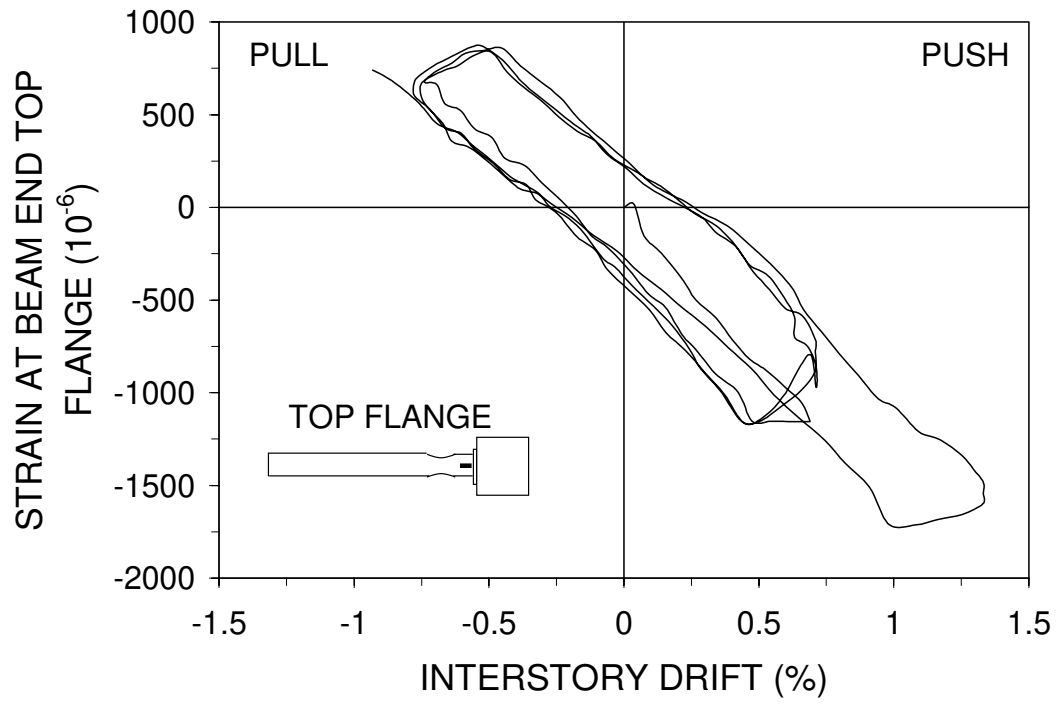


Figure B.1, continued: Interstory drift vs. strain at beam end top flange

B.2 Testing Data of Test Model 2

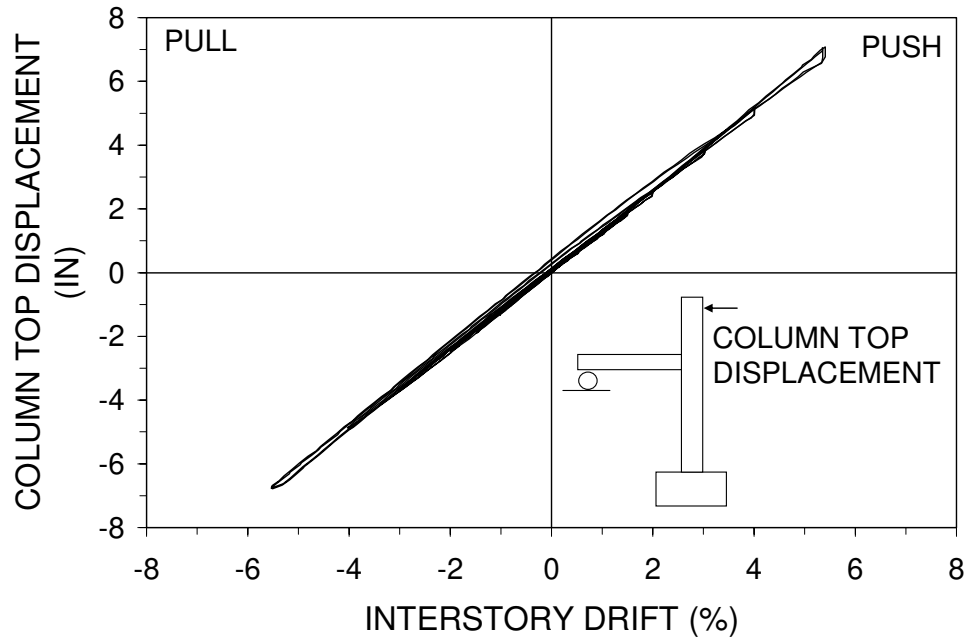


Figure B.2 Interstory drift vs. column top displacement

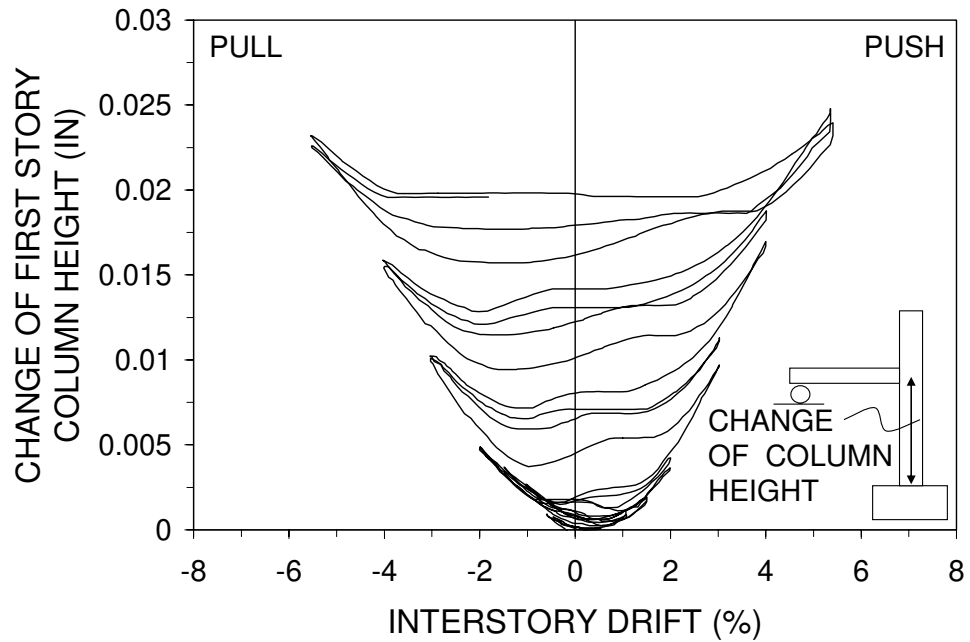


Figure B.2, continued: Interstory drift vs. change of column height

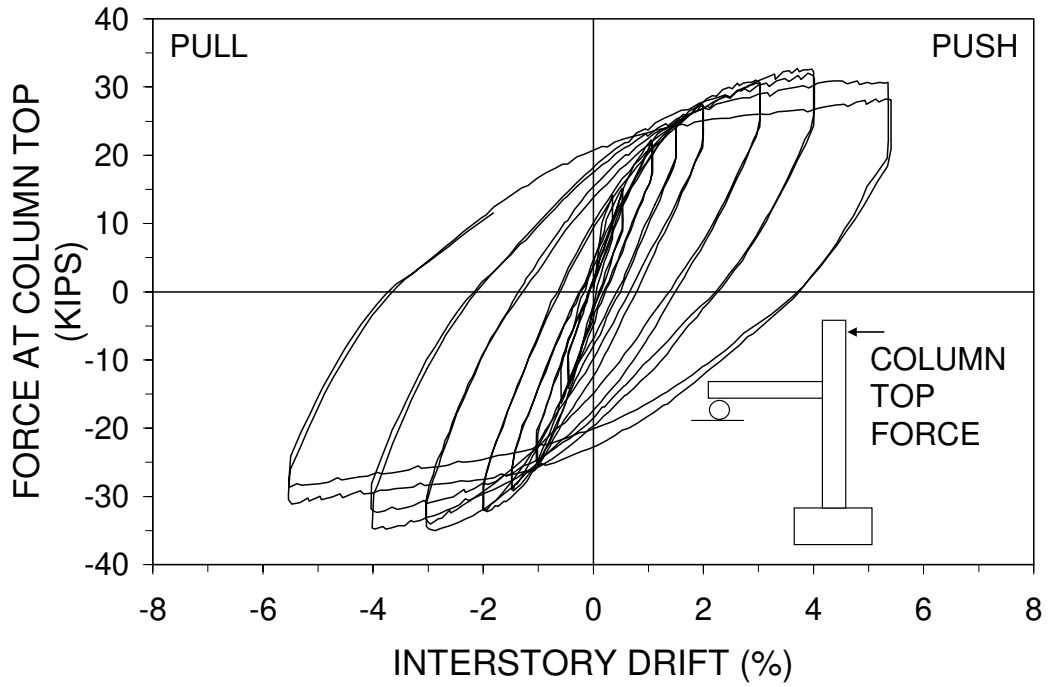


Figure B.2, continued: Interstory drift vs. column top force

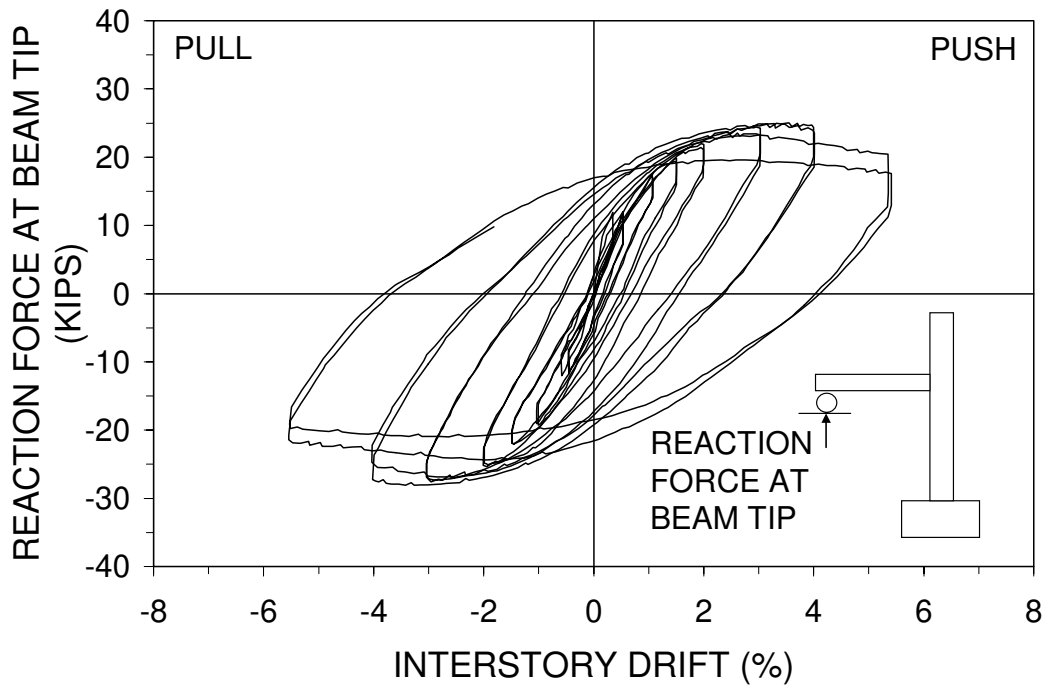


Figure B.2, continued: Interstory drift vs. reaction force at beam tip

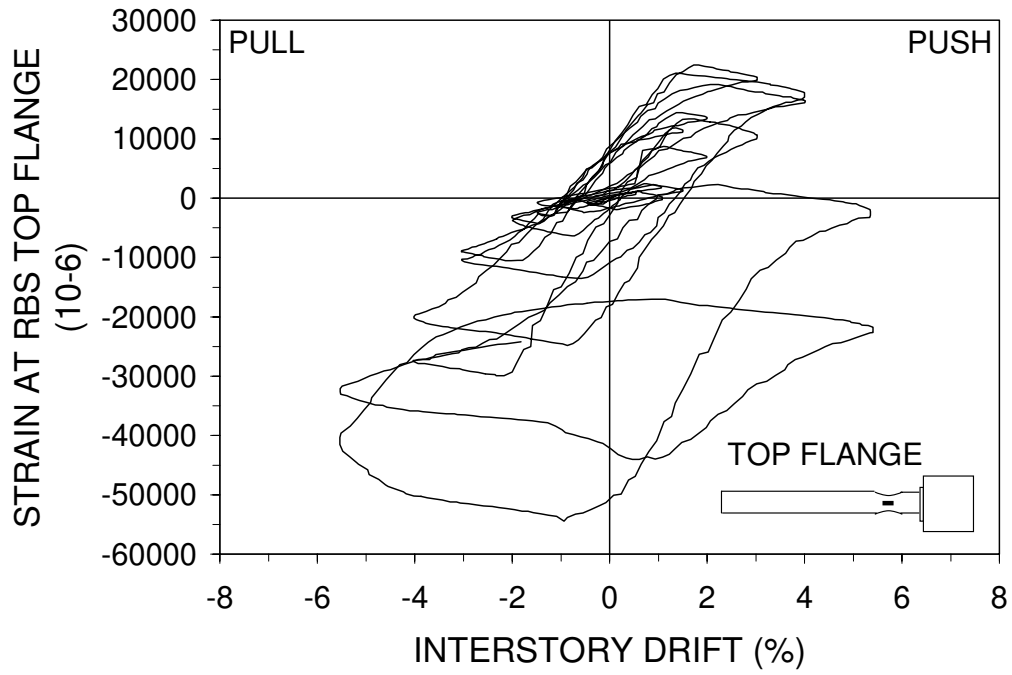


Figure B.2, continued: Interstory drift vs. strain at RBS top flange

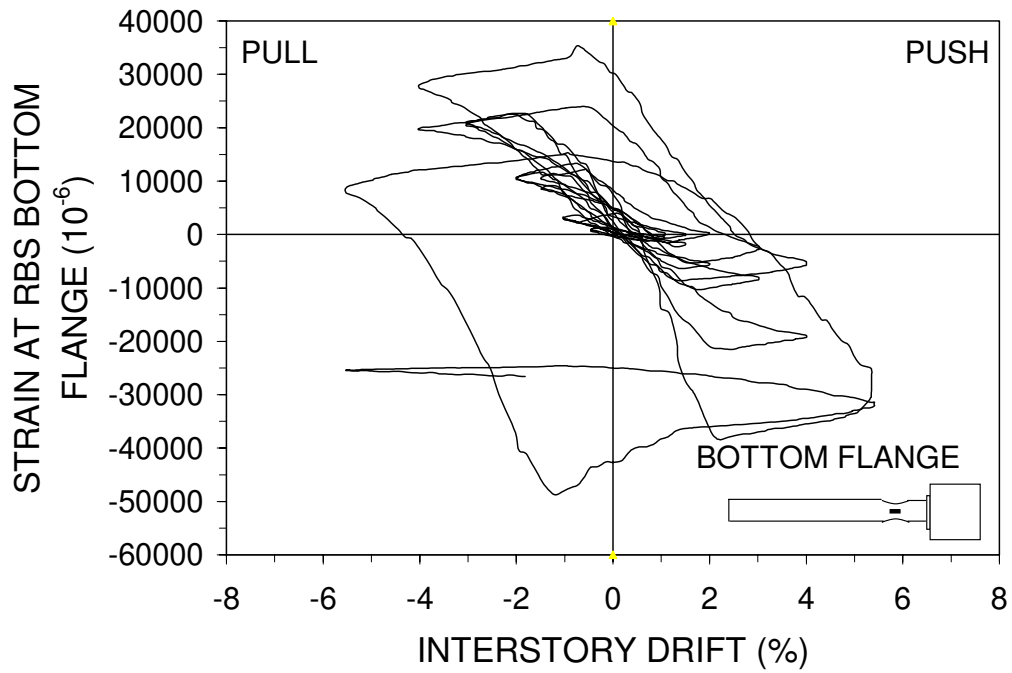


Figure B.2, continued: Interstory drift vs. strain at RBS bottom flange

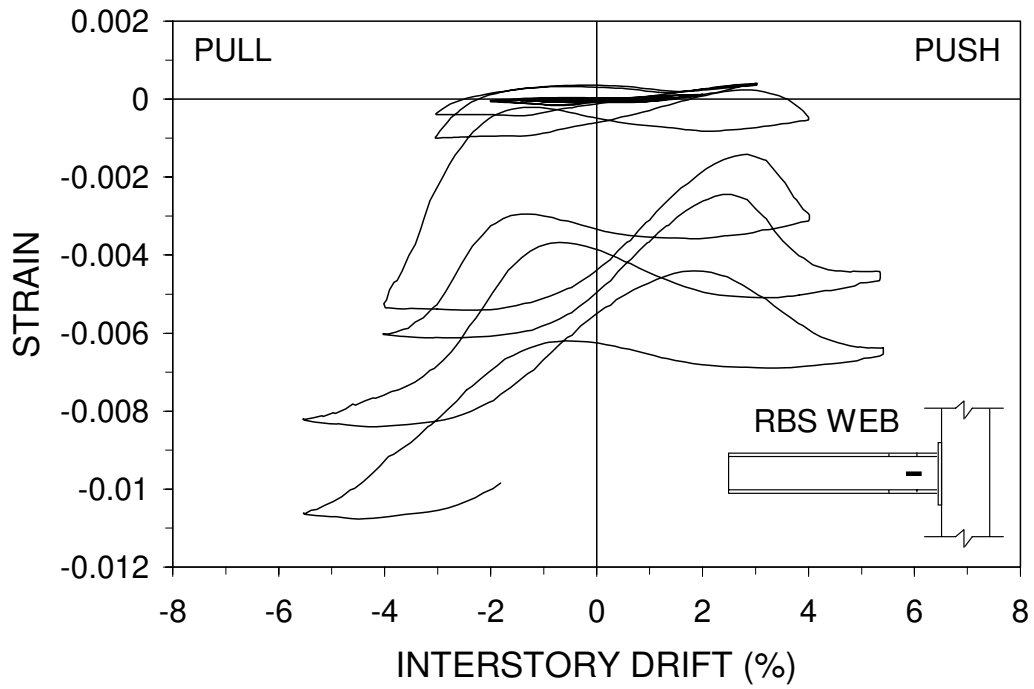


Figure B.2, continued: Interstory drift vs. strain at RBS web

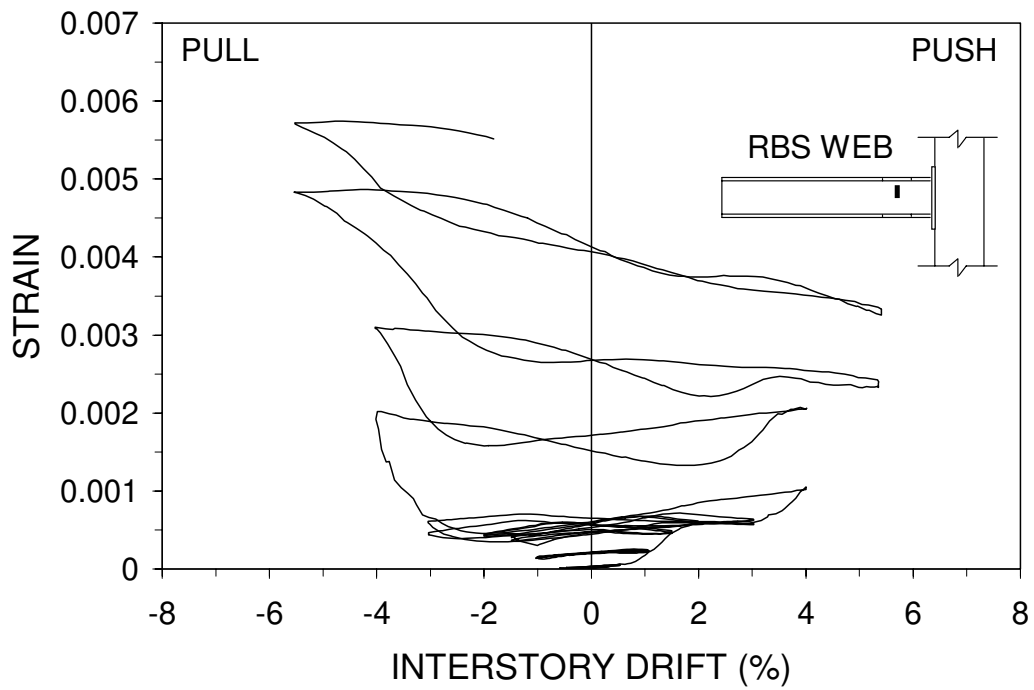


Figure B.2, continued: Interstory drift vs. strain at RBS web

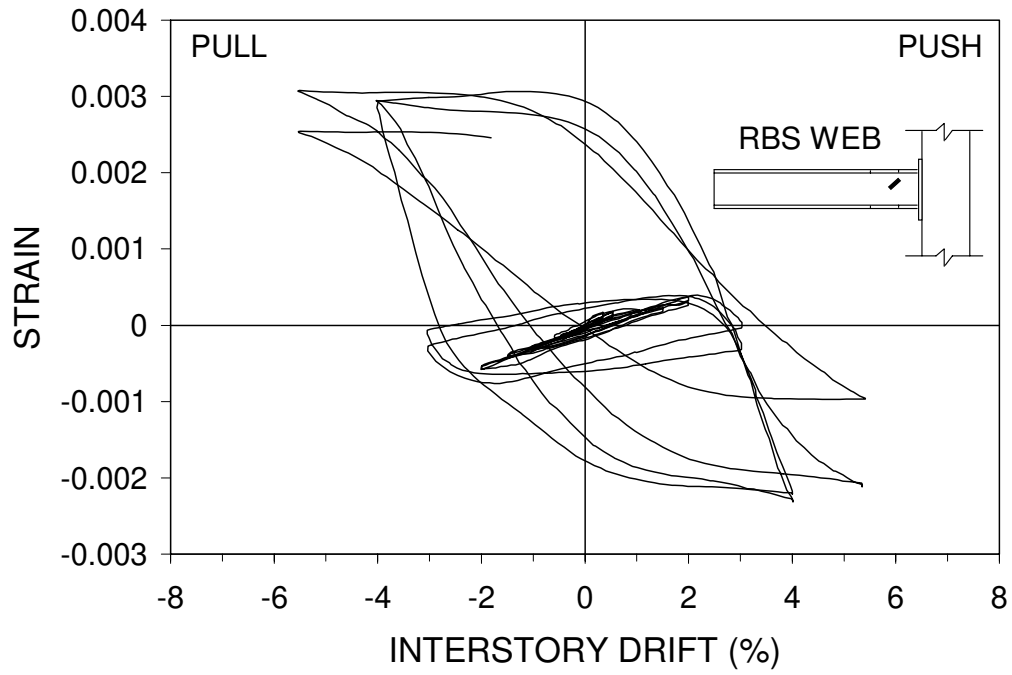


Figure B.2, continued: Interstory drift vs. strain at RBS web

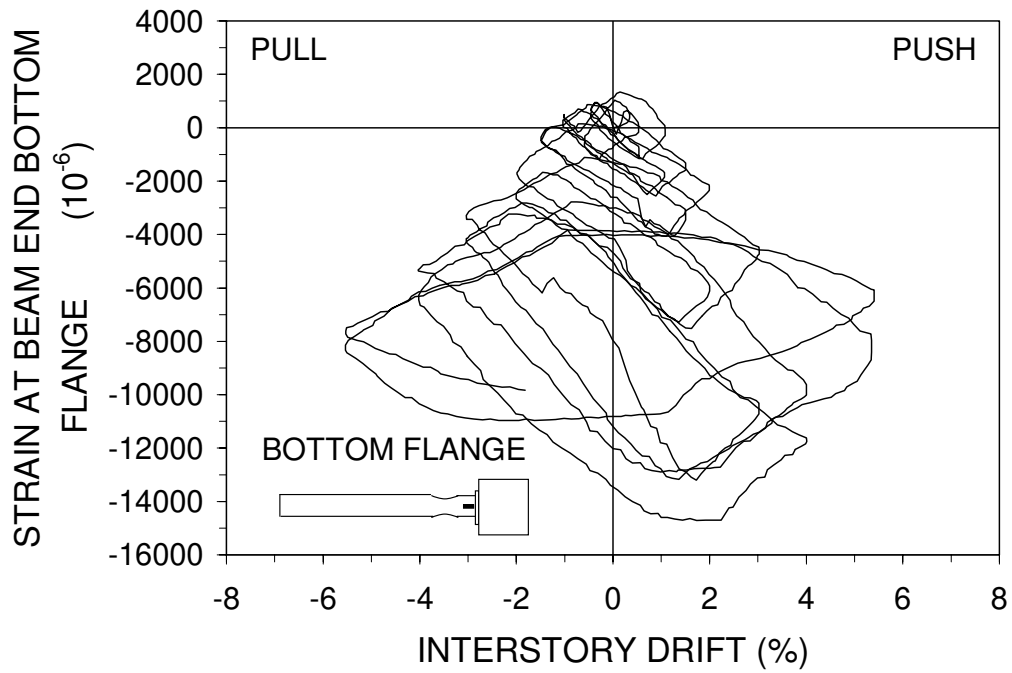


Figure B.2, continued: Interstory drift vs. strain at beam end bottom flange

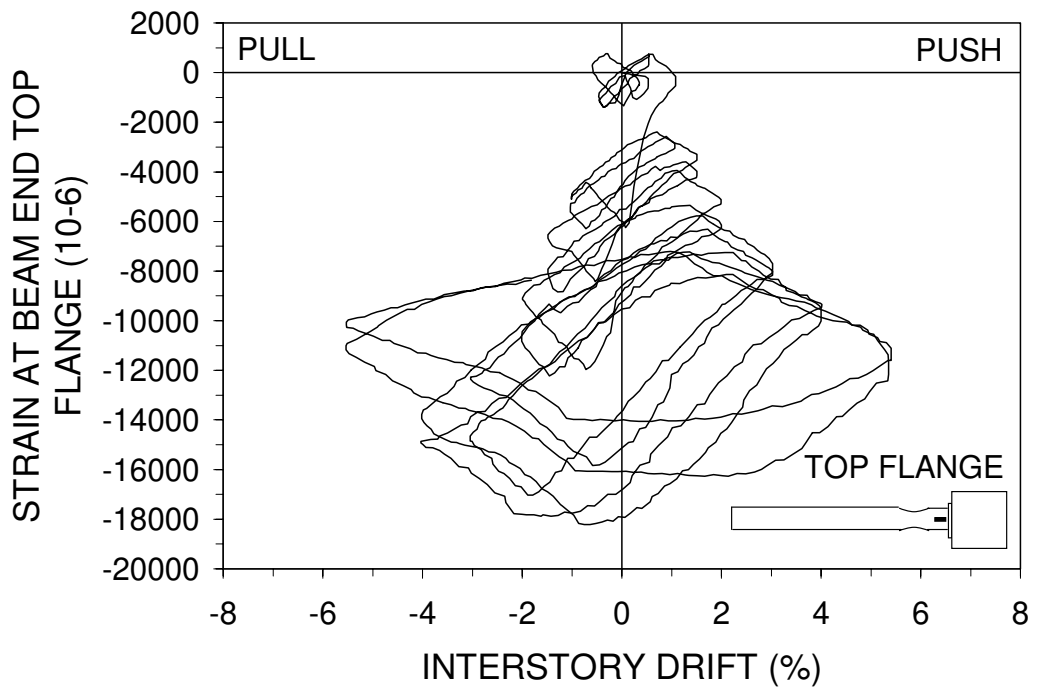


Figure B.2, continued: Interstory drift vs. strain at beam end top flange

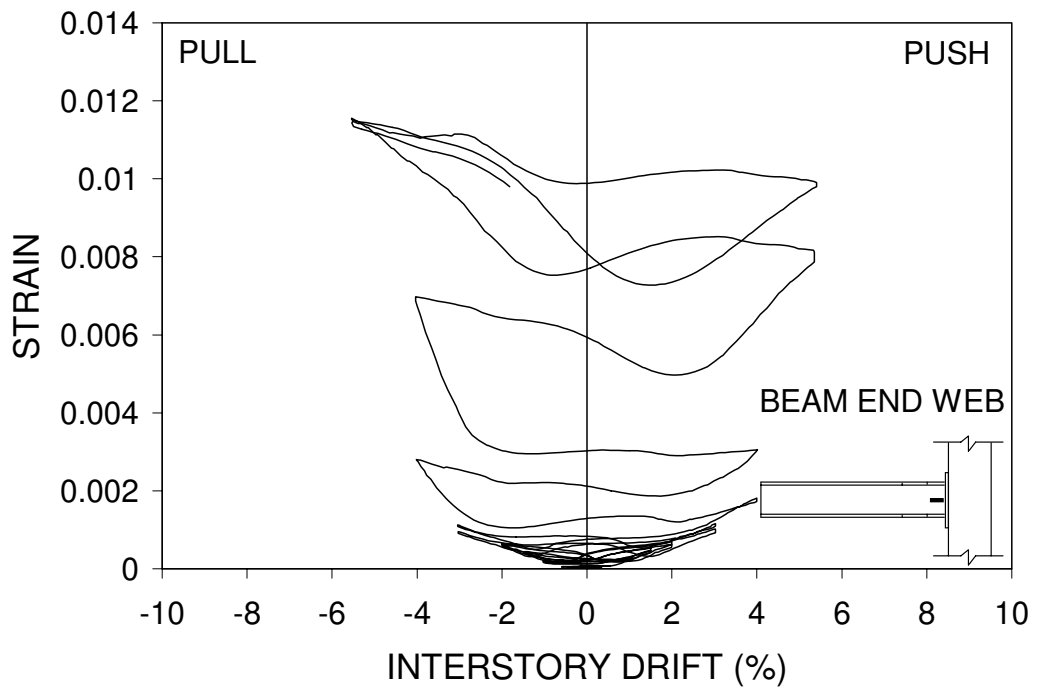


Figure B.2, continued: Interstory drift vs. strain at beam end web

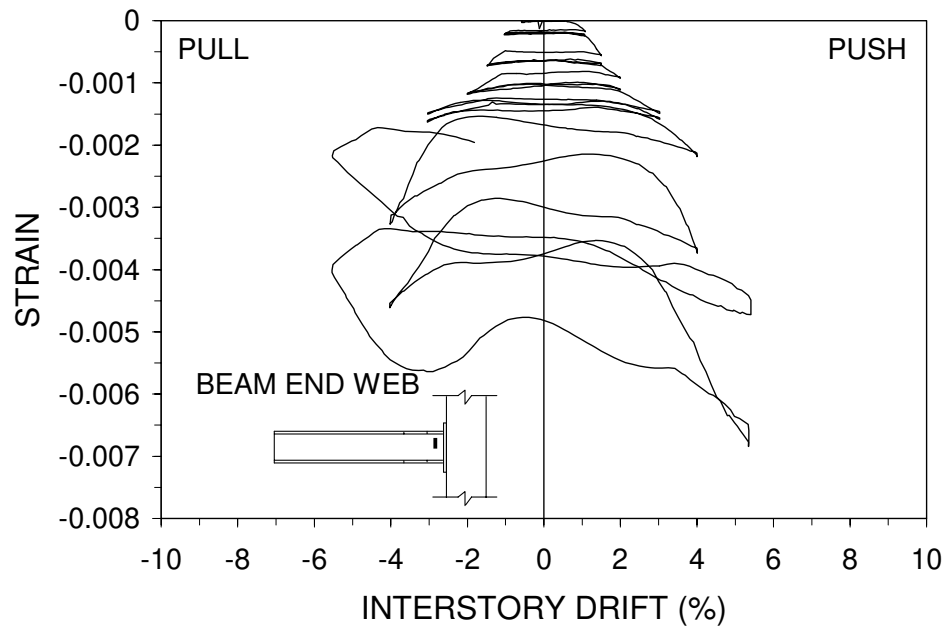


Figure B.2, continued: Interstory drift vs. strain at beam end web

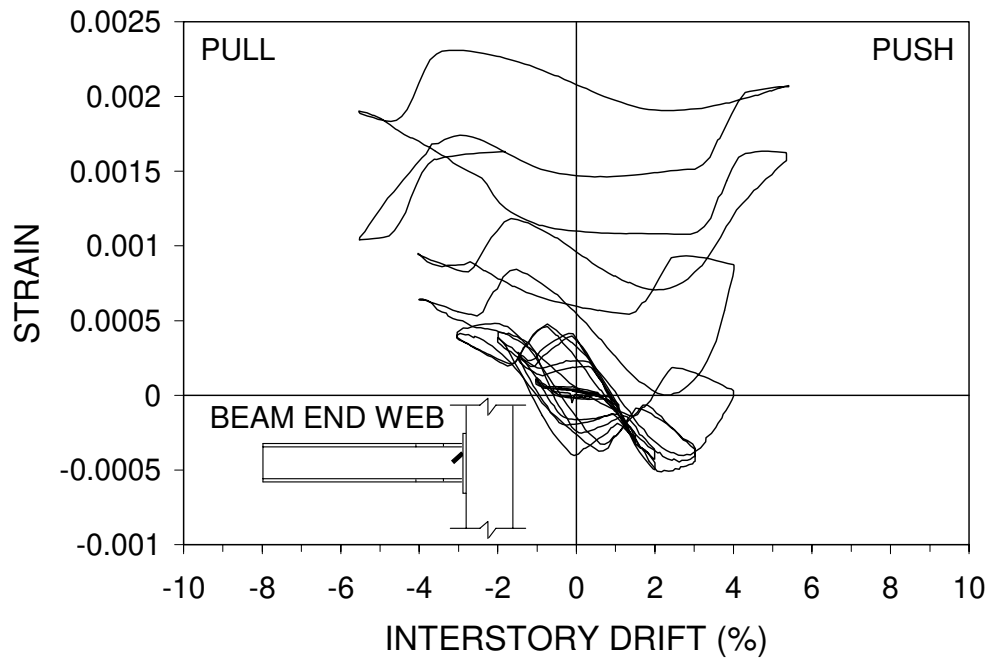


Figure B.2, continued: Interstory drift vs. strain at beam end web

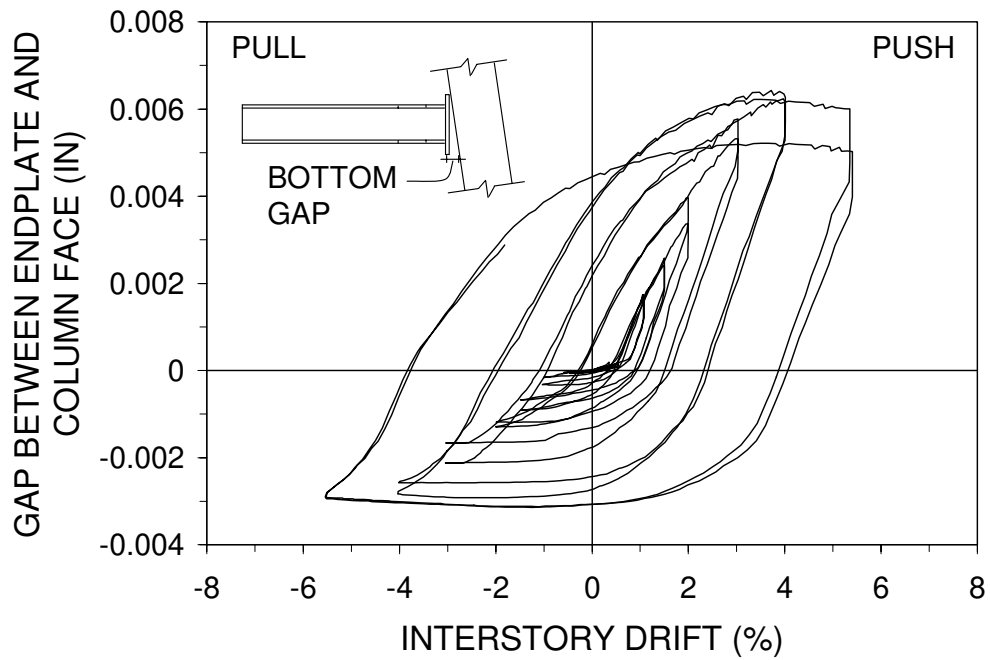


Figure B.2, continued: Interstory drift vs. bottom gap between column and endplate

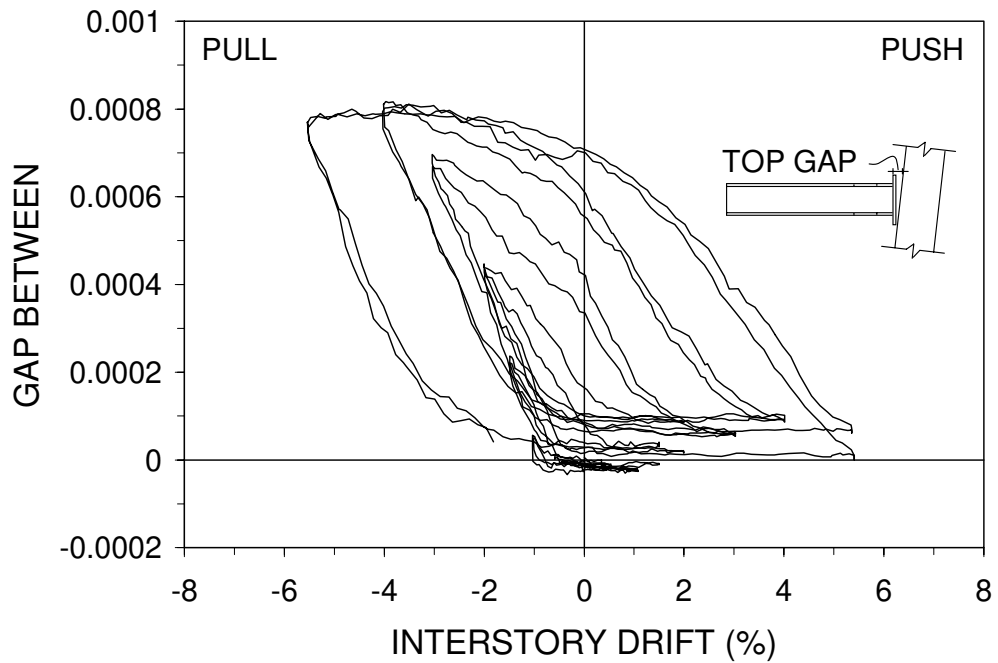


Figure B.2, continued: Interstory drift vs. top gap between column and endplate

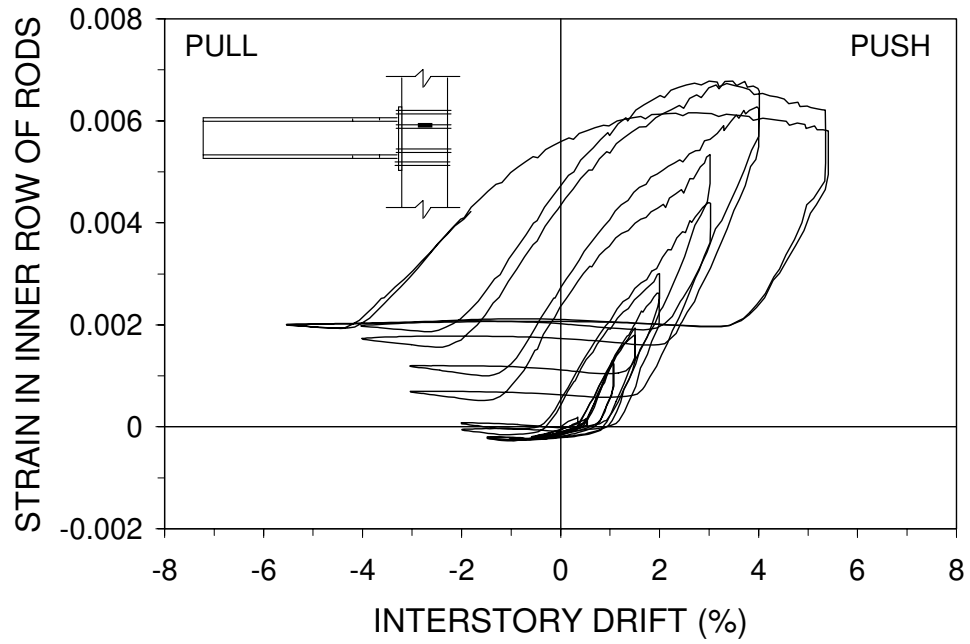


Figure B.2, continued: Interstory drift vs. strain at inner row steel rod

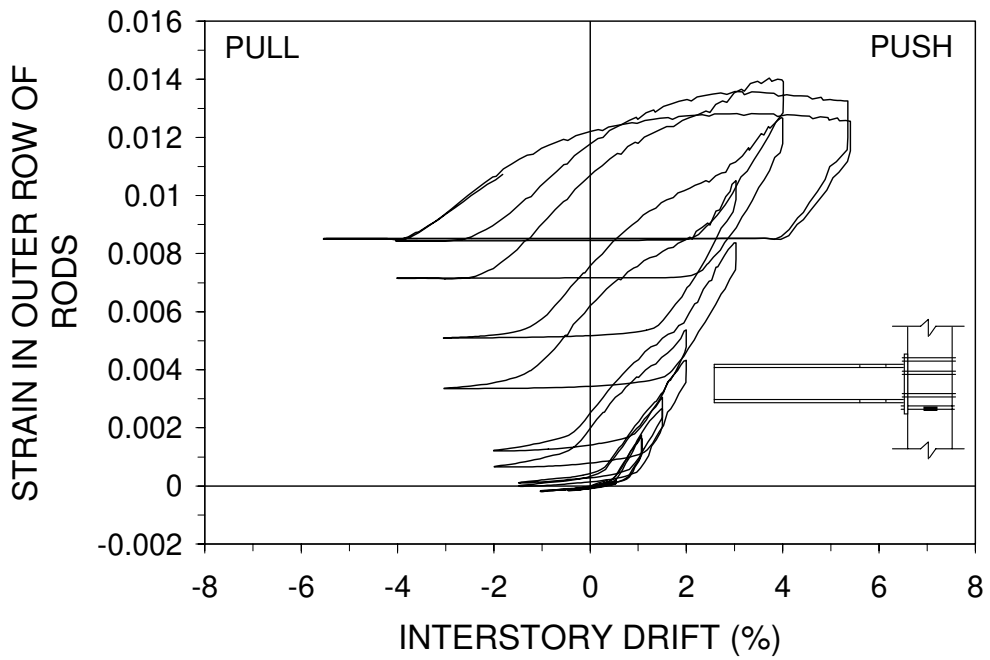


Figure B.2, continued: Interstory drift vs. strain at outer row steel rod

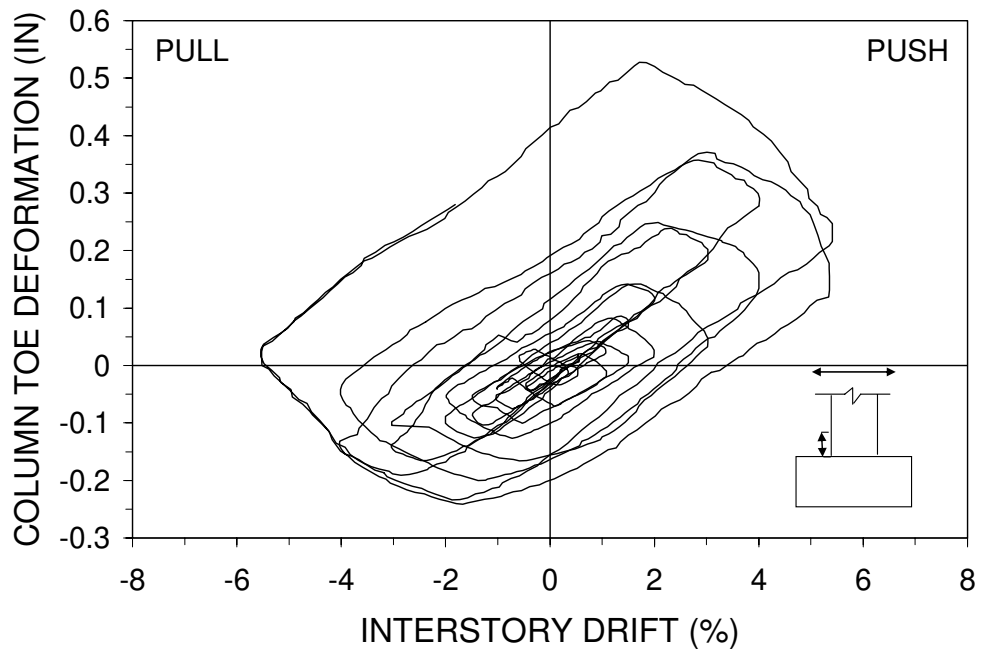


Figure B.2, continued: Interstory drift vs. deformation at column toe

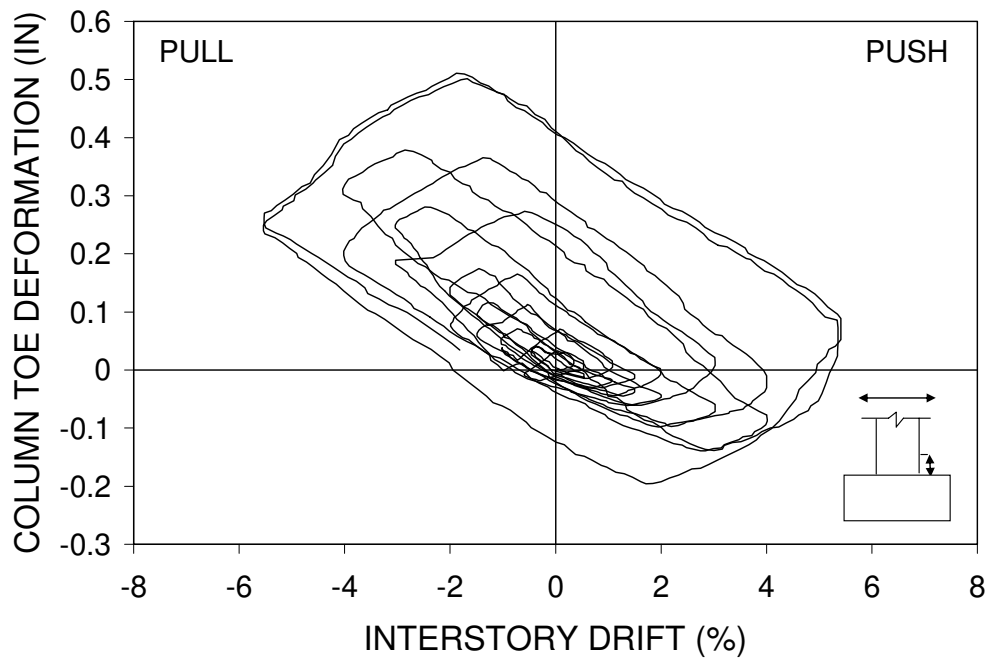


Figure B.2, continued: Interstory drift vs. deformation at column toe

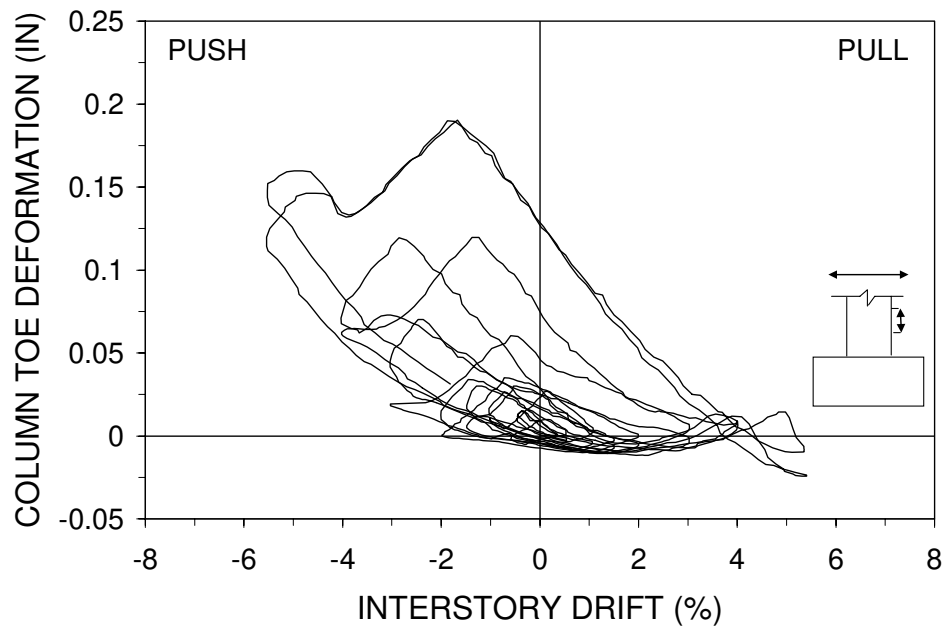


Figure B.2, continued: Interstory drift vs. deformation at column toe

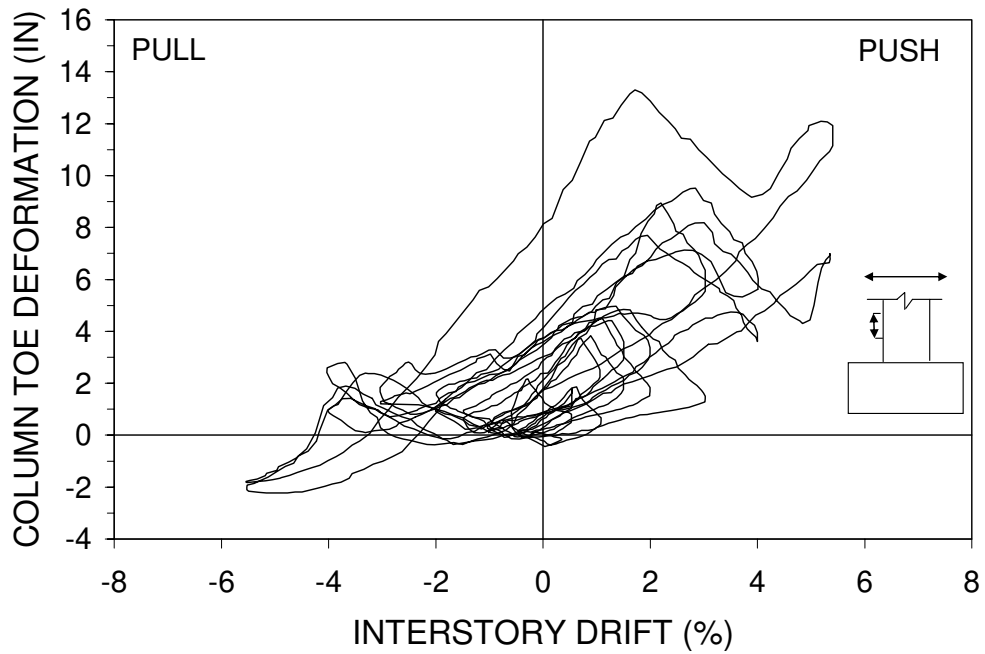


Figure B.2, continued: Interstory drift vs. jeformation at column toe

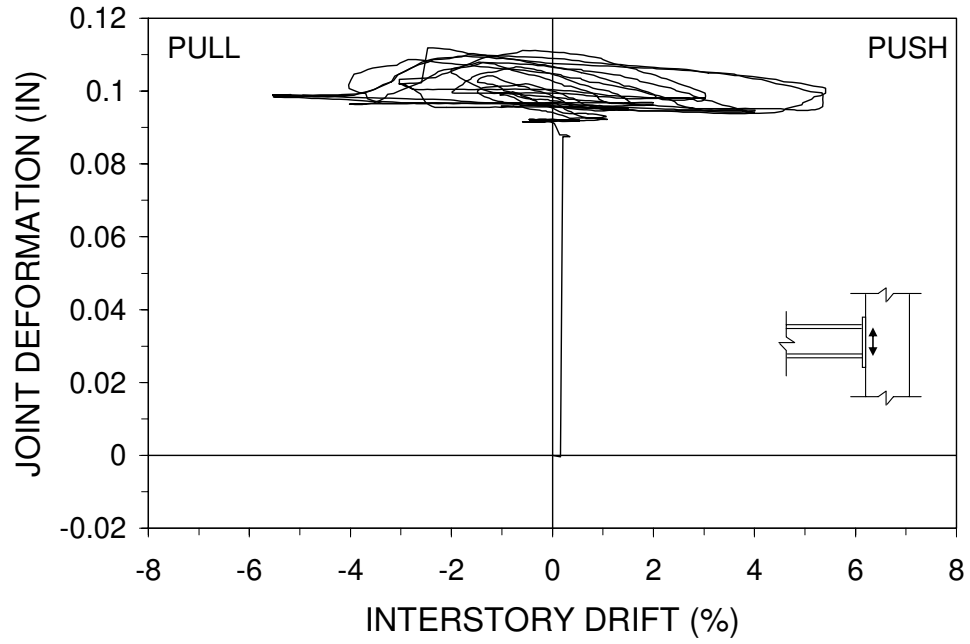


Figure B.2, continued: Interstory drift vs. joint deformation

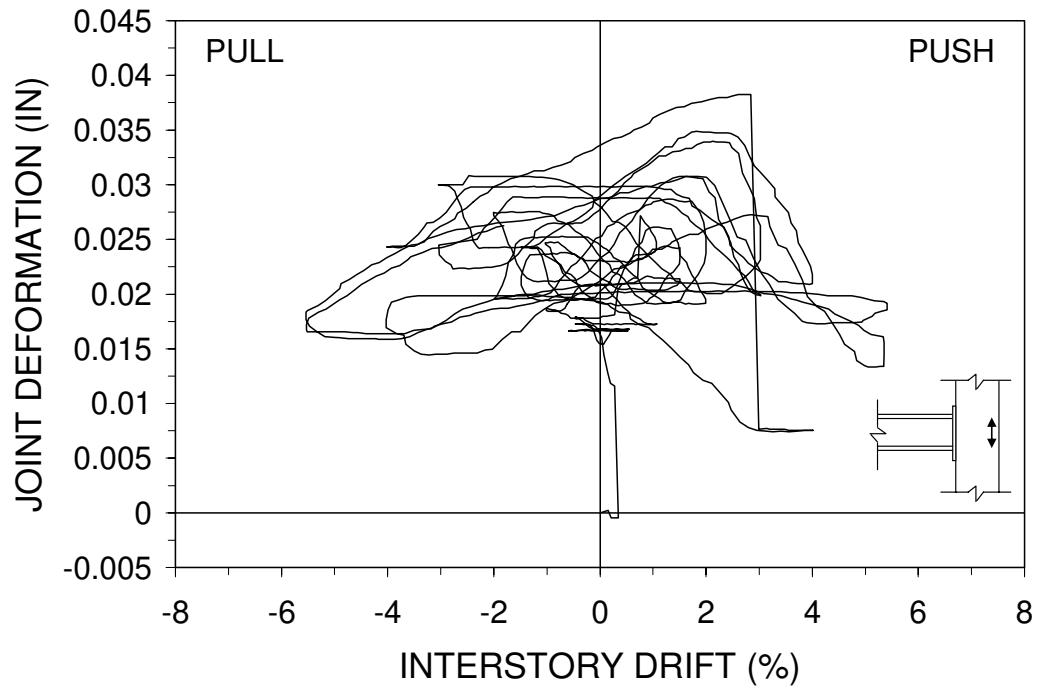


Figure B.2, continued: Interstory drift vs. joint deformation

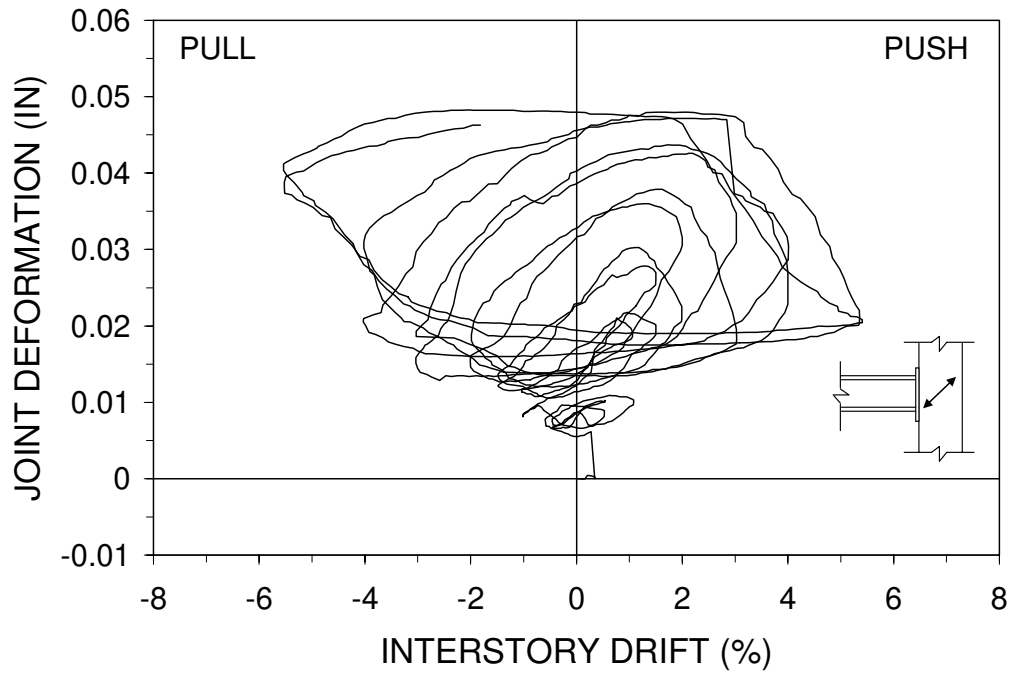


Figure B.2, continued: Interstory drift vs. joint deformation

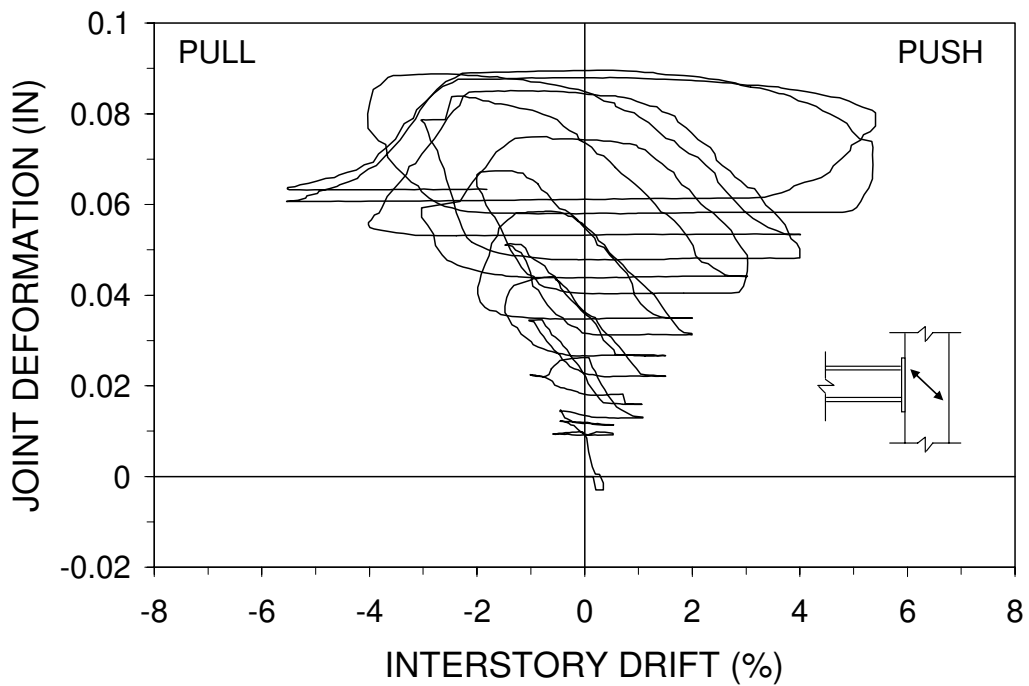


Figure B.2, continued: Interstory drift vs. joint deformation

Appendix C: Material Test Results

In Appendix C, all the material tests related to the research project are summarized.

C.1 Concrete Compressive Test of Cylinders

The concrete used to construct the columns and footings was from the same batch. Totally six 6 in. by 12 in. cylinders were made and tested. Among the six cylinders, three were tested at the construction site by the concrete factory on the 28th day after casting. The results were 6.65ksi, 6.95ksi and 6.85ksi. The rest three cylinders were shipped to the structural lab of USC and tested on the day when test model 1 was tested. The resulted compressive strengths were 7.6ksi, 7.4ksi and 7.6ksi.

C.2 High Strength Steel Rod Tensile Test

The high strength steel rods for test model 1 and 2 were of ASTM A193 type. To obtain the actual mechanical properties two sample specimens were made for the tensile test. The length of the specimen was 21 in., which was also the length necessary to connect the beam and column of test models. A strain gage was attached at about the middle of the specimen to measure the strain. Effective tensile area of 0.334in.² was used to calculate the tensile stress. In the test results, the 0.2% offset yield strengths were shown.

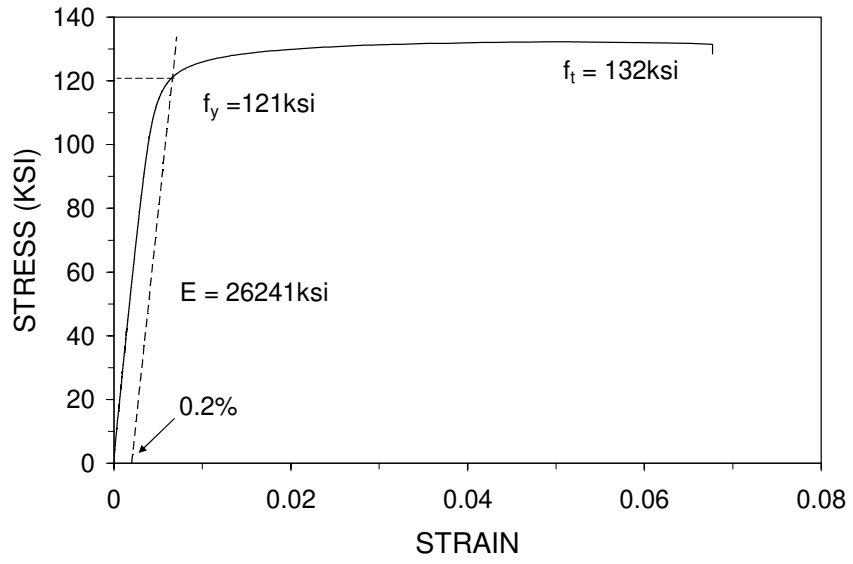


Figure C: Strain-Stress Relationship of Steel Rod Sample

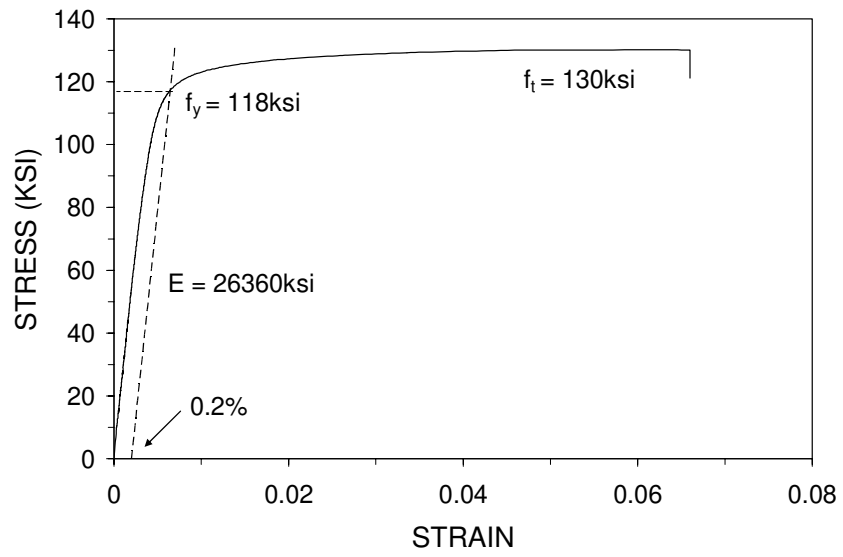


Figure C, continued: Strain-Stress Relationship of Steel Rod Sample

C.3 NMB Splice Sleeve Coupler Tensile Test

In test model 1, the column was connected to the footing through NMB splice sleeves. The connected steel rebars were inserted into the sleeve with certain length and high strength mortar was filled into the sleeve to bond the steel rebars and the sleeve. To obtain the actual tensile strength of the sleeve-rebar coupler, three coupler specimens were made for the tensile tests. The specimens were shown in Figure C.3.1(a). Figure C.3.1(b) shows the test setup of the coupler tensile test. The coupler specimen was gripped at both ends by the testing machine. During the test, the bottom plate, which gripped the bottom end of the coupler, was fixed and the top plate, which gripped the top end of the coupler, moved up to stretch the specimen. The tensile strengths of the three specimens were 16.5kips, 8.6kips and 28.5kips. The typical failure mode of the coupler is illustrated in Figure C.3.2.



(a)



(b)

Figure C, continued: Sleeve-Rebar Couplers for Tensile Tests



Figure C, continued: Failure of NMB Splice Sleeve Coupler

C.4 High Strength Grouting Cement Compression Test

For test model 2, the column was connected to the footing through dowel anchorage of the column longitudinal rebars into the metallic conduit embedded in the footing. High strength grouting cement was filled into the metallic conduit to bond the dowel rebars and the footing. Therefore, the strength of the grouting cement was of significance. Two 2 in. by 4 in. cylinders were made for the compressive tests. The compressive strengths of the two cement cylinders were 5.3ksi and 5.7ksi, respectively.